ENGINEERING CELL BASED BIOMATERIALS FOR NERVOUS TISSUE REPAIR

by

Fanwei Meng

A dissertation submitted to the faculty of
The University of Utah
in partial fulfillment of the requirements for the degree of

Doctor of Philosophy

Department of Bioengineering

The University of Utah

August 2012

The University of Utah Graduate School

STATEMENT OF DISSERTATION APPROVAL

The dissertation of **Fanwei Meng**

has been approved by the following supervisory committee members:

Patrick A. Tresco	, Chair	**5/14** Date Approved
Vladimir Hlady	, Member	**5/14** Date Approved
David W. Grainger	, Member	**5/14** Date Approved
John A. White	, Member	**5/14** Date Approved
Kuberan Balagurunathan	, Member	**5/14** Date Approved

and by **Patrick A. Tresco**, Chair of the Department of **Bioengineering**

and by Charles A. Wight, Dean of The Graduate School.

ABSTRACT

Spinal cord injury (SCI) is extremely debilitating to patients and costly to our healthcare system. Since it is an important contributor to mortality and morbidity, various therapeutic strategies have been investigated, either experimentally or clinically, to improve patients' quality of life. Studies utilizing pharmacological methods to mitigate the inhibitory components of the glial scar and facilitate axonal regeneration have been the primary experimental approaches in the field. However, the results are still not satisfactory. In this research, we aimed to tackle the issue from a novel perspective by developing cell derived, tissue engineered biomaterials that can be used in combination with other therapeutic approaches to improve the efficacy of current treatments.

In this dissertation, a simple method to create either cellularized or acellular ECM biomaterial constructs is described. In particular, by utilizing patterned surface ligands, organized orientation can be introduced to the entire astrocyte derived construct morphologically and with regard to its associated matrix proteins, which mimics the native astrocyte framework within the spinal cord fiber tracts and provides these constructs the ability to guide axonal regeneration *in vitro*. In addition, meningeal fibroblast based biomaterial constructs are also developed taking advantage of the same engineering approach. It has been demonstrated that repairing damaged dura mater with

allografts also benefits the regeneration process of the damaged spinal cord. In particular, acellular meningeal ECM constructs preserve a similar matrix protein profile as the native rat dura mater and support allogeneic meningeal cell adhesion and promote proliferation.

The results suggest these engineered biomaterial constructs derived particularly from cells residing within tissue targeted for repair may carry appropriate tissue specific biological cues and hold therapeutic potentials for spinal cord injury repair as well as dual defect reconstruction.

TABLE OF CONTENTS

LIST OF FIGURES

ACKNOWLEDGMENT

I would like to gratefully acknowledge my advisor, Dr. Patrick Tresco, who provided tremendous guidance and financial support for my research and training in his lab. I also want to thank my advisory committee members: Drs. Vladmir Hlady, David Grainger, John White and Kuberan Balagurunathan for their support and insightful suggestions during my graduate work. Additionally, I would also like to thank other members of the Keck Center for Tissue Engineering for their help and support to my research including Dr. Jeff Wolchock, Dr. Brent Winslow, Dr. Michael Benjamin Christensen, Dr. Elena Budko, John Skousen, Robert Oakes, Nick Nolta and many undergraduates who have come through the lab. Finally, I would like to thank my family for their support.

CHAPTER 1

INTRODUCTION

1.1 General Spinal Cord Injury Facts

The spinal cord is a long, tubular bundle of nervous tissue and cells that locates inside the vertebral canal and it is the main information pathway connecting the brain and peripheral nervous system (PNS). The spinal cord is divided into cervical, thoracic, lumbar and sacral segments (Fig. 1-1:A). Each segment has nerve fibers entering and exiting the spinal cord that are subsequently connecting to different parts of the body. The spinal cord is arranged with white matter on the outside and a butterfly shaped gray matter in the center. The gray matter is subdivided into dorsal horns and ventral horns, which contain groups of sensory or motor neurons that send out axons connecting to different parts of the body, respectively (Fig. 1-1:B and C). The white matter surrounding the gray matter is divided into dorsal, ventral and lateral columns. Each of these columns includes a variety of nerve fiber tracts that contain ascending sensory or descending motor nerve fibers.

Spinal cord Injury (SCI) refers to any injury to the spinal column. Currently, there are nearly 200,000-250,000 people in the United States alone who suffer from SCI with more than 12,000 additional cases every year. In the 1980s, the

Fig.1-1: Gross anatomy of the spinal cord. (A) The spinal cord is a long, tubular bundle of nervous tissue and cells that is located inside the vertebral canal and is generally divided into cervical, thoracic, lumbar and sacral segments. Each segment has nerve fibers entering and exiting the spinal cord that are subsequently connecting to different parts of the body. (B) The spinal cord is arranged with white matter on the outside and a butterfly shaped gray matter in the center. The gray matter is subdivided into dorsal horns and ventral horns. Dorsal horns contain groups of sensory neurons, whose axons receive stimulus information from different parts of the body Ventral horns contain groups of motor neurons, whose axons exit spinal cord and innervate skeletal muscles. (C) The white mater surrounding the gray matter is divided into dorsal, ventral and lateral columns. Each of these columns includes a variety of nerve fiber tracts that contains ascending sensory (shown in blue) or descending motor axons (shown in red). Images adapted from
http://www.chop.edu/healthinfo/acute-spinal-cord-injury
html://biologyonline.us/Online%20A&P/AP%202/Northland/AP2lab/lab2/14.htm

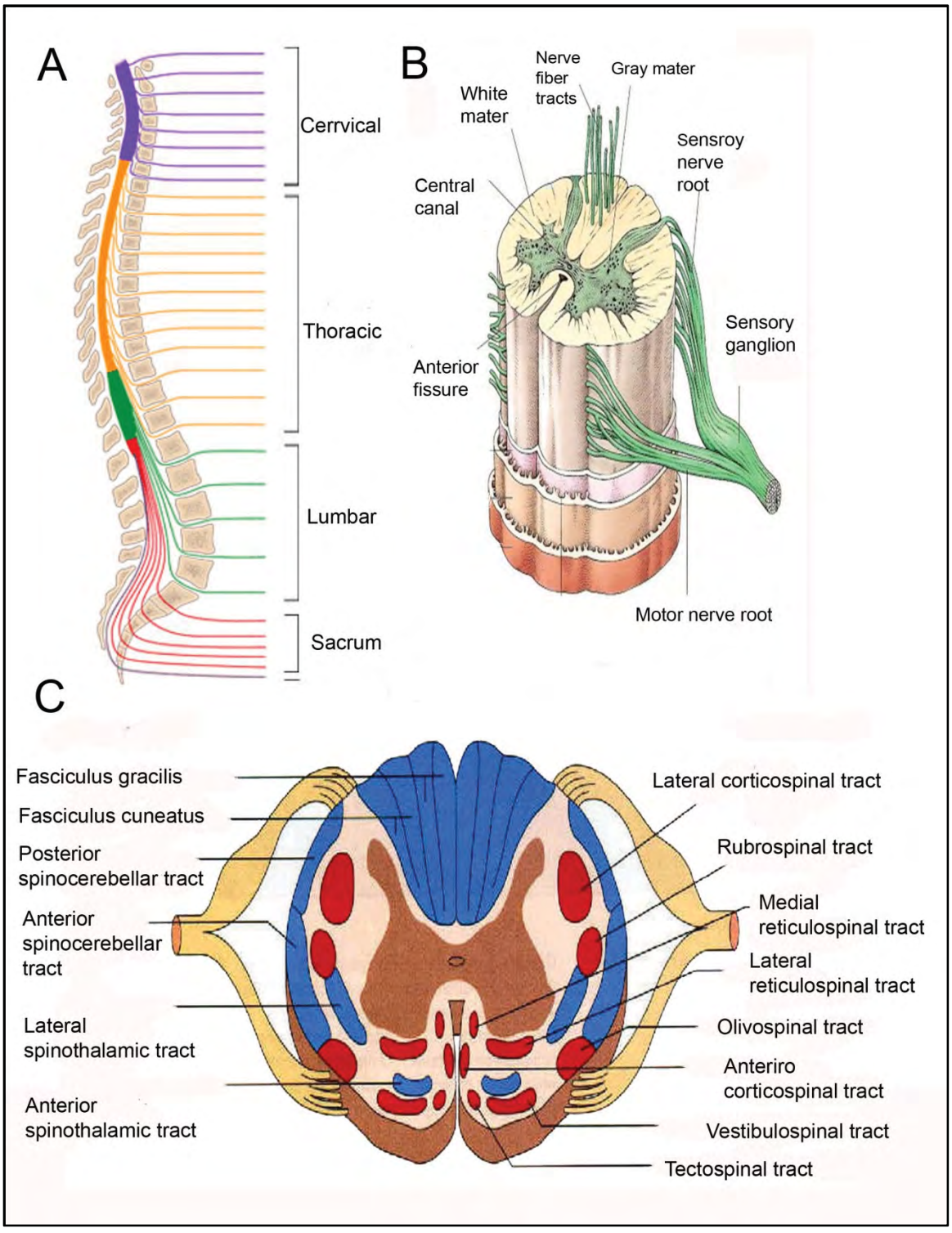
A
Cerrvical
Thoracic
Lumbar
Sacrum
B
Nerve fiber tracts
Gray mater
White mater
Sensroy nerve root
Central canal
Sensory ganglion
Anterior fissure
Motor nerve root
C
Fasciculus gracilis
Fasciculus cuneatus
Posterior spinocerebellar tract
Anterior spinocerebellar tract
Lateral spinothalamic tract
Anterior spinothalamic tract
Lateral corticospinal tract
Rubrospinal tract
Medial reticulospinal tract
Lateral reticulospinal tract
Olivospinal tract
Anteriro corticospinal tract
Vestibulospinal tract
Tectospinal tract

average age of people at time of injury was 28.7 years old, whereas now this number has increased to 39.5 years old due to an increasing average population age. More than 2/3 of SCI patients are males. Motor vehicle accidents are reported to be the most common cause, which accounts for more than 40% of injury incidences, followed by falls (27%) and violent acts (15%). Depending on the severity of the injury, SCIs are categorized into tetraplegia or paraplegia. Over 50% of patients with SCI suffer from tetraplegia. Patients with tetraplegia often have sustained injuries to their cervical segments, which results in the partial or total loss of the use of their limbs and torso. Paraplegia is relatively less severe and patients often maintain the control to their arms. The life expectancy of patients following SCI at high cervical segment levels is reduced by 20 years when compared with healthy people. The severity of the injury also is related directly to lifetime costs. The average cost for the first year for patients with the most severe tetraplegic injuries (at C1-C4 level) is close to 1 million dollars, with an additional $200,000 dollars spent every subsequent year. The total annual cost of SCIs is estimated to be more than 9 billion dollars, including approximately 2.5 billion dollars contributed by lost productivity [117].

1.2 Temporal Pathological Events Following Spinal Cord Injury

A series of pathological events, including blood-spinal cord barrier destruction, different types of inflammatory cell infiltration and glial scar formation take place at the lesion site following SCI. These cellular and molecular responses play important roles that affect the subsequent regenerative phases of the damaged cord tissue (Table 1-1 and Figure 1-2).

Table 1.1: Temporal Events Following SCI

Stage (time)	Events	References
Acute (0-24 hrs)	Vasculature damage -plasma protein extravasation -blood-spinal cord barrier permeability alteration	[1,3,4,5,7]
	Spread of vascular hemorrhage	[1,2]
	Recruitment of inflammatory cells	[11,16,17]
	Edematous condition of surrounding tissue	[11,17]
	Glial cell and neuronal cell necrosis (mechanical damage]	
	Neutrophil infiltration and microglia activation	[11,16.17,18]
Subacute (1-14 days)	Blood-spinal cord barrier permeability alteration and restoration of blood-spinal cord barrier	[1,4,5]
	Decrease of vasculature density	[8,10,11]
	Increase of vasculature density	[9,10,11]
	Secondary elevation of plasma protein extravasation	[7]
	Astrogliosis and accumulation of inhibitory ligands	[30,32,41,44,48]
	Activated microglia become phagocytic	[11,15,17,19]
	Hematogenous macrophage and lymphocyte infiltration	[19]
	Cytokine and growth factor upregulation	[60-62]
	Secondary injury (glial cell and neuronal cell apoptosis)	[15,16]
Chronic (weeks-months)	Blood-spinal cord barrier permeability alteration and restoration of blood-spinal cord barrier	[6]
	Cystic cavity formation	[1-3]
	Decrease of vasculature density due to cavity formation	[8.10.11]
	Reduction in number of activated microglia/macrophage	[16,19]
	Glial scar maturation	[32]
	Accumulation of scar-associated ligands	[30,32,41,44,48]
	Abortive axonal regeneration	[32]

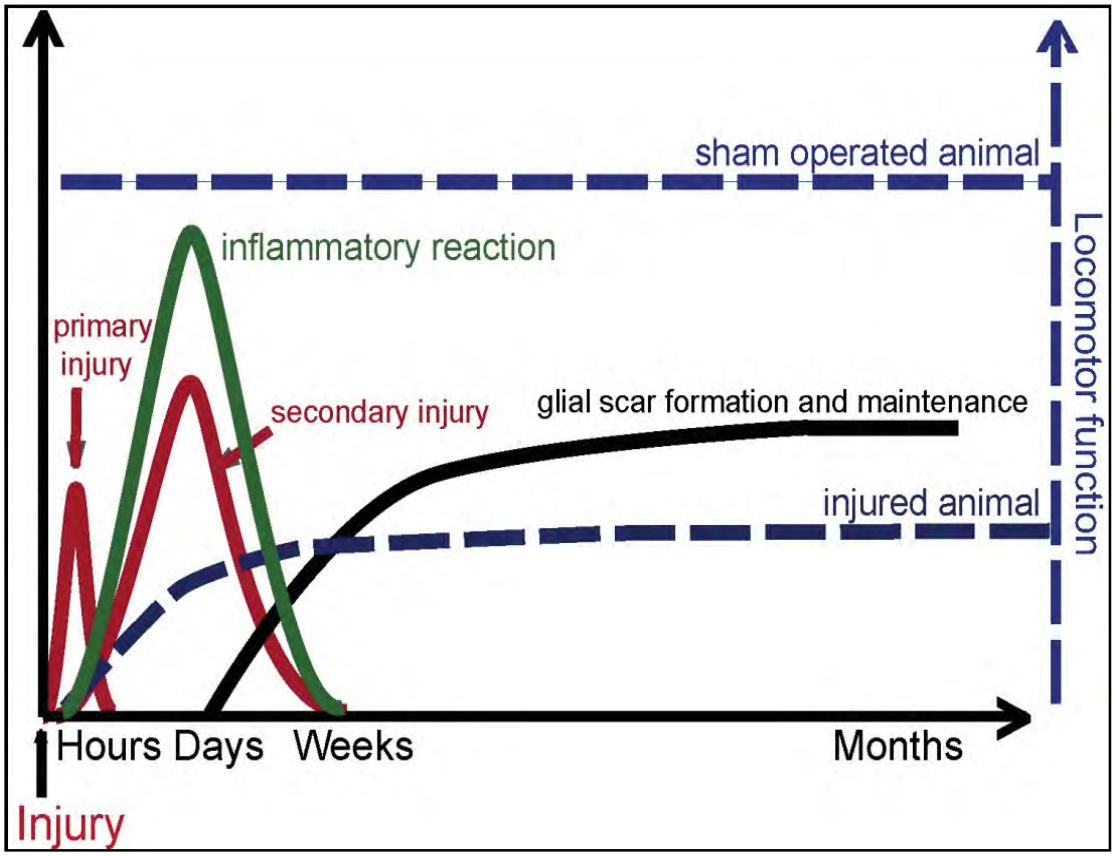

Fig. 1-2: Temporal pattern of the pathological events following spinal cord injury. Adapted from [118].

1.2.1 Vascular Events Following SCI

Following SCI, the integrity of the spinal cord vasculature is compromised due to the primary mechanical impact. Not only does the mechanical insult destroy blood vessels located in the lesion site, it also induces a series of events affecting surrounding intact vasculature, including alternation of blood-spinal cord barrier permeability and extravasation of plasma components into adjacent spinal cord tissue. The exposure of plasma derived cells and soluble molecules to neural tissue is detrimental as demonstrated by the fact that the distribution of

early hemorrhage is often closely associated with the evolution of secondary damage and cystic cavities at chronic healing stages [1-3].

The alteration of blood-spinal cord barrier permeability following injury has been studied by different vascular tracers such as I^{125}-labeled albumin or horseradish peroxidase (HRP) [1, 4, 5]. Acutely, maximal plasma protein extravasation has been reported to occur approximately 2 hrs following contusive SCI where a roughly 20-fold higher protein extravasation rate was observed over control animals. As blood vessel integrity is progressively restored, the extravasation rate has been reported to gradually decline to a roughly 3-fold increase 24 hrs following injury [4].

In a transection SCI model, HRP reactivity showed that vascular hemorrhage extended both caudally and rostrally as far as 1cm away from the lesion site during the first several hours [5]. At 1 day postinjury, while the hemorrhagic pattern was similar to that of the first several hours, an asymmetric HRP reactivity with a more severe hemorrhagic response seen distal to the injury site caudally has been reported [5]. One to two weeks following injury, the blood-spinal cord barrier leakage was restored and little to no HRP reactivity in the spinal cord tissue was observed. As the severity of the injury increased, HRP reactivity showed that the hemorrhagic area spread from the spinal cord grey matter to surrounding white matter and coincided well with the later cystic cavity development [1, 2]

In contrast to the studies where HRP injection demonstrated that leaky blood-spinal cord barrier reestablished between 1-2 weeks, it has been shown

that blood-spinal cord barrier remains leaky for at least 28 days when a small vascular tracer, [14C]-α-aminoisobutyric acid (AIB), is used [6]. Interestingly, a larger permeability change in grey matter than white matter is observed during the first week; however, the pattern is reversed 14-28 days following injury. This higher permeability in white matter at 14-28 days has been found to be in association with a secondary elevation of AIB transfer. A similar biphasic elevation of vascular tracer transfer has also been reported in a mice contusive SCI model [7]. The most pronounced extravasation of another commonly used vascular tracer, Luciferase, has been noticed as early as 35 mins after injury and then gradually decreases. A second elevation is found at 3-7 days and the barrier leakage is restored at 21 days postinjury[7].

Although the majority of blood vessels in the lesion site are destroyed after traumatic impact, the regenerative phase of vasculature occurs rapidly. The number of blood vessels at the injury site has been found to be greatly diminished the first 1-2 days postinjury [8]. Regenerative vascular sprouting and immature capillary formation are then initiated from existing vessels [9]. A significant increase of vessel number has been seen at 3-4 days in the injury epicenter and some vessels have been found to be associated with invading astrocytes [8, 10, 11] Increasing astrocytes and blood vessel association have been observed between 4-7 days. After 7 days, blood vessel number redecreases due to cystic cavity formation and a dramatic decline has been shown to occur by 14 days [8, 10, 11]. More regenerating vessels are often seen in grey matter than in white matter [10]. The regenerated blood vessels usually

have larger lumina and are frequently found to orient longitudinally across the lesion site [11]. In mice, significant regeneration and infiltration of blood vessels have also been reported to occur around 3-7 days; however, in contrast to rats, the vessel number remains afterwards without declining due to the fact that no cavity formation is associated with contusive injury in mice [7].

1.2.2 Inflammatory Response

The inflammatory response following SCI involves a serious of cellular events. Different kinds of immune cells, including neutrophils, microglia, hematogenous monocytes/macrophages and lymphocytes, all play an important role in the natural defensive mechanism following SCI. They remove invading foreign materials and cellular debris at the injury site through secretion of reactive oxygen species, proinflammatory cytokines and proteases [12]. In addition to their active roles in sanitizing the injured tissue environment, they also secret a variety of antiinflammatory cytokines and growth factors which facilitate the postinjury regenerative processes by either promoting cell survival or modifying the extracellular environment to make it proregenerative [13, 14]. However, the interactions between the pro/antiinflammatory responses are often unbalanced with the proinflammatory response being the dominant player. This phenomenon then leads to the development of an inflammation-mediated secondary injury that exacerbates the initial direct mechanical trauma and contributes to delayed cell death and massive enlargement of the lesion area [15, 16].

In animal studies, neutrophils have been reported to be the first immune cell type that arrive the injury site [11, 16, 17] Neutrophils have been seen at the

injury site as early as 1 hr following injury, although in a very small number, probably as a result of mechanical damage to the blood vessels [16]. Typically at this time point, the adjacent tissue appears to be edematous [11, 17]. Numerous neutrophils have been found adhered to the inside blood vessel walls in the wound area 4-6 hrs after injury and very few are present extravascularly. The number of neutrophils present at the injury site has been shown to largely increase 6 hrs postinjury. As the infiltration of neutrophils continues, their numbers peak around 24 hrs. The neutrophil number then gradually decreases after 1 day and activated microglia and macrophages become the dominant cell type seen at the lesion site, taking over the defensive role. Very few neutrophils are still seen 3-4 days postinjury[16]. Similar to rodent injury models, the neutrophil infiltration following human SCI is also observed several hours following injury, peaking around 1 day, gradually decreasing afterwards and eventually disappearing within the first week [18].

Activated microglia and hematogenous macrophages replace neutrophils and become the major inflammatory cell types at the injury site approximately 3 days postinjury [11, 16, 17]. Microglia are the resident macrophages of CNS tissue and are usually maintained in a resting state with highly ramified morphology. They are highly sensitive and can be activated within a short period of time after injury [18]. As early as 1 hr following injury, microglia have been found to shorten and thicken their processes, a sign of microglia activation. However, at this early time point, microglia cell body transformation from an ramified to an amoeboid shape has not begun and the cell, while is positively

stained for OX42, is not strongly stained with antisera against a lysosomal marker CD68 [16, 19] The activation state of microglia continuously increases during the first 24 hrs and many mononuclear cells appear at the injury site after 2 days. Zhang and colleagues have reported that activated microglia transformed into a phagocytic phenotype 2 days following injury [11]. At 3-7 days, these CD68+ cells are the predominant cell type in the lesion area [11, 15, 17, 19]. In addition, a bulk infiltration of activated monocytes and macrophages has also been found at 7 days following injury [11, 19].

Subchronically to chronically, Popovich and colleagues have found that the activation state of activated microglia and macrophages at the lesion site plateaus between 2 and 4 weeks, then gradually decreases after 1 month to a level similar to 14 days postinjury in rat contusive SCI [19]. Activated microglia and macrophages have also been reported to progressively disappear from the injury site between 2 weeks and3 months following partial transection SCI [16]. Zhang and colleagues, on the other hand, observed a great number of macrophages remaining in the primary lesion site even at 6-8 weeks following crush injury [11].

In humans, Fleming and colleagues have reported that the transformation of resting microglia into activated microglia starts at 1-3 days postinjury [18]. Similar to rodent models, the morphology of activated human microglia shift from ramification to an amoeboid shape with enlargement of cell bodies, and thickening, as well as shortening of their processes. Hematogenous monocytes extravasation and the accompanying transformation into an activated

macrophage phenotype occurred roughly at the same time. Around 5-10 days following injury, numerous CD68+ cells were found in necrotic areas and CD68+ immunoreactivity remained significantly elevated weeks to months following injury [18].

In rodents, lymphocytes infiltrate the lesion site following a similar temporal pattern as activated macrophages. The number of lymphocytes has been reported to significantly increase at 3 days following injury, peak around 1 week and then gradually decrease afterwards. In particular, the distribution of lymphocytes has been found to concentrate more in the injury epicenter and to a lesser extent in the nearby lesion extensions [19].

The temporal profile of lymphocyte recruitment differs in human patients compared to animal models. In human patients, only a limited number of lymphocytes have been observed extravascularly in the haemorrhagic and necrotic area up to 10 days after injury [18]. However, after this initial period the number of lymphocytes increases from weeks to months in humans.

1.2.3 Glial Scar Formation

In the spinal cord, the trajectories of ascending sensory fibers and descending motor fibers extend along white matter fiber tracts paved by longitudinally aligned glial cells [20-23] (Fig.1-3:A). Following SCI, the subsequent cellular and molecular responses interrupt the continuity of the organized glial framework and lead to the formation of a dense cellular structure, termed the glial scar [15, 20, 24]. The glial scar is a highly disorganized cellular structure that is primarily composed of hypertrophied, reactive astrocytes [15, 24].

The glial scar can be anatomically identified by increased expression of glial fibrillary acidic protein (GFAP), an intermediate filament found exclusively in astrocytes[25-27], as well as other intermediate filament proteins such as vimentin [28, 29]. The GFAP and vimentin expression are generally observed to be upregulated during the first week following SCI [19, 30-32]. This upregulation is initially seen at the injury core and subsequently spreads both caudally and rostrally [33]. This spread of the reactive astrocyte response away from the injury site has been correlated with animal maturity. Extensive astrogliosis and long distance spreading into adjacent spinal cord segments has been observed in adult animals following injury whereas the reactive astrocyte response in neonatal animals is mild and confined to the injury site [33]. In addition, the GFAP upregulation has been found to be region-dependent where more GFAP+ reactive astrocytes are seen in spinal cord segments proximal to the injury center than distal segments and persisted for at least 30 days [30].

Depending on the nature of the injury, the lesion center can either form a necrotic core surrounded by a rim of reactive astrocytes or eventually become filled by them [15, 17, 19]. Although the reactive astroglial responses take place acutely after injury where the increased mitotic activity and the hypertrophy of reactive astrocytes become noticeable within 7 days, the maturation of the glial scar may take several months to accomplish [32] (Fig. 1-3:B, C, D and E). In cases of laceration of penetration SCI where the continuity of dura mater breaks down, the glial scar also contains connective tissue elements derived from invading meningeal fibroblasts[34, 35].

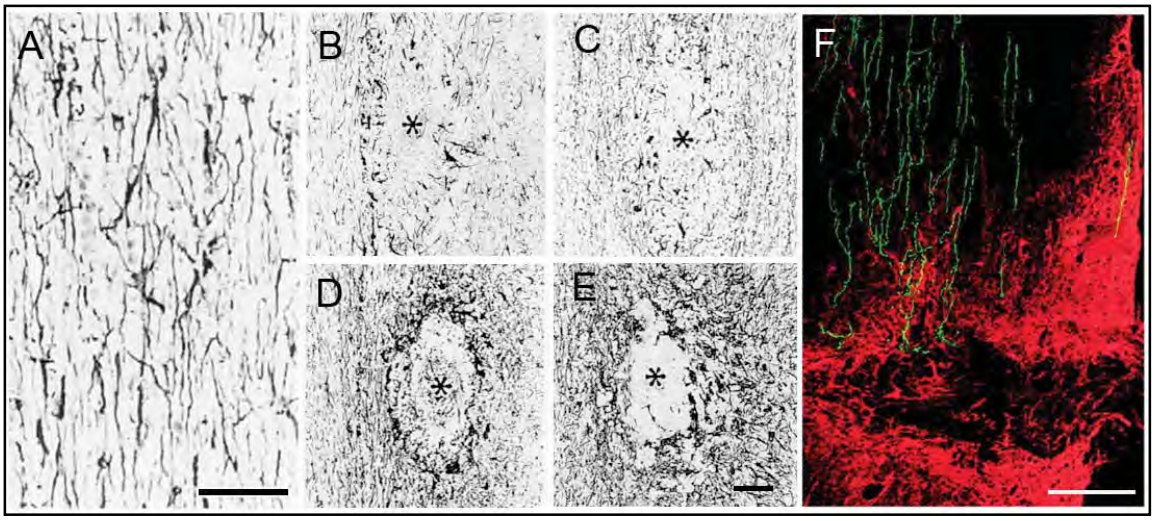

Fig. 1-3: Inhibitory glial scar formation. (A) In the spinal cord, the fiber tracts are paved by longitudinally oriented astroglial cells. Here, a network of organized astrocytic processes, visualized by GFAP, is found lining along the corticospinal motor fiber tract. The development of the glial scar at (B) 1, (C) 3, (D) 7, and (D) 13 weeks. The glial scar formation is a hallmark cellular response following SCI and a mature scar may take months to form. Adapted from [32] (D) The glial scar is repulsive to axonal regeneration due to both its disorganized cellular structure and associated inhibitory ligands. GFP labeled DRG axons (shown in green) have been shown to stall at the margin of the scar tissue (stained for chondroitin sulfate proteoglycan (CSPG) in red). Adapted from [24]. Scale bar=50 µm in (A), 100 µm in (B-E), 250 µm in (F).

In contrast to the strong astrogliosis reaction seen in rodent SCI models, the reactive astroglial response in humans is not only delayed by 4 months following injury but also accompanied with only slight GFAP upregulation. The intensity of GFAP immunoreactivity decreases to a level lower than normal spinal cord by 1 year following injury and persist for 23 years [18].

The glial scar is considered the major impediment for axonal regeneration as many *in vivo* studies have established the close association between axonal regeneration failures and scar formation [15, 20, 24, 36] (Figure 1-3:F). Regenerating axons have been found to stall at the border of the scar tissue and

are incapable of penetrating though the entire scar territory. The glial scar was originally thought to act simply as a physical barrier impeding axonal regeneration [37-39]; however, recent studies have demonstrated that the molecular composition of the scar tissue also contributes to its inhibitory nature [40-42]. These putative inhibitory molecules include subtypes of chondroitin sulfate proteoglycans (CSPGs) [43-46] and tenascins [42, 47] that are secreted by activated glial cells, as well as myelin associated molecules [48-50] which are expressed by cells of oligodendrocytes lineage or exposed due to myelin sheath damage. Semaphorin and deposited collagenous materials have also been shown or suggested to contribute to the inhibitory nature of the glial scar when there is meningeal fibroblast infiltration following SCI [34, 35, 51].

1.3 The Protective Role of Astrocytes Following Spinal Cord Injury

As mentioned previously, reactive astrogliosis is a prominent cellular feature following SCI and the inhibitory effect of the astroglial scar on axonal regeneration has been well established both *in vitro* and *in vivo* [20, 24, 40, 41, 45]. However, recent studies have started to reveal the positive roles of reactive astrocytes following SCI. Astrocytes play important housekeeping roles as they scavenge excess extracellular glutamate and ions to prevent excitotoxicity, maintain homeostasis and secrete a variety of neurotrophic factors that are essential for neuronal activities [52-56]. Following injury, the expression of astrocyte associated glutamate transporters has been shown to upregulate in response to the elevated extracellular glutamate level due to neuronal dysfunction and cellular death [52, 57]. A study that experimentally ablated

reactive astrocytes after injury demonstrated a down-regulation of available glutamate transporters, which in turn resulted in neuronal degeneration similar to the pathology of direct excitotoxicity induced by excess glutamate [58]. These results suggest that even in an activated hypertrophied state, reactive astrocytes continue regulating the extracellular glutamate level to prevent neuronal toxicity. In addition, astrocytes sustain metabolic homeostasis by storing energy in the form of glycogen and their metabolic activities become hyperactive following injury, which metabolize stored glycogen to provide energy for surviving neurons [59].

Reactive astrocytes also continue providing trophic support essential for the neuronal survival in the vicinity of the injury site [53-56]. Following exposure to proinflammatory cytokines, such as interleukin-1 beta (IL-1β) and interleukin-6 (IL-6), reactive astrocytes have been shown to increase the production of nerve growth factor (NGF), fibroblast growth factor-2 (FGF-2) and neurotrophin-3 (NT-3), which all are important for neuronal survival or regeneration [60, 61]. Additional to the beneficial effects on surviving neurons, reactive astrocyte secreted vascular endothelial growth factor (VEGF) promotes angiogenesis and revascularization, which are essential for nutrient and oxygen transport and wound healing [55]. Insulin growth factor-1 (IGF-1), secreted by reactive astrocytes as a result of IL-1β signaling, regulates oligodendrocyte precursor proliferation and maturation into myelin synthesizing mature oligodendrocytes, which facilitate the remyelination following injury [62].

Although at the chronic stages, disorganized scar tissue has been clearly demonstrated as an obstacle to axonal regeneration, acutely the scar tissue demarcates a boundary separating the lesion area and surrounding healthy tissue, suggesting a potential role of reactive astrocytes in regulating the spatial distribution of these inflammatory cells and preventing adjacent tissue damage [63]. In particular, reactive astrocytes play an important role in restoration of disrupted blood-spinal cord barrier and reestablishment of extracellular homeostasis, both are critical for proper neuronal functions [58, 63]. As shown in the transgenic mice studies where reactive astrocyte proliferation is ablated, animals without reactive astrocyte proliferation are associated with more severe hemorrhage, tissue destruction and increased cell death [63, 64]. The reactive astrocyte infiltration into lesion center has also been demonstrated to result in improved locomotor recovery [65, 66].

It was proposed by Rolls and colleagues [67] that the process of reactive astrogliosis could be divided into two phases, a first (early) phase where reactive astrocytes contribute positively to preserve tissue function and a second (chronic) phase where a mature, disorganized glial scar forms and inhibits axonal regeneration. Therefore, therapeutic interventions that could modify the glial scar formation during the acute to subacute phases (~weeks) to make the scar tissue more proregenerative at the chronic stage could be promising for SCI repair.

1.4 Astroglia Mediated Neuronal Outgrowth

A rich body of evidence has demonstrated that astroglia cells actively interact with neuronal processes through their associated ligands to either

support or provide guidance to either pioneering axons during development or regenerating axons following injury [24, 68-75]. The underlying molecular and cellular mechanisms by which astroglia support and guide neuronal pathfinding have been elucidated by many *in vitro* and *in vivo* studies [74, 76-82]. It has been shown that astroglia deposit or express a variety of permissive molecules, including laminin (LN), fibronectin (FN), N-Cadherin and neural cell adhesion molecules (NCAM), that contribute to neuronal pathfinding by providing an adhesive pathway that attracts axonal trajectories (Fig. 1-4).

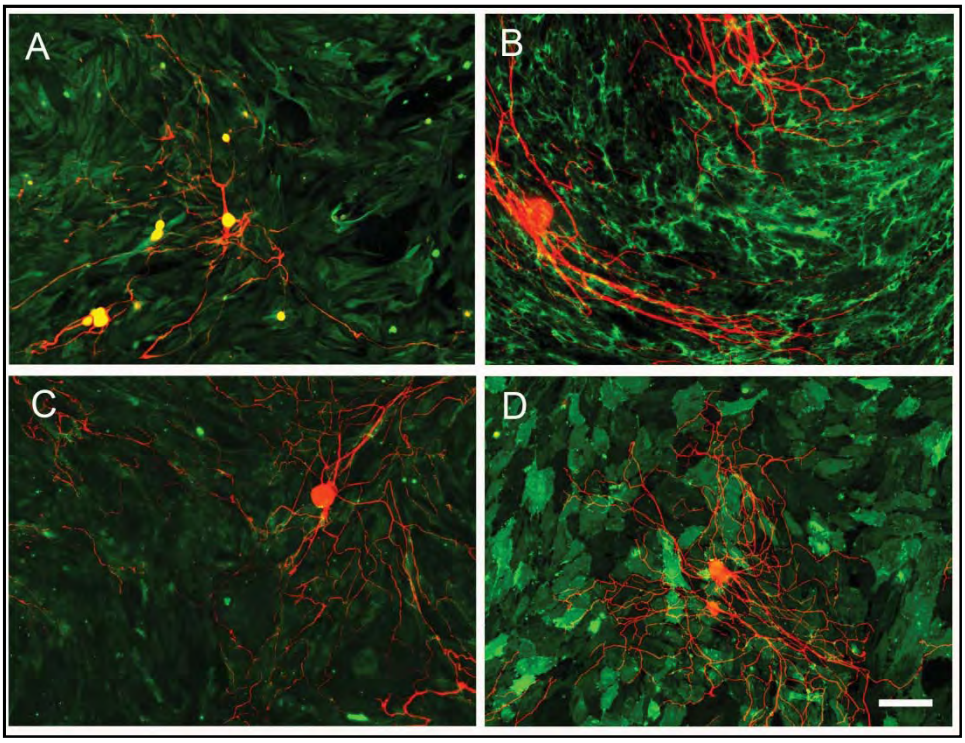

Fig. 1-4: Astrocytes support neuronal cell outgrowth *in vitro*. (A) Dissociated DRG neurons (shown in red) extend lengthy neurites on astrocyte monolayers (stained for GFAP in green) *in vitro*. Various astrocyte associated permissive ligands, such as FN (green in B), LN (green in C) and NCAM (green in D) have been shown to act as permissive substrates in supporting neuronal cell outgrowth (red in B-E). Scale bar=100 µm.

The expression of LN, one of the major axonal growth promoting molecules expressed by astrocytes, has been shown to precede and closely associate with pioneering axon entry into the optic nerve in the optic nervous system development [76]. Punctate patterns of LN immunoreactivity have also been found at the marginal area of the ventral longitudinal pathway in the mouse embryo and in close association with invading axons [77]. In addition to serving as a guidance cue, astrocyte associated LN has also been shown to be an important ligand for that provides a permissive substrate to support neuronal outgrowth *in vitro* [81].

FN is another astrocyte derived permissive extracellular matrix (ECM) protein that supports neurite outgrowth and studies have revealed at least 2 binding sites on FN molecules that interact with central nervous system (CNS) or PNS neurons with different affinities [83, 84]. In addition, astrocyte derived FN have been shown to be critical for sensory fiber regeneration in the adult rat white matter [74]. The role of astrocyte associated FN in guiding neuronal pathfinding has also been suggested *in vitro* using confocal microscopy where regenerating dorsal root ganglion (DRG) neurites were found to be closely associated with linear arrays of astrocyte derived FN bundles [85].

N-cadherin and NCAM are two membrane-bound axonal growth promoting ligands expressed by astrocytes whose roles in guiding axonal outgrowth along astroglial cells have been revealed *in vitro*[78, 80]. Functional antisera blocking N-cadherin and β1 ECM receptors has been found to reduce embryonic day 7 (E7) retinal neurite extension on astrocyte surfaces, suggesting

the important role of Ca^{2+} mediated cell surface molecules and ECM proteins in supporting neurite outgrowth at early developmental stages. NCAM, on the other hand, has been shown to regulate mature retinal neuron neurite outgrowth (E14) on astrocytes [78]. In contrast to retinal neurons, NCAM is not involved in mediating ciliary ganglion neuron neurite outgrowth whereas N-cadherin plays an important role in regulating both E8 and E14 ganglion neurons [80].

In addition to guiding axonal pathfinding via expression of permissive ligands, astroglia are recognized to deposit inhibitory ligands to form molecular boundaries for regulating neurite trajectories and patterning. CSPG is the major repulsive ECM molecule deposited by astrocytes. This inhibitory ligand has been shown to serve such a function both *in vivo* and *in vitro*[42, 86-88]. During development, the deposition of CSPG-rich territories by astroglial cells is believed to form repulsive barriers restricting axonal infiltration into unwanted areas. The functional role of CSPG-rich molecular barriers in organizing axonal growth patterns is demonstrated by an experiment utilizing chondroitinase ABC (ChABC), an enzyme that digests away the glycosaminoglycan (GAG) chains attached to the CSPG core protein. Injection of ChABC into developing zebrafish embryo has been found to induce abnormal ventral motor axonal outgrowth and branches formation [89]. *In vitro*, neurite trajectories on astroglial surfaces have also been observed to avoid regions rich in CSPG [42, 86].

1.5 Astrocyte Transplantation for Central Nervous System Repair

Numerous studies have shown that astrocytes are permissive substrates that supports neurite outgrowth from a variety of neuronal cell types *in vitro* [78-

81]. However, this supportive ability of astrocytes has been shown to be dependent on their maturation state [79, 90]. As astrocytes age *in vitro*, they gradually become less permissive as the result of the altered molecular basis underlying astrocyte-neuron interactions [79]. Moreover, insoluble factors derived by mature astrocytes have been suggested to be the critical factors that contribute to the reduced permissiveness to support neurite outgrowth [90].

Contrary to the decreased permissiveness of aged astrocytes to support neurite outgrowth, studies have found therapeutic potential for immature astrocytes in CNS injury repair applications [91-97] (Fig. 1-5). When young astrocytes (i.e., 4 days in culture) coated nitrocellulose grafts are implanted into adult mice forebrain, it suppresses glial scar formation and implanted young astrocytes are able to migrate away from the graft and integrate with the surrounding CNS tissue. On the other hand, aged astrocyte (i.e., 28 days in culture) coated implants are associated with intense glial scar formation and little integration between the grafts and the host tissue is seen [94]. Embryonic astrocyte coated polymer implants have also been applied at injured dorsal root entry zone to facilitate dorsal root nerve fiber regeneration [92]. Similarly, these young astrocyte coated grafts are well integrated with adjacent spinal cord parenchyma and dorsal root fibers with varying degrees of regeneration back into the spinal cord are found in few animals. In the lesioned rat fornix fiber tract, transplantation of immature astrocyte suspensions results in a significant increase of myelinated axons seen proximal to the lesion site 8 weeks follow inginjury [96]. Transplantation of young astrocytes, either on gelforms or in cell

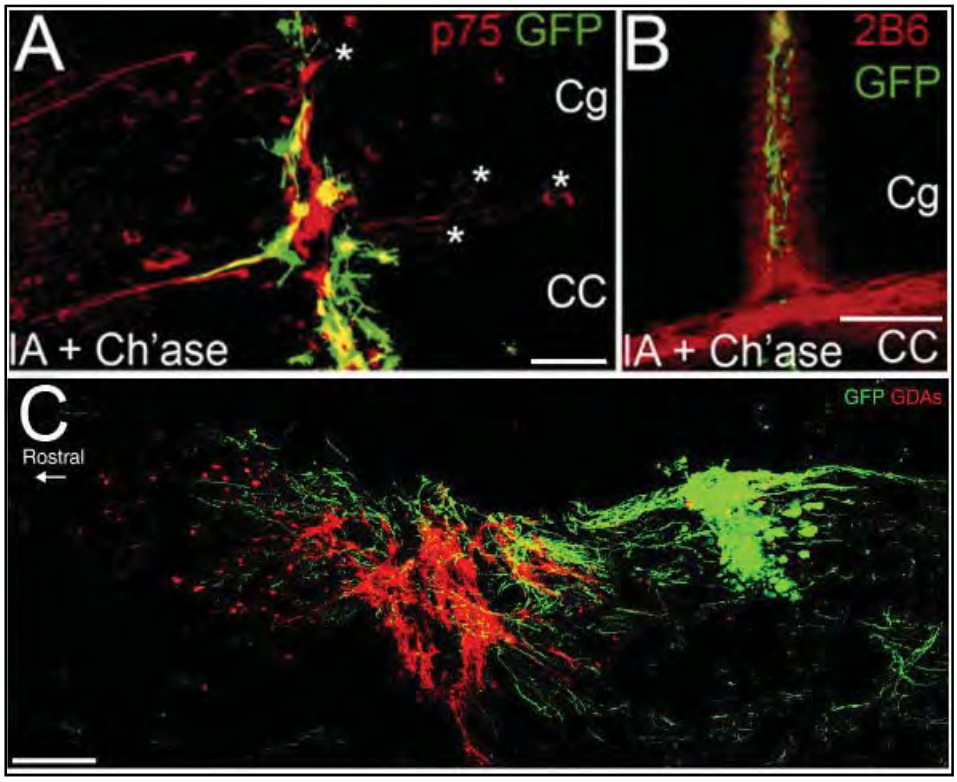

Fig. 1-5: Transplantation of immature astrocytes for spinal cord injury repair. (A) Injection of GFP labeled immature astrocytes (IA, shown in green) in combination of ChABC (Ch'ase) promote regeneration of p75+ axons (shown in red) across the lesion site in a rat brain microlesion injury (asterisks). (B) ChABC injection effectively digests away the GAG chains on CSPG, confirmed by positive 2B6 antisera detection (shown in red). Adapted from [97]. (C) Transplantation of astrocytes (shown in red) derived from glial restricted precursors cells promotes GFP labeled DRG axons (shown in green) regenerating across the lesion center and enter the rostral side of the host spinal cord tissue. Adapted from [75]. Scale bar=50 µm in (A), 100 µm in (B),=300 µm in (C).

suspensions, also has been demonstrated to induce increased number of neurofilament positive axonal fibers penetrating into the lesion site [95]. In addition, when incorporated in a collagen matrix, immature astrocytes have been shown to attract regenerating axons penetrating into the implant, but only to a limited extent [91]. Furthermore, transplantation of immature astrocyte in combination with ChABC treatment have been found to facilitate CNS axonal regeneration across the injury site in microlesioned cingulum [97].

Recently, transplantation of a specific type of astrocyte derived from embryonic glial restricted precursor has been shown to greatly benefit the regeneration outcome following unilateral transection SCI in rats [75]. These glial restricted precursor derived astrocytes (GDA) are generated by exposing precursor cells to bone morphogenetic protein-4 (BMP-4) *in vitro* and are able to promote extensive axonal regeneration *in vivo* and functional recovery. Injured animals that receive GDA transplantation achieve indistinguishable outcomes in the volitional foot placement test when compared to uninjured rats [75, 98].

In particular, transplantation of GDA induced a significant realignment of the reactive astrocytes around the lesion border where the usually seen misaligned glial scar tissue is replaced by organized arrays of astrocytic processes parallel to the normal spinal cord rostral-caudal axis [75, 98]. This aligned astrocyte framework has been suggested to at least partially contribute to the observed extensive axonal regeneration since growth cone pathfinding would be more efficient when exploring a maze of misaligned reactive astrocytic processes and their associated disorganized ligands is not required.

1.6 Organized Glial Structure for Axonal Guidance

During CNS development, pioneering axons extend a long distance toward their targets through interactions with a variety of directional cues and a part of the directional information is provided by interacting with surrounding astroglial cells. The astroglial cells crosstalk with pioneering axons temporally and spatially by organizing into organized glial frameworks and extending their processes parallel to the presumptive fiber tracts at specific periods during development [68-73, 99-101].

In the developing chick retina, Müller cells (i.e., astroglia in the retinal system) have been shown to arrange their endfeet to form organized cellular tunnels filled with axons, suggesting their role in organizing and directing retinal axonal outgrowth [101]. A similar close association of Müller cells to the optic axons in the developing mice retinal system has also been demonstrated [101]. In addition, GFAP+ astroglia have been reported to form organized glial structures preceding the arrival of callosal commissural axons during the fusion of two brain hemispheres [71]. Moreover, it has been shown that during midline decussation, commissural fibers interact with GFAP+ cells and their processes in the formation of anterior commissure [73]. Organized astroglia patterns have also been found in the adult mouse and rat spinal cord, being parallel to the neuronal processes [100, 102].

Following SCI, available evidence has suggested that an organized glial structure could be utilized by regenerating axons as supporting scaffolds to provide guidance information [24, 74, 75, 98, 103-107] (Fig. 1-6). The trajectories

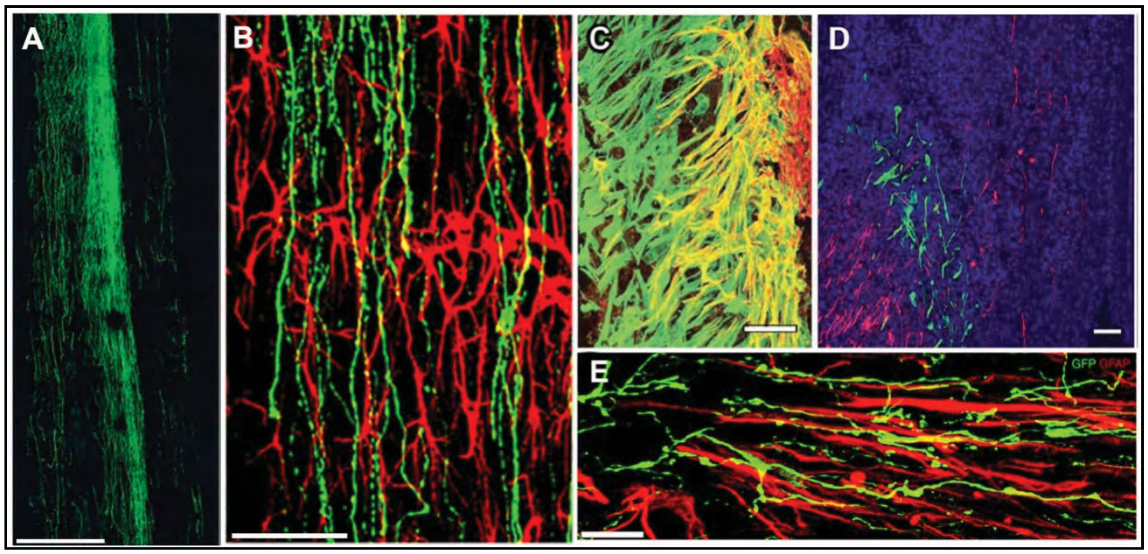

Fig. 1.6: Organized glial frameworks facilitate axonal regeneration. (A) Transplanted GFP labeled DRG neurons (shown in green) showed robust and long distance outgrowth in degenerating spinal cord white mater. (B) In particular, these GFP+ axons (shown in green) are found to be in a close association and growing parallel to the longitudinally aligned host astrocytic processes (shown in red) Adapted from [24]. (B) Following olfactory ensheathing cell transplantation, the astrocytic processes (shown in red) and Schwann cell processes (shown in green) at the injury interface are found to form ladder-like, parallel bridging structures that aligned in the normal oblique orientation of dorsal roots. (D) Regenerating sensory fibers (shown in red) follow the oriented glial cell processes at the interface and cross the lesion site. OECs are shown in green and DAPI is used as counterstain. Adapted from [105]. (E) GDA transplantation reorganize the reactive astrocyte processes at the lesion margin and regenerating DRG axons (shown in green) are found to follow the oriented astrocytic processes at lesion margin (shown in red) penetrating into the lesion center. Adapted from [75]. Scale bar=500 µm in (A), 50 µm in (B),100 µm in (C), 200 µm in (D), 25 µm in (E)

of DRG neurons transplanted into degenerating adult rat spinal cord have been found to extend long distances parallel to, and closely associated with, longitudinally aligned host astrocytic processes. This robust outgrowth is found to stall when regenerating axons enter the disorganized glial scar territory [24]. Similar neuronal outgrowth patterns that followed the processes of host astrocytes have also been observed when different types of embryonic neurons are transplanted into myelinated adult rat fiber tracts [107]. In addition, when cultured on tissue slices containing corpus callosum, a white matter fiber tract in the brain, DRG neurites also generally extend along GFAP+ astrocytic processes [74]. The regenerating endogenous rubrospinal motor fibers have also been found to follow the orientation of realigned reactive astrocytic processes at the lesion margin, which then penetrated into the lesion center [75, 98].

The hypothesis that an organized glial structure could potentially facilitate axonal regeneration is reinforced by transplantation studies of olfactory ensheathing cells (OECs) [103, 105, 108]. In injured dorsal root entry zones, transplanted OECs have been found to induce a ladder-like bridging structure, established by host CNS astrocytic processes and PNS Schwann cell processes. Regenerating sensory fibers are found to extend across the injury site in alignment with these oriented glial processes at the interface [105]. OECs transplantation has also been shown to induce regenerating corticospinal tract axons advancing through the transplant and back into host spinal cord tissue without interruption [103]. The fact that OECs can reorganize the configuration of astrocytes they interact with to form a continuous bridging pathway is suggested

to be one of the underlying cellular mechanisms by which OECs facilitate regeneration [108]. Longitudinally oriented axons have also been observed to be associated with organized Schwann cell frameworks that infiltrated into the lesion site following rat contusive SCI, reinforcing the idea that organized glial structures direct and facilitate axonal regeneration [104].

1.7 Engineering Oriented Glial Framework *In Vitro*

Given the knowledge that astroglia guide neuronal pathfinding via formation of organized glial structures and deposition of both permissive and repulsive ligands, it is intriguing to think that axonal regeneration could be supported, promoted and directed if an oriented glial substrate were able to be engineered to restore the organized glial framework at the injury site.

Mechanical cues such as topographical grooves have been shown to successfully induce alignment of different glial cell types *in vitro* [85, 109-114] (Fig. 1-7). Substrates containing microgrooves made of poly (D,L-lactic acid) have been fabricated and coated with LN to align Schwann cells *in vitro*[112]. The groove width is found to be the critical parameter in inducing Schwann cells organization rather than the depth of the grooves. In particular, groove width falling into the 10-20 μm range, slightly larger than the width of a Schwann cell body, is demonstrated to be optimal. When rat spinal neurons are cultured atop the aligned Schwann cell monolayers, neurite trajectories are found to be parallel to the orientation of underlying Schwann cells, presumably guided through both topographical and molecular mechanisms [110].

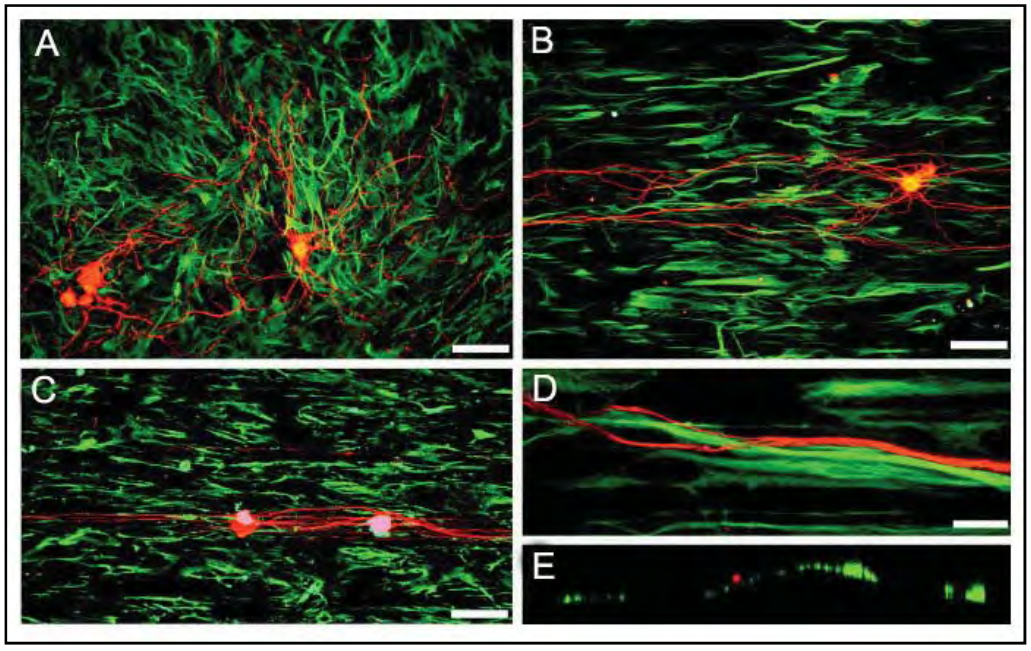

Fig. 1-7: Oriented astrocyte monolayers guide neurite outgrowth *in vitro*. (A) No biased neurite outgrowth is observed when DRG neurons are cultured on randomly organized astrocyte monolayers. (B) Directed neurite outgrowth is observed when DRG neurons are cultured on oriented astrocyte monolayers induced by grooved substrates. (C) Similar guided outgrowth behavior is also observed with adult DRG neurons. (D, E) Reconstructed 3D confocal images confirm neurite outgrowth atop astrocyte monolayers. Adapted from [85]. Neurites are shown in red and astrocytes are shown in green in (A-E). Scale bar=100 µm in (A-C), 16 µm in (D)

Organized astrocyte frameworks have also been successfully engineered *in vitro* [85, 109, 113-115]. Oriented astrocyte monolayers are engineered by culturing primary rat cortical astrocytes on grooved polystyrene substrates [85]. The roughness of surface undulation has been shown to play an important role in organizing astrocyte orientation and a threshold value must be achieved in order to provide directional information. Aligned astrocyte monolayers successfully direct adjacent regenerating DRG neurite outgrowth in a direction parallel to the orientation of astrocytic processes, irrespective of the developmental stage of the neuron. In addition, the spatial pattern of various astrocyte associated ligands is found to be related to astrocyte morphology such that a network of corresponding insoluble ligands (i.e., ECM proteins and membrane bound molecules) is observed to be present anisotropically on aligned astrocyte monolayers. In particular, confocal microscopy reveals a close association between the trajectories of regenerating DRG neurons and linear arrays of astrocyte derived FN, suggesting a potential role of FN in guiding DRG pathfinding. The directed outgrowth length (i.e., neurite outgrowth in a particular direction of interest) of neurites grown on aligned astrocyte structure is found to be significantly increased when compared to those grown on randomly organized astrocytes [85]. Similar astrocyte alignment is also achieved on micropatterned polystyrene substrates [113]. It has been shown that astrocyte alignment induced by microtopography can be maintained for at least 3 weeks *in vitro* [114]. Although neurite alignment on oriented astrocyte monolayers engineered by microtopography is lower than that of neurites grown directly on the grooved

polymeric substrates, neuronal survival on the astrocyte coated substrates is significantly prolonged [114].

Astrocyte alignment has also been successfully induced by the application of external electric fields in the absence of physical cues, which then guide the directional outgrowth of regenerating DRG neurons [109]. Moreover, it is demonstrated that directed neurite outgrowth is maintained even when neurons are grown on fixed, oriented astrocyte monolayers, suggesting the insoluble ligands derived from astrocytes play the critical role in mediating neurite outgrowth [109, 119].

1.8 Summary

In summary, a large body of evidence has suggested the beneficial roles of astrocytes following SCI. Astrocytes are the critical player in maintaining ion homeostasis, regulating extracellular glutamate level, reestablishing the blood-spinal cord barrier integrity and restricting the spread of infiltrating inflammatory cells into healthy tissues following injury. In addition, they secret neurotrophic factors that support the survival of neuronal cells postinjury. Although reactive astrocytes are known to be the major component of the inhibitory glial scar, studies have also shown that they can be proregenerative following exposure to postinjury cytokines.

In addition, rich evidence has suggested that the regenerative ability of injured axons could be promoted when an organized astrocyte framework is provided. Regenerating axons have been found to be able to retrieve directional information from the organized glial structure following injury to guide their

trajectories, potentially through interactions with a network of anisotropically organized ligands expressed and deposited by astrocytes, both permissive and repulsive. Particularly, astrocyte derived FN might be a potent guiding ligand as neurite trajectories were found to be directly atop of linear bundles of astrocyte derived FN *in vitro*.

However, there are still questions that remain to be asked in order to get a more complete understanding of the underlying molecular mechanism that oriented astrocytes guide neuronal pathfinding, and how to translate this knowledge to develop novel biomaterials to improve current treatments. Although Biran and colleagues observed a close association between linear arrays of astrocyte derived FN and DRG neurites, the fact that the culture system was based on grooved substrates makes it difficult to rule out the involvement of the mechanical effect on influencing neurite trajectories. Similarly, Alexander and colleagues failed to demonstrate what the key insoluble ligand(s) on aligned astrocyte monolayers provides the directional information for adjacent neuronal cells. Moreover, despite studies that have demonstrated the feasibility of engineering aligned glial structures *in vitro* to induce directional axonal regeneration, it is unclear if an oriented glial framework could be transferred for *in vivo* applications. Our studies were designed to investigate these unanswered but important questions.

1.9 References

1. Noble LJ, Wrathall JR. Distribution and time course of protein extravasation in the rat spinal cord after contusive injury. Brain Res 1989;482:57-66.

2. Noble LJ, Wrathall JR. Correlative analyses of lesion development and functional status after graded spinal cord contusive injuries in the rat. Exp Neurol 1989;103:34-40.

3. Mautes AE, Weinzierl MR, Donovan F, Noble LJ. Vascular events after spinal cord injury: contribution to secondary pathogenesis. Phys Ther 2000;80:673-687.

4. Hsu CY, Hogan EL, Gadsden RHS, Spicer KM, Shi MP, Cox RD. Vascular permeability in experimental spinal cord injury. J Neurol Sci 1985;70:275-282.

5. Noble LJ, Wrathall JR. The blood-spinal cord barrier after injury pattern of vascular events proximal and distal to a transection in the rat. Brain Res 1987;424:177-188.

6. Popovich PG, Horner PJ, Mullin BB, Stokes BT. A quantitative spatial analysis of the blood-spinal cord barrier. I. Permeability changes after experimental spinal contusion injury. Exp Neurol 1996;142:258-275.

7. Whetstone WD, Hsu JY, Eisenberg M, Werb Z, Noble-Haeusslein LJ. Blood spinal cord barrier after spinal cord injury relation to revascularization and wound healing. J Neurosci Res 2003;74(227-239).

8. Imperato-Kalmar EL, McKinney RA, Schnell L, Rubin BP, Schwab ME. Local changes in vascular architecture following partial spinal cord lesion in the rat. Exp Neurol 1997;145:322-328.

9. Beggs JL, Waggener JD. Microvascular regeneration following spinal cord injury: The growth sequence and permeability properties of new vessels. Adv Neurol 1979;22:191-206.

10. Casella GT, Marcillo A, Bunge MB, Wood PM. New vascular tissue rapidly replaces neural parenchyma and vessels destroyed by a contusion injury to the rat spinal cord. Exp Neurol 2002;173:63-76.

11. Zhang Z, Guth L. Experimental spinal cord injury: Wallerian degeneration in the dorsal column is followed by revascularization, glial proliferation, and nerve regeneration. Exp Neurol 1997;147:159-171.

12. David S, Kroner A. Repertoire of microglial and macrophage responses after spinal cord injury. Nat Rev Neurosci 2011;12:388-399.

13. Schwartz M, Lazarov-Spiegler O, Rapalino O, Agranov I, Velan G, Hadani M. Potential repair of rat spinal cord injuries using stimulated homologous macrophages. Neurosurgery 1999;44(5):1041-1045.

14. Prewitt CM, Niesman IR, Kane CJ, Houlé JD. Activated macrophage/microglial cells can promote the regeneration of sensory axons into the injured spinal cord. Experimental Neurology 1997;148:433-443.

15. Fitch MT, Doller C, Combs CK, Landreth GE, Silver J. Cellular and molecular mechanisms of glial scarring and progressive cavitation: *in vivo* and *in vitro* analysis of inflammation-induced secondary injury after CNS trauma. J Neurosci 1999;19:8182-8198.

16. Dusart I, Schwab ME. Secondary cell death and the inflammatory reaction after dorsal hemisection of the rat spinal cord. Eur J Neurosci 1994;6:712-724.

17. Carlson SL, Parrish ME, Springer JE, Doty K, Dossett L. Acute inflammatory response in spinal cord following impact injury. Exp Neurol 1998;151:77-88.

18. Fleming JC, Norenberg MD, Ramsay DA, Dekaban GA, Marcillo AE, Saenz AD, et al. The cellular inflammatory response in human spinal cords after injury. Brain 2006;129:3249-3269.

19. Popovich PG, Wei P, Stokes BT. Cellular inflammatory response after spinal cord injury in Sprague-Dawley and Lewis rats. J Comp Neurol 1997;377:443-464.

20. Davies SJ, Fitch MT, Memberg SP, Hall AK, Raisman G, Silver J. Regeneration of adult axons in white matter tracts of the central nervous system. Nature 1997;390:680 - 683.

21. Suzuki M, Raisman G. Multifocal pattern of postnatal development of the macroglial framework of the rat fimbria. Glia 1994;12:294-308.

22. Suzuki M, Raisman G. The glial framework of central white matter tracts: segmented rows of contiguous interfascicular oligodendrocytes and solitary astrocytes give rise to a continuous meshwork of transverse and longitudinal processes in the adult rat fimbria. Glia 1992;6:222-235.

23. Barry D, McDermott K. Differentiation of radial glia from radial precursor cells and transformation into astrocytes in the developing rat spinal cord. Glia 2005;50.

24. Davies SJ, Goucher DR, Doller C, Silver J. Robust regeneration of adult sensory axons in degenerating white matter of the adult rat spinal cord. J Neurosci 1999;19:5810-5822.

25. Ridet JL, Malhotra SK, Privat A, Gage FH. Reactive astrocytes: cellular and molecular cues to biological function. Trends Neurosci 1997;20:570-577.

26. Bignami A, Dahl D. Astrocyte-specific protein and neuroglial differentiation. An immunofluorescence study with antibodies to the glial fibrillary acidic protein. J Comp Neurol 1974;153:27-38.

27. Eng LF. Glial fibrillary acidic protein (GFAP): the major protein of glial intermediate filaments in differentiated astrocytes. J Neuroimmunol 1985;8:203-214.

28. Chiu FC, Norton WT, Fields KL. The cytoskeleton of primary astrocytes in culture contains actin, glial fibrillary acidic protein, and the fibroblast-type filament protein, vimentin. J Neurochem 1981;37:147-155.

29. Yang HY, Lieska N, Shao D, Kriho V, Pappas GD. Proteins of the intermediate filament cytoskeleton as markers for astrocytes and human astrocytomas. Mol Chem Neuropathol 1994;21:155-176.

30. Baldwin SA, Broderick R, Blades DA, Scheff SW. Alterations in temporal/spatial distribution of GFAP- and vimentin-positive astrocytes after spinal cord contusion with the New York University spinal cord injury device. J Neurotrauma 1998;15:1015-1026.

31. Barrett CP, Guth L, Donati EJ, Krikorian JG. Astroglial reaction in the gray matter lumbar segments after midthoracic transection of the adult rat spinal cord. Exp Neurol 1981;73:365-377.

32. Li Y, Raisman G. Sprouts from cut corticospinal axons persist in the presence of astrocytic scarring in long-term lesions of the adult rat spinal cord. Exp Neurol 1995;134:102-111.

33. Barrett CP, Donati EJ, Guth L. Differences between adult and neonatal rats in their astroglial response to spinal cord injury. Exp Neurol 1984;84:374-385.

34. Iannotti C, Zhang YP, Shields LB, Han Y, Burke DA, Xu XM, et al. Dural repair reduces connective tissue scar invasion and cystic cavity formation after acute spinal cord laceration injury in adult rats. J Neurotrauma 2006;23:853-865.

35. Hermanns S, Reiprich P, Müller HW. A reliable methodmtomreduce collagen scar formation ing the lesioned rat spinal cord. J Neurosci Methods 2001;110:141-146.

36. Rudge JS, Silver J. Inhibition of neurite outgrowth on astroglial scars *in vitro*. J Neurosci 1990;10:3594-3603.

37. Clemente CD, Windle WF. Regeneration of severed nerve fibers in the spinal cord of the adult cat. J Comp Neurol 1954;101:691-731.

38. Windle WF, Clemente CD, Chambers WW. Inhibition of formation of a glial barrier as a means of permitting a peripheral nerve to grow into the brain. J Comp Neurol 1952;96:359-369.

39. Windle WF, Chambers WW. Regeneration in the spinal cord of the cat and dog. J Comp Neurol 1950;93:241-257.

40. McKeon RJ, Schreiber RC, Rudge JS, Silver J. Reduction of neurite outgrowth in a model of glial scarring following CNS injury is correlated with the expression of inhibitory molecules on reactive astrocytes. J Neurosci 1991:3398-3411.

41. McKeon RJ, Höke A, Silver J. Injury-induced proteoglycans inhibit the potential for laminin-mediated axon growth on astrocytic scars. Exp Neurol 1995;136:32-43.

42. Meiners S, Powell EM, Geller HM. A distinct subset of tenascin/CS-6-PG-rich astrocytes restricts neuronal growth *in vitro*. J Neurosci 1995;15:8096-8108.

43. McKeon RJ, Jurynec MJ, Buck CR. The chondroitin sulfate proteoglycans neurocan and phosphacan are expressed by reactive astrocytes in the chronic CNS glial scar. J Neurosci 1999;19:10778-10788.

44. Levine JM. Increased expression of the NG2 chondroitin-sulfate proteoglycan after brain injury. J Neurosci 1994;14.

45. Bradbury EJ, Moon LD, Popat RJ, King VR, Bennett GS, Patel PN, et al. Chondroitinase ABC promotes functional recovery after spinal cord injury. Nature 2002;416:636-640.

46. Monnier PP, Sierra A, Schwab JM, Henke-Fahle S, Mueller BK. The Rho/ROCK pathway mediates neurite growth-inhibitory activity associated with the chondroitin sulfate proteoglycans of the CNS glial scar. Mol Cell Neurosci 2003;22:319-330.

47. Lochter A, Vaughan L, Kaplony A, Prochiantz A, Schachner M, Faissner A. J1/tenascin in substrate-bound and soluble form displays contrary effects on neurite outgrowth. J Cell Biol 1991;113:1159-1171.

48. Schnell L, Schwab ME. Axonal regeneration in the rat spinal cord produced by an antibody against myelin-associated neurite growth inhibitors. Nature 1990;343:269-272.

49. Mukhopadhyay G, Doherty P, Walsh FS, Crocker PR, Filbin MT. A novel role for myelin-associated glycoprotein as an inhibitor of axonal regeneration. Neuron 1994:757-767.

50. Wang KC, Koprivica V, Kim JA, Sivasankaran R, Guo Y, Neve RL, et al. Oligodendrocyte-myelin glycoprotein is a Nogo receptor ligand that inhibits neurite outgrowth. Nature 2002;417:941-944.

51. Niclou SP, Franssen EH, Ehlert EM, Taniguchi M, Verhaagen J. Meningeal cell-derived semaphorin 3A inhibits neurite outgrowth. Mol Cell Neurosci 2003;24:902-912.

52. Hertz L, Zielke HR. Astrocytic control of glutamatergic activity: astrocytes as stars of the show. Trends Neurosci 2004;27:735-743.

53. Chen LW, Zhang JP, Kwok-Yan Shum D, Chan YS. Localization of nerve growth factor, neurotrophin-3, and glial cell line-derived neurotrophic factor in nestin-expressing reactive astrocytes in the caudate-putamen of 1-methyl-4-phenyl-1,2,3,6-tetrahydropyridine-treated C57/Bl mice. J Comp Neurol 2006;497:898-909.

54. Schwartz JP, Nishiyama N. Neurotrophic factor gene expression in astrocytes during development and following injury. Brain Res Bull 1994;35:403-407.

55. Papavassiliou E, Gogate N, Proescholdt M, Heiss JD, Walbridge S, Edwards NA, et al. Vascular endothelial growth factor (vascular permeability factor) expression in injured rat brain. J Neurosci Res 1997;49:451-460.

56. Muller HW, Junghans U, Kappler J. Astroglial neurotrophic and neurite-promoting factors. Pharmacology & Therapeutics 1995;65:1-18.

57. Krum JM, Phillips TM, Rosenstein JM. Changes in astroglial GLT-1 expression after neural transplantation or stab wounds. Exp Neurol 2002;174:137-149.

58. Cui W, Allen ND, Skynner M, Gusterson B, Clark AJ. Inducible ablation of astrocytes shows that these cells are required for neuronal survival in the adult brain. Glia 2001;34:272-282.

59. Liberto CM, Albrecht PJ, Herx LM, Yong VW, Levison SW. Proregenerative properties of cytokine-activated astrocytes. J Neurochem 2004;89:1092-1100.

60. März P, Heese K, Dimitriades-Schmutz B, Rose-John S, Otten U. Role of interleukin-6 and soluble IL-6 receptor in region-specific induction of astrocytic differentiation and neurotrophin expression. Glia 1999;26:191-200.

61. Messersmith DJ, Murtie JC, Le TQ, Frost EE, Armstrong RC. Fibroblast growth factor 2 (FGF2) and FGF receptor expression in an experimental demyelinating disease with extensive remyelination. J Neurosci Res 2000;62:241-256.

62. Mason JL, Suzuki K, Chaplin DD, Matsushima GK. Interleukin-1beta promotes repair of the CNS. J Neurosci 2001;21:7046-7052.

63. Faulkner JR, Herrmann JE, Woo MJ, Tansey KE, Doan NB, Sofroniew MV. Reactive astrocytes protect tissue and preserve function after spinal cord injury. J Neurosci 2004;24:2143-2155.

64. Pekny M, Johansson CB, Eliasson C, Stakeberg J, Wallén A, Perlmann T, et al. Abnormal reaction to central nervous system injury in mice lacking glial fibrillary acidic protein and vimentin. J Cell Biol 1999;145:503-514.

65. Okada S, Nakamura M, Katoh H, Miyao T, Shimazaki T, Ishii K, et al. Conditional ablation of Stat3 or Socs3 discloses a dual role for reactive astrocytes after spinal cord injury. Nat Med 2006;12:829-834.

66. White RE, Yin FQ, Jakeman LB. TGF-alpha increases astrocyte invasion and promotes axonal growth into the lesion following spinal cord injury in mice. Exp Neurol 2008;214:10-24.

67. Rolls A, Shechter R, Schwartz M. The bright side of the glial scar in CNS repair. Nat Rev Neurosci 2009;10:235-241.

68. Misson JP, Edwards MA, Yamamoto M, Caviness VSJ. Identification of radial glial cells within the developing murine central nervous system: studies based upon a new immunohistochemical marker. Brain Res Dev Brain Res 1988;44:95-108.

69. Voigt T. Development of glial cells in the cerebral wall of ferrets: Direct tracing of their transformation from radial glia into astrocytes. J Comp Neurol 1989;289:74-88.

70. Silver J, Lorenz SE, Wahlsten D, Coughlin J. Axonal guidance during development of the great cerebral commissures: Descriptive and experimental

studies, *in vivo*, on the role of preformed glial pathways. J Comp Neurol 1982;210:10-29.

71. Silver J, Edwards MA, Levitt P. Immunocytochemical demonstration of early appearing astroglial structures that form boundaries and pathways along axon tracts in the fetal brain. J Comp Neurol 1993;328:415-436.

72. Silver J, Rutishauser U. Guidance of optic axons *in vivo* by a preformed adhesive pathway on neuroepithelial endfeet. Dev Biol 1984;106:485-499.

73. Cummings DM, Malun D, Brunjes PC. Development of the anterior commissure in the opossum: Midline extracellular space and glia coincide with early axon decussation. J Neurobiol 1997;32:403-414.

74. Tom VJ, Doller CM, Malouf AT, Silver J. Astrocyte-associated fibronectin is critical for axonal regeneration in adult white matter. J Neurosci 2004;24:9282-9290.

75. Davies JE, Huang C, Proschel C, Noble M, Mayer-Proschel M, Davies SJ. Astrocytes derived from glial-restricted precursors promote spinal cord repair. J Biol 2006;5:7.

76. Liesi P, Silver J. Is astrocyte laminin involved in axon guidance in the mammalian CNS? . Dev Biol 1988;130:774-785.

77. Letourneau PC, Madsen AM, Palm SL, Furcht LT. Immunoreactivity for laminin in the developing ventral longitudinal pathway of the brain. Dev Biol 1988;125:135-144.

78. Neugebauer KM, Tomaselli KJ, Lilien J, Reichardt LF. N-cadherin, NCAM, and integrins promote retinal neurite outgrowth on astrocytes *in vitro*. J Cell Biol 1988;107:1177-1187.

79. Smith GM, Rutishauser U, Silver J, Miller RH. Maturation of astrocytes *in vitro* alters the extent and molecular basis of neurite outgrowth. Dev Biol 1990;138:377-390.

80. Tomaselli KJ, Neugebauer KM, Bixby JL, Lilien J, Reichardt LF. N-cadherin and integrins: Two receptor systems that mediate neuronal process outgrowth on astrocyte surfaces. Neuron 1988;1:33-43.

81. Costa S, Planchenault T, Charriere-Bertrand C, Mouchel Y, Fages C, Juliano S, et al. Astroglial permissivity for neuritic outgrowth in neuron-astrocyte cocultures depends on regulation of laminin bioavailability. Glia 2002;37:105-113.

82. Kuhn TB, Schmidt MF, Kater SB. Laminin and fibronectin guideposts signal sustained but opposite effects to passing growth cones. Neuron 1995;14:275-285.

83. Liesi P, Kirkwood T, Vaheri A. Fibronectin is expressed by astrocytes cultured from embryonic and early postnatal rat brain. Exp Cell Res 1986;163:175-185.

84. Rogers SL, Letourneau PC, Peterson BA, Furcht LT, McCarthy JB. Selective interaction of peripheral and central nervous system cells with two distinct cell-binding domains of fibronectin. J Cell Biol 1987;105:1435-1442.

85. Biran R, Noble MD, Tresco PA. Directed nerve outgrowth is enhanced by engineered glial substrates. Exp Neurol 2003;184:141-152.

86. Snow DM, Lemmon V, Carrino DA, Caplan AI, Silver J. Sulfated proteoglycans in astroglial barriers inhibit neurite outgrowth *in vitro*. Exp Neurol 1990;109:111-130.

87. Snow DM, Steindler DA, Silver J. Molecular and cellular characterization of the glial roof plate of the spinal cord and optic tectum: A possible role for a proteoglycan in the development of an axon barrier. Dev Biol 1990;138:359-376.

88. Steindler DA, Cooper NG. Glial and glycoconjugate boundaries during postnatal development of the central nervous system. Brain Res 1987;433:27-38.

89. Bernhardt RR, Schachner M. Chondroitin sulfates affect the formation of the segmental motor nerves in zebrafish embryos. Dev Biol 2000;221:206-219.

90. Geisert EEJ, Stewart AM. Changing interactions between astrocytes and neurons during CNS maturation. Dev Biol 1991;143:335-345.

91. Joosten EA, Veldhuis WB, Hamers FP. Collagen containing neonatal astrocytes stimulates regrowth of injured fibers and promotes modest locomotor recovery after spinal cord injury. J Neurosci Res 2004;77:127-142.

92. Kliot M, Smith GM, Siegal JD, Silver J. Astrocyte-polymer implants promote regeneration of dorsal root fibers into the adult mammalian spinal cord. Exp Neurol 1990;109:57-69.

93. Smith GM, Miller RH. Immature type-1 astrocytes suppress glial scar formation, are motile and interact with blood vessel. Brain Res 1991;543:111-122.

94. Smith GM, Silver J. Transplantation of immature and mature astrocytes and their effect on scar formation in the lesioned central nervous system. Prog Brain Res 1988;78:353-361.

95. Wang JJ, Chuah MI, Yew DT, Leung PC, Tsang DS. Effects of astrocyte implantation into the hemisected adult rat spinal cord. Neuroscience 1995;65:973-981.

96. Wunderlich G, Stichel CC, Schroeder WO, Müller HW. Transplants of immature astrocytes promote axonal regeneration in the adult rat brain
Glia 1994;10:49-58.

97. Filous AR, Miller JH, Coulson-Thomas YM, Horn KP, Alilain WJ, Silver J. Immature astrocytes promote CNS axonal regeneration when combined with chondroitinase ABC. Dev Neurobiol 2010;70:826-841.

98. Davies JE, Pröschel C, Zhang N, Noble M, Mayer-Pröschel M, Davies SJ. Transplanted astrocytes derived from BMP- or CNTF-treated glial-restricted precursors have opposite effects on recovery and allodynia after spinal cord injury. J Biol 2008;19:24.

99. Silver J, Sidman RL. A mechanism for the guidance and topographic patterning of retinal ganglion cell axons. J Comp Neurol 1980;189:101-111.

100. Bitner C, Benjelloun-Touimi S, Dupouey P. Palisading pattern of subpial astroglial processes in the adult rodent brain: Relationship between the glial palisading pattern and the axonal and astroglial organization. Brain Res 1987;465:167-178.

101. Suburo A, Carri N, Adler R. The environment of axonal migration in the developing chick retina: A scanning electron microscopic (SEM) study. J Comp Neurol 1979;184:519-535.

102. Oudega M, Marani E. Expression of vimentin and glial fibrillary acidic protein in the developing rat spinal cord: an immunocytochemical study of the spinal cord glial system. J Anat 1991;179:97-114.

103. Li Y, Field PM, Raisman G. Regeneration of adult rat corticospinal axons induced by transplanted olfactory ensheathing cells. J Neurosci 1998;18:10514-10524.

104. Brook GA, Plate D, Franzen R, Martin D, Moonen G, Schoenen J, et al. Spontaneous longitudinally orientated axonal regeneration is associated with the Schwann cell framework within the lesion site following spinal cord compression injury of the rat. J Neurosci Res 1998;53:51-65.

105. Li Y, Carlstedt T, Berthold CH, Raisman G. Interaction of transplanted olfactory-ensheathing cells and host astrocytic processes provides a bridge for axons to regenerate across the dorsal root entry zone. Exp Neurol 2004;188:300-308.

106. Ramón-Cueto A, Cordero MI, Santos-Benito FF, Avila J. Functional recovery of paraplegic rats and motor axon regeneration in their spinal cords by olfactory ensheathing glia. Neuron 2000;25:425-435.

107. Davies SJ, Field PM, Raisman G. Long interfascicular axon growth from embryonic neurons transplanted into adult myelinated tracts J Neurosci 1994;14:1596-1612.

108. Li Y, Li D, Raisman G. Interaction of olfactory ensheathing cells with astrocytes may be the key to repair of tract injuries in the spinal cord: The 'pathway hypothesis. J Neurocytol 2005;34:343-351.

109. Alexander JK, Fuss B, Colello RJ. Electric field-induced astrocyte alignment directs neurite outgrowth. Neuron Glia Biol 2006;2:93-103.

110. Thompson DM, Buettner HM. Neurite outgrowth is directed by schwann cell alignment in the absence of other guidance cues. Ann Biomed Eng 2006;34:161-168.

111. Deumens R, Koopmans GC, Den Bakker CG, Maquet V, Blacher S, Honig WM, et al. Alignment of glial cells stimulates directional neurite growth of CNS neurons *in vitro*. Neuroscience 2004;125:591-604.

112. Miller C SH, Witt A, Rutkowski G, Mallapragada S. Oriented Schwann cell growth on micropatterned biodegradable polymer substrates. Biomaterials 2001;22:1263-1269.

113. Recknor JB, Recknor JC, Sakaguchi DS, Mallapragada SK. Oriented astroglial cell growth on micropatterned polystyrene substrates. Biomaterials 2004;25:2753-2767.

114. Sørensen A, Alekseeva T, Katechia K, Robertson M, Riehle MO, Barnett SC. Long-term neurite orientation on astrocyte monolayer aligned by microtopography. Biomaterials 2007;28:5498-5508.

115. East E, de Oliveira DB, Golding JP, Phillips JB. Alignment of astrocytes increases neuronal growth in three-dimensional collagen gels and is maintained following plastic compression to form a spinal cord repair conduit. Tissue Eng Part A 2010;16:3173-3184.

116. Pasterkamp RJ, Giger RJ, Ruitenberg M-J, D. HAJG, De Wit J, De Winter F, et al. Expression of the gene encoding the chemorepellent semaphoring III is induced in the fibroblast component of neural scar tissue formed following injuries of adult but not neonatal CNS. Mol Cell Neurosci 1999;13:143–166.

117. Spinal cord injury facts and figures at a glance. The National Spinal cord Injury Statistical Center, Birmingham, AL, 2011.

118. Renault-Mihara F, Okada S, Shibata S, Nakamura M, Toyama Y, Okano H. Spinal cord injury: emerging beneficial role of reactive astrocytes' migration. Int J Biochem Cell Biol 2008;40:1649-53

119. Meng F, Hlady V, Tresco PA. Inducing alignment in astrocyte tissue constructs by surface ligands patterned on biomaterials 2012;33:1323-1335.

CHAPTER 2

INDUCING ALIGNMENT IN ASTROCYTETISSUE CONSTRUCTS BY SURFACE LIGANDS PATTERNED ON BIOMATERIALS

2.1 Introduction

The ability of astroglia to guide neuronal pathfinding during development, *in vitro* and following injuries is well established. During development, astroglia provide directional information to pioneering axons by organizing into glial frameworks or boundaries at specific periods [1-6]. In addition, available evidence indicates that regenerating axons extend long distances following longitudinally aligned glial cells [7-11]. *In vitro*, various studies have shown that astrocytes and their secreted extracellular matrix (ECM) support neurite outgrowth of a variety of neuronal cell types [12-16]. In addition to acting as a permissive substrate, astrocytes also guide neurite extension through depositing inhibitory ECM [17-19].

Given the knowledge that astroglia serve as guidepost cells during development, as well as following injuries and support neurite outgrowth *in vitro*,

understanding how regenerating axons interact with astroglia may shed light on developing new therapeutic approaches to reconstruct parts of the damaged nervous system or to bypass the disorganized astroglial scar. To facilitate functional recovery, severed and/or spared sprouting axons must reinnervate specific and not random targets so methods that allow control over the trajectory of regenerating axons may provide technology to enhance functional recovery [23].

Several groups are studying how to engineer oriented glial substrates to study the underlying cellular and molecular mechanisms by which glial cells guide neuronal pathfinding [24-27]. It was previously demonstrated that oriented, engineered astrocyte substrates are useful for enhancing directed neurite outgrowth [25, 26, 28]. In one approach, topographical grooves and indentations in growth culture substrates have been used to orient astrocyte morphology [25, 26, 29]. Nerve cells plated on top of the directionally oriented astrocytes extend neurites in the same direction as the underlying oriented astrocyte monolayers [25, 26]. However, using such an approach, it is not clear whether the architectural features themselves are responsible for the directional orientation of the overlying neurons as grooved substrates alone are effective in directing neurite elongation [30, 31].

To better elucidate the mechanisms involved in astrocyte mediated neuronal outgrowth, planar substrates with patterned nanometer–level anisotropic guidance cues were produced with soft lithographic methods in which continuous lanes of laminin (15 μm wide) were interspersed by continuous lanes

of untreated glass (15 μm wide). We used this approach to exclude the influence of physical undulations on directing neurite trajectories, and examined how engineered astrocyte constructs affect the directional outgrowth of adjacent regenerating neurites, as well as, how they affected the orientation of adjacent astrocytes in thick tissue engineered constructs.

2.2 Materials and Methods

2.2.1 Micropatterning Device Fabrication

Polydimethylsiloxane (PDMS, R-2615, Nusil) contact printing stamps were designed using software L-edit and fabricated in the University of Utah Microfabrication laboratory. Stamps were designed to have anisotropic continuous lanes (15 μm wide) interspersed with continuous bare coverslip surfaces (15 μm wide) in order to provide directional information to align astrocytes.

Photolithographic masks of the designed pattern were fabricated using a micropattern generator (Electromask). Resulting masks were used directly as molds to produce PDMS stamps. PDMS two component kit was mixed in a 1:10 ratio, vacuumed treated to remove bubbles till no bubbles were observed, poured into a mold and then cured at 100℃ for 30 mins. The cured PDMS stamps were peeled off against the mold and cut into approximately $1\times1.5cm^2$ blocks. PDMS stamps were immersed in hexane overnight to remove residual uncured PDMS prior used for protein pattern transferring.

2.2.2 Microcontact Printing

Glass coverslips were cleaned by rinsing with acetone, isopropanol followed by double distilled deionized (DD) water, then sonicated for 15 mins and autoclaved. Ten µl laminin solution (LN, 400 µg/ml in sterile PBS; Sigma) was applied to each PDMS stamp and covered by a coverslip to help the solution spread the entire stamp surface for 25 mins. After adsorption, stamps were rinsed with sterile DD water and briefly dried under a nitrogen stream. LN adsorbed stamps with and without a lane pattern were brought into contact with clean coverslips and then removed to generate both isotropic and anisotropic protein pattern.

2.2.3 Astrocyte and DRG Isolation and Preparation

Purified primary rat postnatal astrocytes were isolated as previously described [32]. Cerebral cortices from postnatal Day 1 (P1) Sprague–Dawley rats were dissected out with meninges removed, then minced and digested (1.33% collagenase, 30 mins, Worthington Biochemical) followed by 0.25% trypsin treatment (30 mins, Worthington Biochemical). The cells were triturated and suspended in DMEM/F12 medium (Invitrogen) with 10% fetal bovine serum (FBS, Atlantic Biological). The dissociated cells were plated in 75 cm^2 flasks. After one week, purified astrocytes were obtained by overnight shake-off at 175 rpm. Dorsal root ganglion neurons (DRG) were isolated from P1 rats as previously described [23]. Individual neurons were removed from their location near the spinal column. Then the attached nerve roots were removed and the ganglia neurons were suspended in a trypsin/collagenase (0.25%/0.33%) mixture for 30

mins. The tissue was then triturated. The resulting cell suspension was centrifuged, suspended in 1 ml DMEM/F12 plus 50 µl of DNase. Then dissociated DRG neurons were plated on astrocytes monolayers on various patterns in DMEM/F12 with 10% FBS.

2.2.4 Astrocyte and DRG Culture

Purified astrocytes were seeded on LN lanes patterned or onto homogeneous fields of LN surfaces at a density of 17,300 cells/cm^2 in serum free medium (SATO-) over the first 4–6 hrs and then switched to 10% FBS for the remainder of the 4-day period to create confluent oriented and randomly, organized astrocytes monolayers, respectively. Medium was changed every other day. To produce fixed oriented and randomly organized astrocyte monolayers, astrocytes were cultured as described above and fixed by immersion in 4% paraformaldehyde for 15 mins after 4 days in culture. After fixation, cell layers were rinsed with sterile PBS once and then immersed in DMEM/F12 medium at 37℃ for 2 days to remove and deactivate residual aldehyde groups generated during the fixation process. Fresh medium was changed every day.

DRG neurons were seeded on both live and fixed astrocytes monolayer cultures (both oriented and randomly, organized) at a density of 580 DRG neurons/cm^2 in 10% FBS supplemented with 10 ng/ml 2.5S nerve growth factor (NGF; Invitrogen). The co-cultures were cultured for an additional 48 hrs and then treated with 4% paraformaldehyde for 15 min and then stored in PBS with azide.

Purified astrocytes were seeded on patterned (anisotropic) and unpatterned (isotropic) surfaces at a density of 52,000 cells/cm^2 with serum free medium (SATO-) over the first 4–6 hrs and switched to 10% FBS for 2 days to create the first confluent, oriented and random astrocyte monolayers, respectively. Then, the seeding process was repeated every other day with 52,000 cells/cm^2 in 1.5 ml 10% FBS. Half of the culture medium in each well was replaced with fresh medium the next day following cell seeding. The seeding process was repeated 3–4 times to create multilayered astrocyte cultures, which were then fixed using 4% paraformaldehyde.

2.2.5 Anti-FN Antisera Blocking Experiment

Fixed oriented astrocyte monolayers were treated with mouse anti-FN antisera (45 µg/ml, Sigma) for 3 hrs then rinsed with sterile PBS prior to adding dissociated DRG neurons. DRG neurons were seeded at a density of 580 DRG neurons/cm^2 in 10% FBS, supplemented with 10 ng/ml 2.5S NGF. DRGs were cultured for an additional 48 hrs and treated with 4% paraformaldehyde for 15 mins and then stored in PBS with azide. Untreated, fixed oriented astrocyte monolayers served as controls. There were four repeat experiments for each group.

2.2.6 Immunohistochemistry and Image Acquisition

For intracellular antigens, fixed cultures were treated with 0.05% Triton X-100 in PBS for 5 mins and rinsed with PBS three times. No Triton was applied for the extracellular matrix molecular immunohistochemical detection. Fixed cell

layers were blocked with 4% goat serum and 0.1% sodium azide in PBS for 1 hr and incubated with primary antisera against glial fibrillary acidic protein (GFAP, DAKO, 1:1000), neurofilament (NF160, Sigma, 1:500), laminin (LN, Sigma, 1:500), cellular fibronectin (FN, Sigma, 1:500), chondroitin sulfate proteoglycan (CS-56, Sigma, 1:500) and neural cell adhesion molecule (NCAM, Sigma, 1:500). Appropriate conjugated secondary antibodies (Molecular Probes) were applied at dilution of 1:500 except for GFAP (1:1000). All antibodies were diluted in 4% goat serum with 0.1% azide and applied for 24 hrs at room temperature. Fixed cell layers were rinsed with PBS three times both after primary and secondary antibody application. DAPI (10 μM; Molecular Probes) was used for all cell nuclei visualization. Coverslips were mounted with Fluoromount–G (Southern Biotechnology). Images were acquired using a Nikon epifluorescence microscope equipped with a CCD camera or using an Olympus FVX laser scanning confocal microscope.

2.2.7 Astrocyte Orientation Analysis

The orientation of elliptical DAPI+ astrocytes cell nuclei was used to determine astrocyte orientation as well as their overall appearance. For astrocytes cultured on unpatterned LN surface, the vertical axis of each image was chosen as the reference axis. For astrocytes cultured on the patterned LN substrate, the long axis of the printed LN lane pattern was used as the reference axis for calculating cell orientation. A built-in function of ImagePro (Media Cybernetics) was used to generate elliptical outlines for all cell nuclei and the angle made between the long axis of each elliptical mask and the designated

axis of the image was calculated. Nuclei that were cut off by the edge of images and clusters of nuclei that overlapped, which the program could not distinguish and recognize, were manually removed from the data set. Each measurement was placed into a data bin of plus or minus 10° off the designated axis of each image. Angle bins ranged from –90° to 90° with 0° being parallel to the designated vertical axis of each image. Four random images were taken from each coverslip and there were four repeats for each condition (oriented and random).

2.2.8 Neurite Length and Alignment Quantification

NF-160 antibody was used to visualize neuronal cell bodies and their processes. Neurite angle and length measurement were conducted using NIH Image J software. Directed length was measured and defined as the vector length of each neurite growing in the direction of interest. To calculate the directed length, a straight line was first drawn from the tip of the neurite to the cell soma. Then the directed length of each neurite was calculated by multiplying the length of the straight line by the cosine of the angle made between the straight line and the direction of interest. A designated axis of each image was chosen as the direction of interest for DRGs grown on astrocytes monolayers cultured on unpatterned substrates (both live and fixed) whereas the long axis of the LN lane pattern was used for DRGs grown on oriented astrocyte layers (both live and fixed).

Orientation of neurite outgrowth was quantified by measuring the angle between the straight line drawn from the tip of the neurite to the cell soma and

the reference axis. Each measurement was placed into a data bin of 10° ranging from –90° to 90° with 0° being parallel to the reference axis. There were three repeats for each condition (live random, fixed random, fixed oriented and live oriented).

2.2.9 Multilayered Astrocyte Analysis

Two dimensional fast fourier transform (FFT) has been used to analyze anisotropy in cells [24] and [61]. Multilayered astrocyte cultures (random and aligned) were stained for FN and the spatial distribution of astrocyte derived FN was used as an indicator for cellular orientation. Confocal microscopy was used to image through the thickness of the multilayered astrocyte cultures. Two dimensional FFT was applied on the z-stack images of both random and aligned multilayered cultures using NIH Image J software. The “Oval Profile” plug-in was used to determine radial sums over the 2D FFT image from 0° to 360° with discrete sampling of every 10°. These data were summarized so that the sum is unity. As the 2D FFT is symmetrical, only data points from 0° to 180° were used. It should be noted that the FFT image was first rotated 90° counterclockwise because the results of the FFT yield frequencies orthogonal to those in the original image. The anisotropy index was determined by the cell orientation distributions extracted from the 2D FFT [61]. The anisotropy index was determined by dividing the maximum value of the orientation distribution with the expected distribution value at that angle for a perfectly isotropic sample. Three random images were taken from each multilayered astrocyte cultures and there were three independent repeats.

2.2.10 AFM

The height in nanometers of stamped LN patterns was analyzed using a commercial AFM (Dimension 3000, Digital Instruments) in the University of Utah Microfibrication laboratory using the tapping mode.

2.2.11. Statistical Analysis

All quantitative data were reported as the mean ± standard deviation or as a frequency distribution. One way ANOVA was used to compare the means. Astrocyte morphological orientation distributions and neurite angle distributions were analyzed for differences using a chi square test for independence. The relationship between astrocyte and DRG alignment was also assessed using a Pearson's correlation coefficient. Two-tailed student *t*-test was used to pair-wise compare for anisotropy of multilayered astrocyte cultures. *p*-values < 0.05 were considered statistically significant.

2.3 Results

2.3.1 Astrocyte Orientation on Printed LN Pattern

Microcontact printing (Fig. 2-1:A) was used to generate continuous LN lanes of 15 μm width interspersed with continuous lanes of untreated glass strips of 15 μm width (Fig. 2-1:C). Clean coverslips stamped with a homogenous LN field (Fig. 2-1:B) were used to evaluate the ability of anisotropic LN lanes to direct astrocyte orientation. The height of the stamped LN lanes was approximately 5 nm as measured by AFM using tapping mode (Fig. 2-1:D and E). Primary P1 astrocytes cultured on the printed LN pattern exhibited an elongated morphology

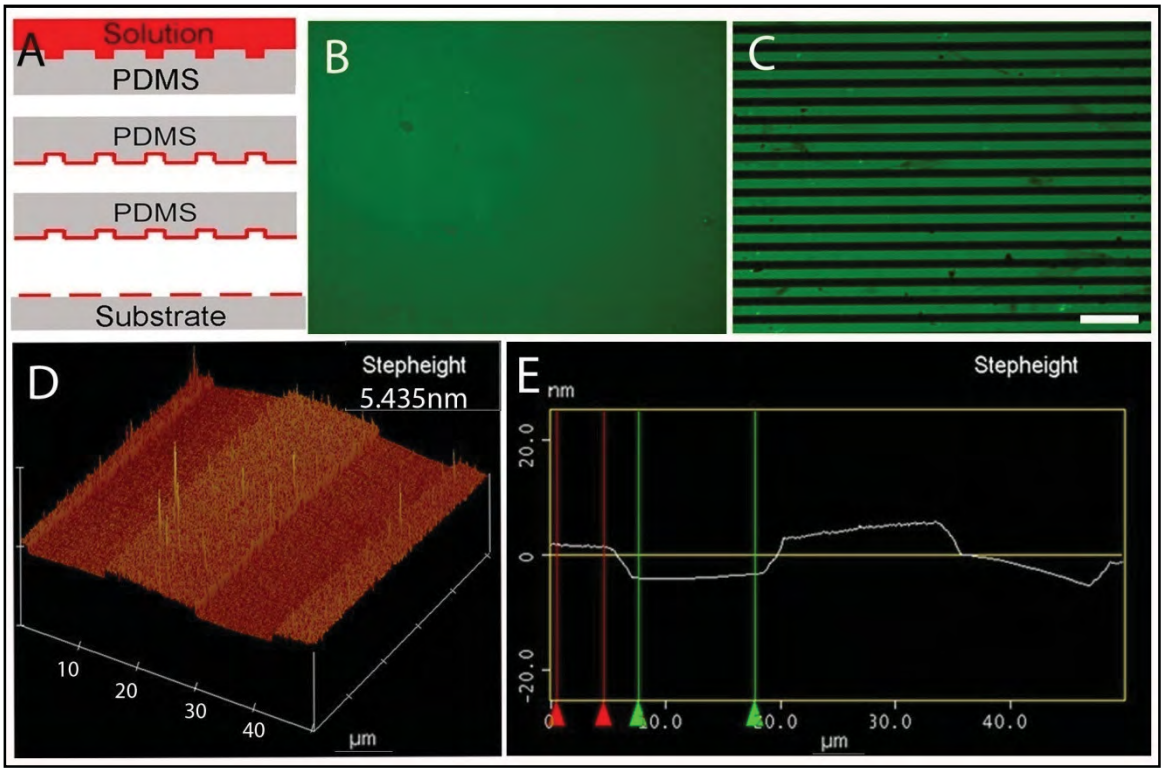

Fig. 2-1: Microcontact printing. (A) Casting method for generating patterns of extracellular matrix ligand (red) onto the surface of glass coverslips. (B) Representative fluorescent image of stamped homogeneous laminin (LN) field (green). (C) Representative fluorescent image of micropatterned LN lane pattern consisting of alternating 15 µm wide LN lanes (green) and 15 µm wide lanes of the unpatterned glass coverslip surface (black). (D and E) Representative atomic force microscopy (AFM) image of the topography of a printed LN lane pattern on the glass coverslip. The light color plateaus represent the printed LN lanes and the darker color represents the bare glass coverslip surface. The step height between the printed LN lanes and bare coverslip surface is approximately 5 nm as determined by AFM. Scale bar=100 µm.

that followed the underlying LN lanes 6 hrs after plating and the oriented morphology was maintained throughout the whole culture period (Fig. 2-2:G, H and I). Astrocytes cultured on the homogenous LN fields had no preferred directional orientation (Fig. 2-2:A, B and C). A second cytoskeletal marker, actin, was used to confirm the orientation of astrocytes cultured on either isotropic LN fields or anisotropic LN lane pattern. When seeded on LN lanes, the orientation of actin microfilaments was closely associated with the observed morphological orientation of the cells (Fig. 2-2:J, K and L). No preferred orientation of actin was observed on isotropic surfaces (Fig. 2-2:D, E and F). These observations demonstrated a haptotactic influence of the anisotropic LN substrate distribution on the guidance behavior of astrocytes. Confluent astrocytes (both aligned and random) were formed 4 days after initially seeding.

Astrocyte alignment on both patterned and homogeneous LN field (unpatterned) surfaces was quantified. The nuclei of oriented astrocytes exhibited elliptical morphology with their long axis oriented parallel to the underlying LN lane pattern, whereas equal proportions of astrocyte orientation on unpatterned surfaces fell within any particular angle bin, indicating random orientation on the homogenous LN field (Fig. 2-2:M). Approximately 81% of the cells were aligned within 20° of parallel to the long axis of underlying lane pattern (Fig. 2-2:N). The difference between the two groups was significant (Chi Square Test for Independence, $p<0.05$). The data demonstrated that nanometer level guidance cues can influence the morphology and directional bias of astrocytes on planar substrates.

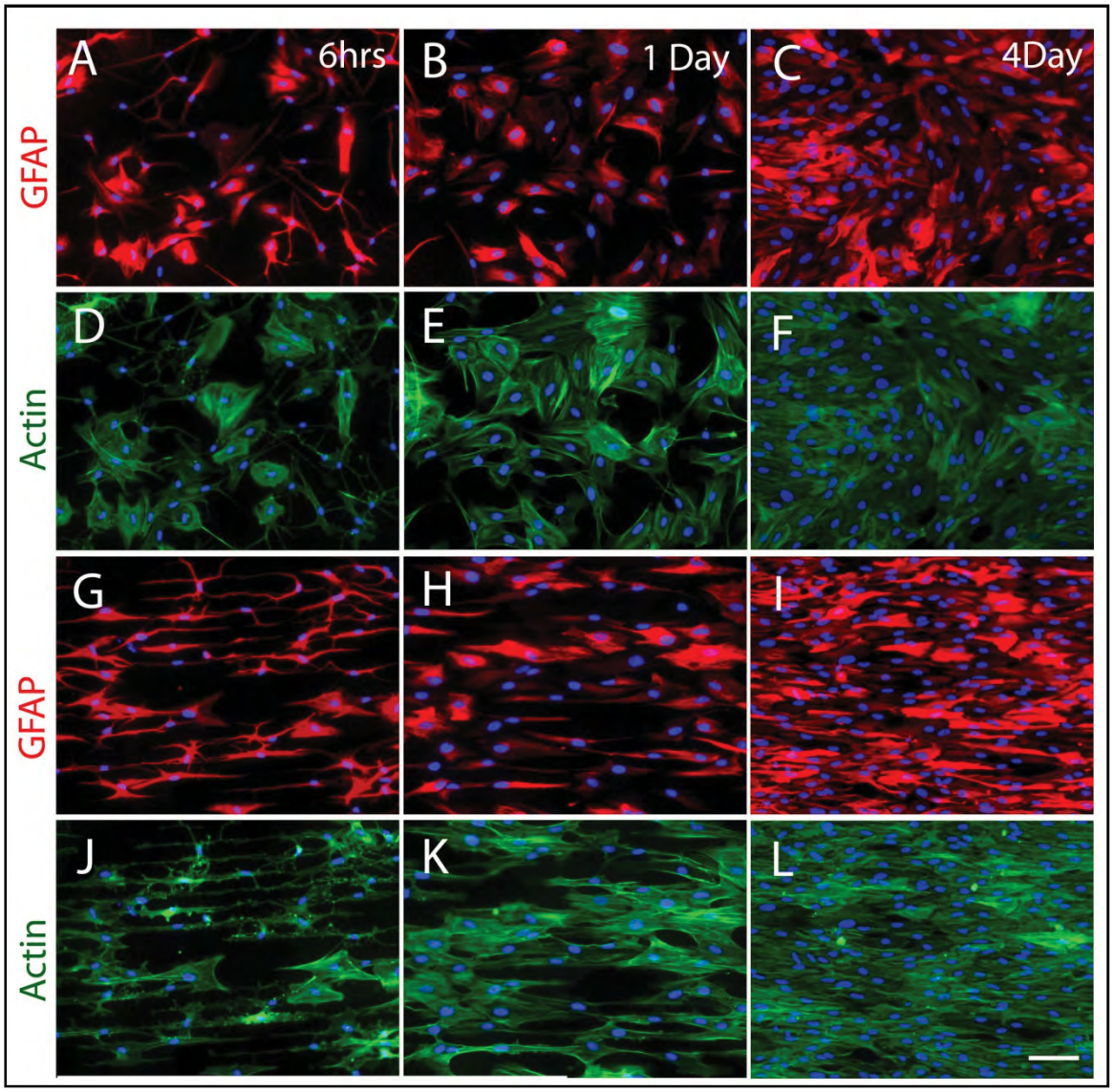

Fig.2-2: Representative astrocyte orientation behavior on homogeneous and patterned LN surfaces stamped on glass coverslips. On homogenous LN fields, astrocytes showed nopreferred orientation at 6 h (A), 1 day (B) and 4 days (C) as visualized with the indirect immunofluorescent histochemistry (IHC) against the intermediate filament Glial Fibrillary Acidic Protein (GFAP) (red), or using fluorescently labeled phalloidin to visualize actin microfilament orientation (D-F). In sharp contrast, the orientation of GFAP (G-I) and fluorescently labeled actin (J-L) on stamped LN lane patterned surfaces revealed considerable anisotropy.

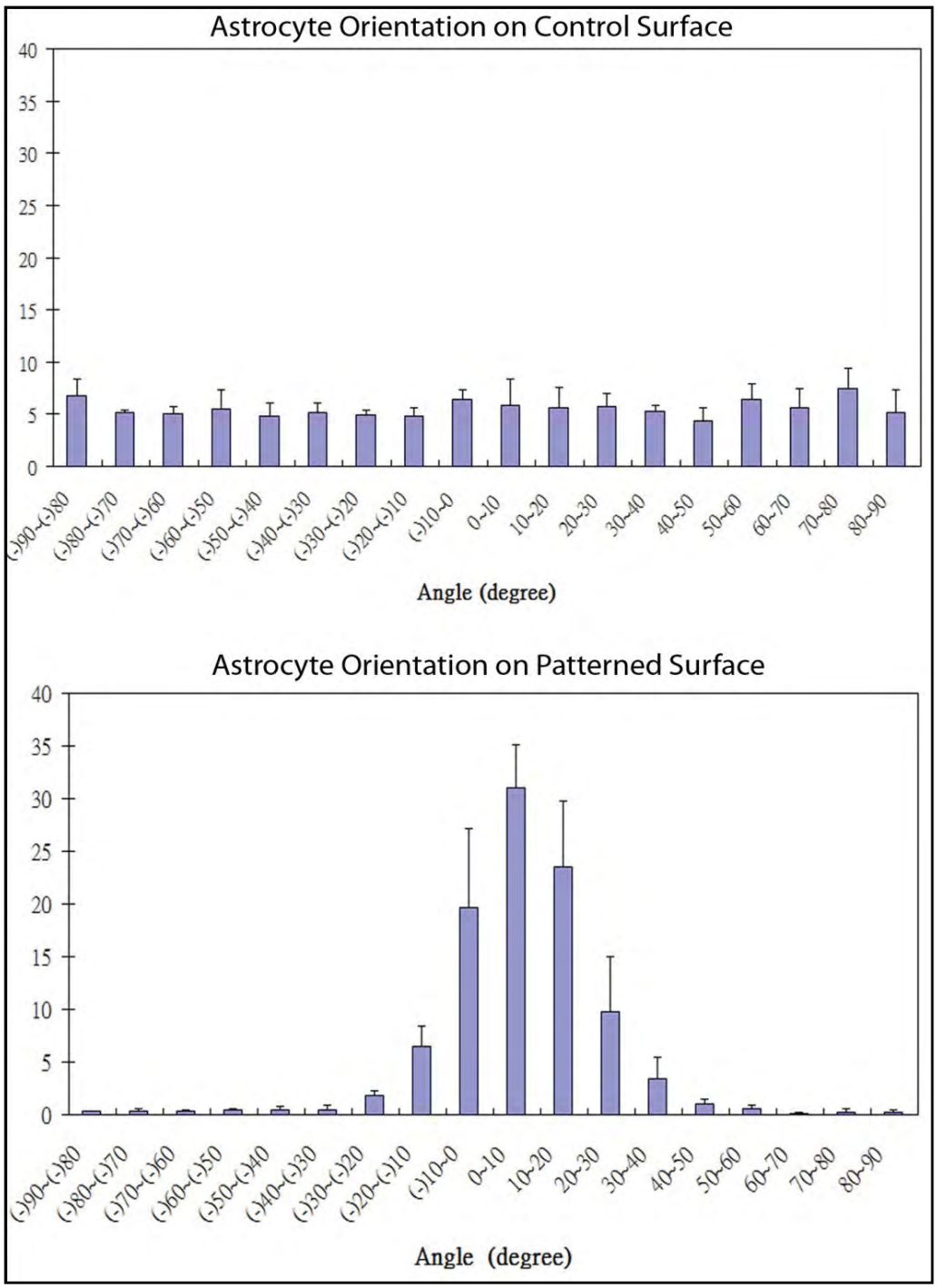

Fig.2-2 continued: A quantitative analysis of astrocyte alignment on homogeneous stamped LN surfaces (M) showed no preferred directionality, whereas a strong bias in the direction of astrocyte alignment on the stamped LN lane patterns (N) was evident. The two groups were significantly different as determined with the Chi Square Test for Independence at a $p < 0.05$

2.3.2 Neurite Outgrowth Directionality

A close association was found between the orientation of overlying DRG neurite outgrowth trajectory and the morphological orientation of the underlying astrocytes. The direction of neurite outgrowth was generally in a direction parallel to the aligned astrocytes (Fig. 2-3:C). In general, when DRGs were put on top of random astrocytes (cultured on LN field), no overall preferred orientation of neurite outgrowth was found (Fig. 2-3:A). DRGs were also cultured on both fixed random and fixed oriented astrocytes cultures to assess whether simply the presence and the spatial distribution of nondiffusible factors (e.g., ECM proteins and cell surface bound ligands) derived from astrocytes were principally responsible for the guidance behavior. Similarly, neurite outgrowth exhibited strong alignment on the fixed, oriented astrocytes cultures (Fig. 2-3:D). Again, no directional biased neurite outgrowth was found on fixed random astrocytes cultures (Fig. 2-3:B). The 3D reconstructed confocal images (flipped around the *Y*-axis of a series z-stack images) demonstrated that although neurites penetrated into the astrocyte culture they rarely if ever reached the plane of the top of the coverslip, suggesting the observed guided neurite outgrowth was purely biological mechanism associated with the orientation of the astrocytes (Fig. 2-3:E and F). Similar to the orientation distribution pattern of the random astrocytes cultures, neurite outgrowth angles were near uniformly distributed on both live and fixed random astrocytes cultures (Fig. 2-4:A and B). By contrast, approximately 89% of neurite angles on both live and fixed oriented astrocytes were within 20° of the long axis of LN lane pattern (Fig. 2-4:C and D). The neurite

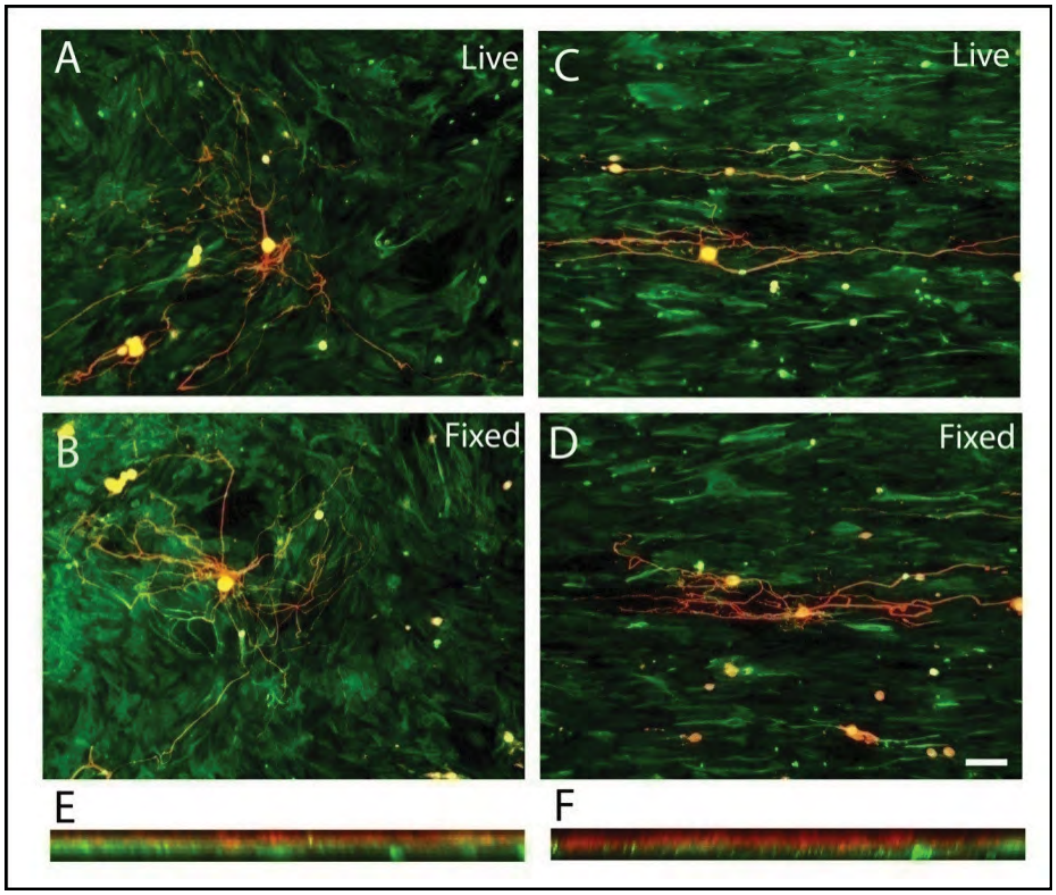

Fig.2-3: Representative confocal images of DRG outgrowth on astrocyte monolayers grown on stamped homogeneous LN fields (left panels) or patterned LN lanes (right panels). (A) Representative DRG outgrowth (red) on live astrocyte monolayers grown on homogeneous LN substrates (GFAP-green) showed no overall preferred directional outgrowth. (B) Similarly, no directionally biased DRG outgrowth was observed on fixed astrocytes cultures grown on homogeneous LN substrates. (C) In sharp contrast, DRG outgrowth on aligned astrocytes monolayers grown on patterned LN substrates extended in the direction of the underlying astrocytes whether alive (C) or fixed (D). Representative, 3D reconstructed confocal images of DRG outgrowth on unaligned astrocytes (E, grown on homogeneous stamped LN) or on aligned astrocyte monolayers (F) demonstrated that DRG outgrowth rarely penetrated into underlying astrocytes and did not reach the surfaces of the stamped coverslips showing that all DRG outgrowth was determined by the interaction with the astrocytes cell layers. Scale bar= 100 μm. Astrocytes were visualized with IHC against GFAP (green) while DRG outgrowth was visualized with antisera directed against neurofilament (red).

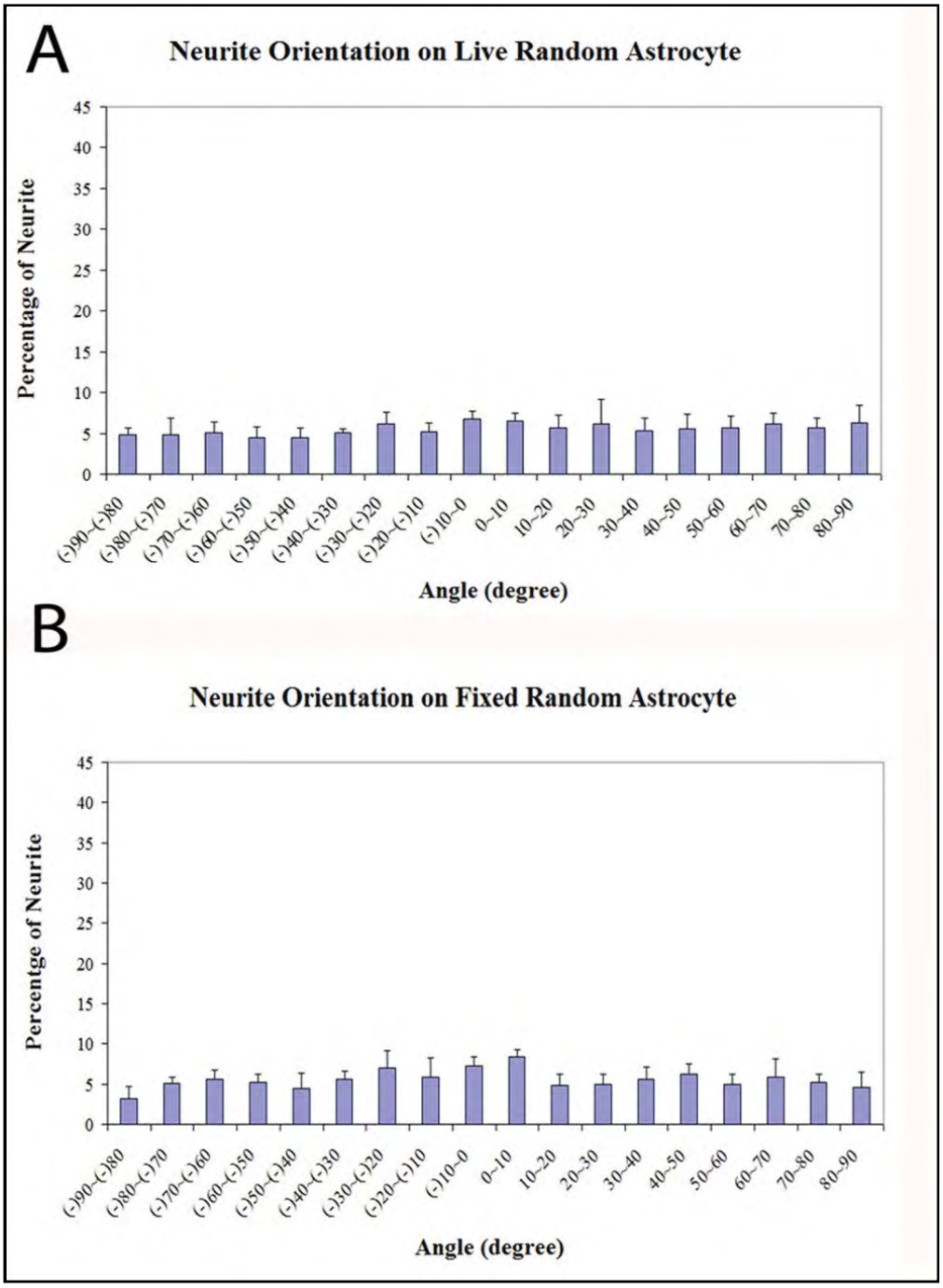

Fig. 2-4: Quantitative analysis of DRG outgrowth direction on astrocyte monolayers grown on stamped homogeneous (left panels) or patterned LN surfaces (right panels). The distribution of DRG outgrowth orientation on live (A) and on fixed astrocytes monolayers (B) cultured on homogeneous LN substrates showed no preferred directional outgrowth.

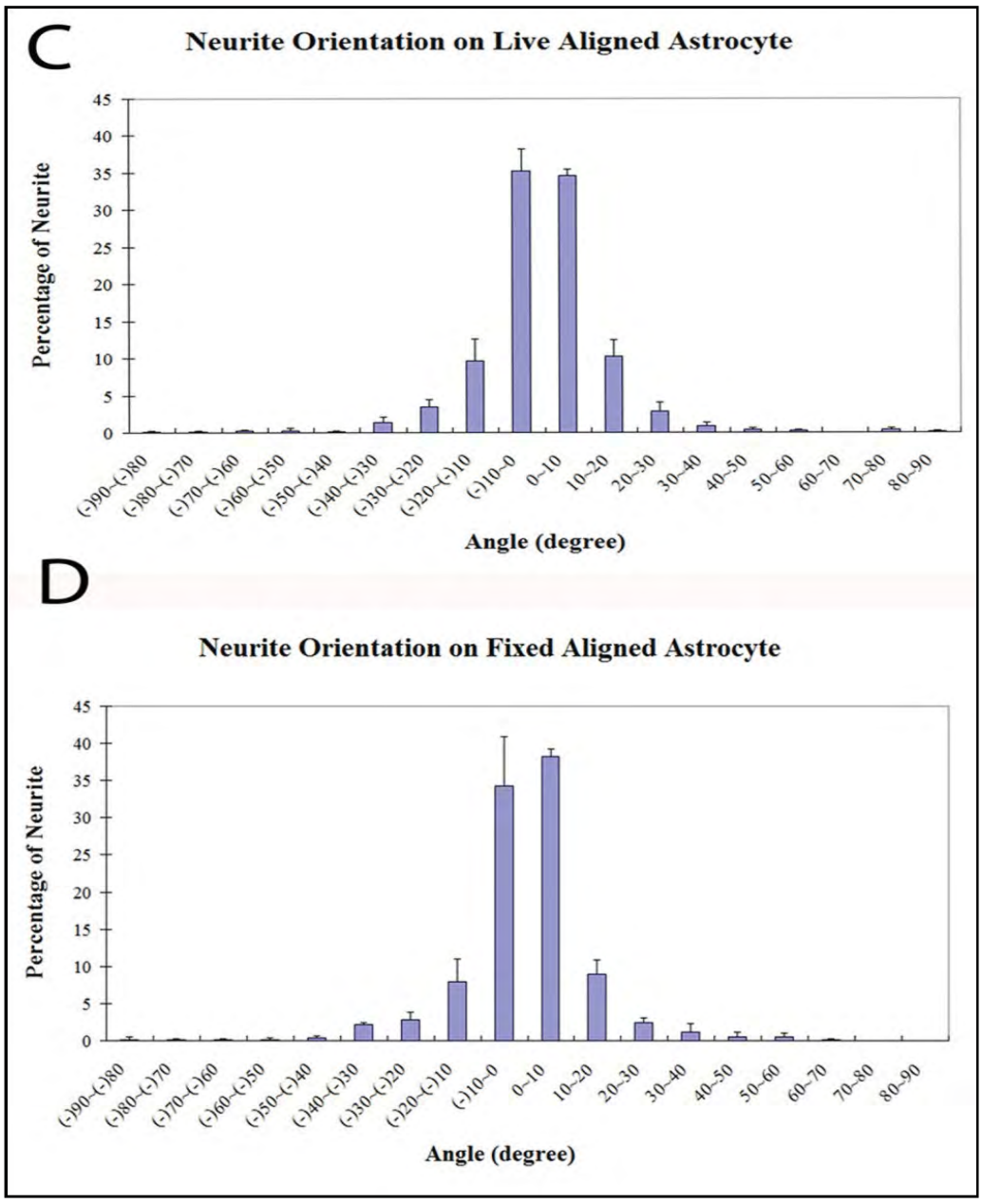

Fig.2-4 continued: In sharp contrast, DRG outgrowth on live (C) or fixed (D) astrocytes grown on patterned LN surfaces showed a strong bias in the direction of the orientation of the underlying astrocytes with a high proportion of neurites growing within 20^{o} parallel to the direction of the orientation of the underlying astrocyte monolayer. The DRG outgrowth direction distribution on astrocyte monolayers grown on patterned surfaces (both live and fixed) was significantly different from those grown on astrocyte monolayers cultured on stamped homogeneous LN fields (both live and fixed) (Chi Square Test for Independence, $p < 0.05$).

angle distribution was significantly different between random and oriented astrocyte groups (Chi Square Test for Independence, $p<0.05$). Overall, the relationship between the orientation of astrocytes and that of neurite outgrowth exhibited a strong correlation (Pearson's correlation coefficient > 0.87).

2.3.3 Oriented Astrocytes Direct Outgrowth of Neurites

In an attempt to determine the relationship between neurite trajectory and outgrowth length, the directed outgrowth of neurites parallel to the long axis of LN lanes (both live and fixed) and that of neurites parallel to a designated axis on random astrocytes (both live and fixed) was calculated. DRG outgrowth on oriented astrocytes resulted in greater directed outgrowth where 370% and 280% increase of directed length were seen on live and fixed oriented astrocytes, respectively, than that on fixed random astrocytes, respectively. When compared to live random astrocytes, the increase of directed outgrowth dropped to 250% and 190%, respectively (Fig. 2-5:A). There was a significant difference in the directed length comparison between any two conditions (fixed random, live random, fixed oriented and live oriented, one-way ANOVA, $p<0.05$). The distribution of directed neurite length on four conditions was evaluated and it was found the maximum value of directed neurite length increased gradually from fixed randomly organized, live randomly organized, fixed oriented to live oriented astrocytes (Fig. 2-5:B). These results indicated that the alignment as well as the viability of astrocytes affected directed length of neurite trajectories.

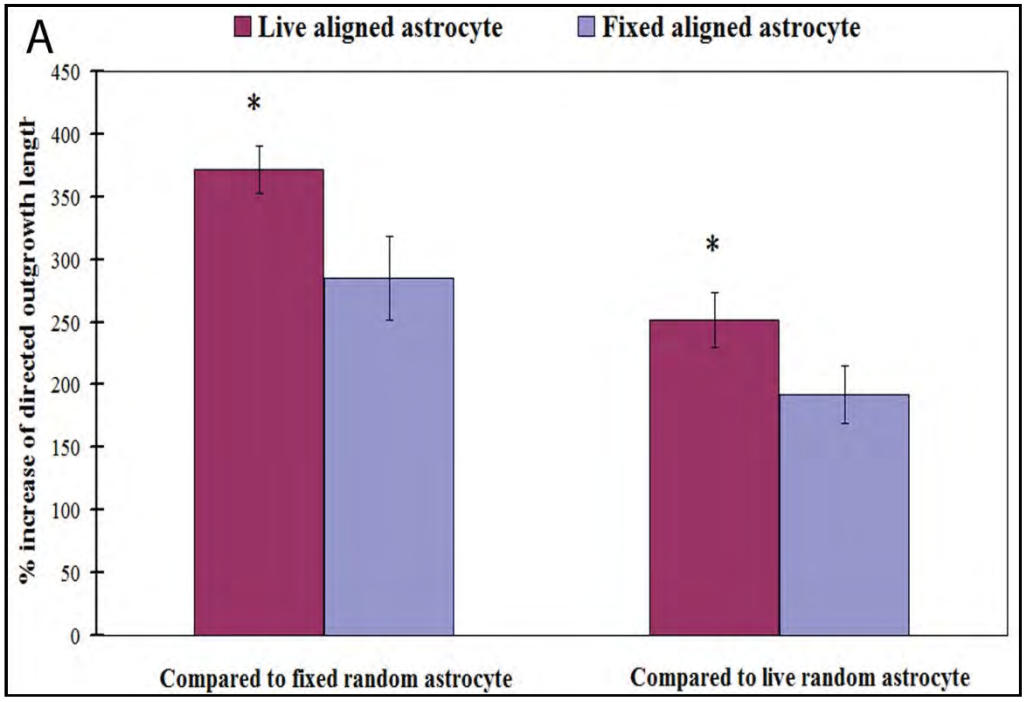

Fig.2-5: Directed neurite outgrowth and directed outgrowth length distributions. (A) DRG outgrowth on oriented astrocytes resulted in greater length in a particular direction (directed outgrowth) where we observed a 370% and 280% increase of the directed length on live and fixed oriented astrocytes monolayers, respectively, compared to that observed on fixed random astrocytes, respectively. When compared to outgrowth on live random astrocytes, the increase of directed outgrowth dropped to 250% and 190%, respectively (ANOVA, post hoc,$p<0.05$).

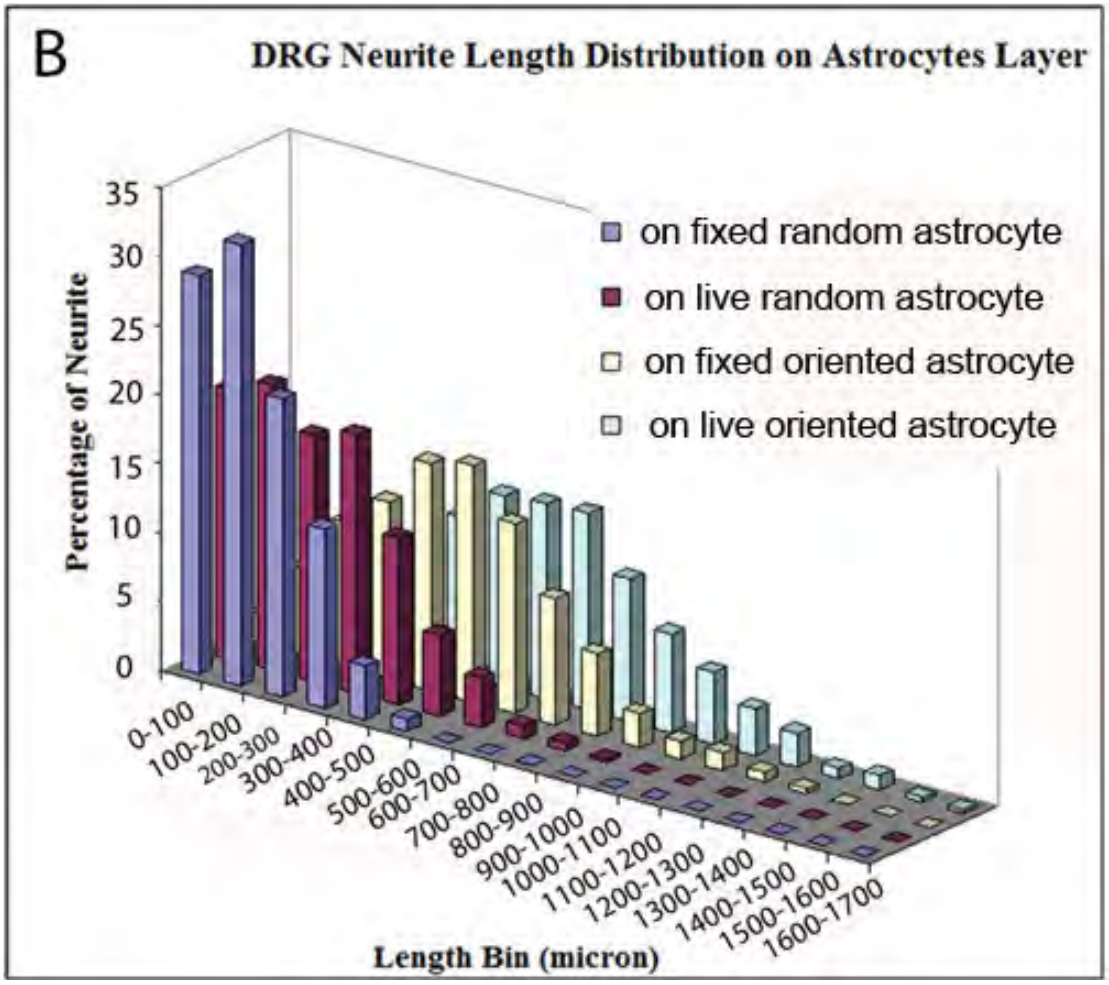

Fig. 2-5 continued: (B) A comparison of the distribution of directed DRG outgrowth lengths under the four conditions showed that the DRG outgrowth was consistently longer in a larger proportion of the population when the astrocytes monolayers were oriented.

2.3.4 ECM Expression of Astrocytes and Neurite Outgrowth

Immunofluorescent staining with antisera against astrocyte associated FN, CSPG, LN and NCAM all revealed a spatial arrangement parallel to the long axis of LN lanes at a certain degree on the oriented astrocyte monolayers (Fig. 2-6:B, D, F, and H). The parallel spatial distribution was the most evident with FN, which formed fibrillar bundles and was closely associated with the underlying stamped LN pattern (Fig. 2-6:B, colocalization data of FN and LN lanes not shown). Similarly, the CSPG expression pattern also delineated the underlying printed LN lane pattern; however, it was not as distinct as FN and no fibrillar structure of CSPG was seen (Fig. 2-6:D). NCAM is a cell membrane associated adhesion molecule expressed on astrocyte surface and its expression pattern seemed to outline the astrocytes cell membrane (Fig. 2-6:F).

Although the general pattern of NCAM on aligned astrocytes appeared to follow the long axis of printed LN lanes, we did not see similar fibrillar structure to what we observed for FN. In order to investigate the distribution pattern of astrocytes derived LN, FN lanes (400 µg/ml, Invitrogen) was patterned on the underlying substrate. The anisotropic nature of oriented astrocytes derived LN was the least obvious. (Fig. 2.6H). The spatial pattern of immunostaining of all four extracellular matrix molecules on random astrocytes revealed no preferred orientation (Fig. 2-6:A, C, E and G). Although the overall pattern of FN on random astrocytes was not organized, small patches appeared organized where we observed that neurite outgrowth followed these oriented ligands (Fig. 2-6:A arrow). Neurite outgrowth on oriented astrocytes did not seem to be affected

Fig. 2-6: Spatial distribution of extracellular matrix molecules expressed by astrocytes and their association with DRG outgrowth on homogeneous LN substrates (left panels) and (patterned LN substrates (right panels). Astrocyte derived FN had a fibrillar structure when grown on homogeneous LN substrates (A) and patterned LN lanes (B). Neurite outgrowth was found to be closely associated with astrocytes derived FN. Although the overall pattern of FN expressed by astrocytes grown on homogeneous LN substrates was not organized, neurite outgrowth tended to follow locally oriented FN fibers (see arrow in panel A). CSPG expression appeared as punctuate expression pattern that was unorganized on the homogeneous LN substrates astrocytes (C) and on aligned astrocytes, as seen with FN (B), appeared to co-align with the underlying pattern of the stamped LN lanes (D). Neurites were found to extend through areas with both high and low expression of CSPG in both culture conditions. The expression of NCAM by both random (E) and aligned astrocyte (F) seemed to delineate astrocyte membranes and act as permissive substrates for neurite to grow. Astrocyte derived LN had similar punctate expression pattern as CSPG on both random (G) and aligned (H) culture and acted as supportive substrates for neurite outgrowth. FN was in green in (A, B); CSPG was in green in (C, D); NCAM was in green in (E, F) and LN was in green in (G, H). Neurites were in red in (A-H). Scale bar=100 µm.

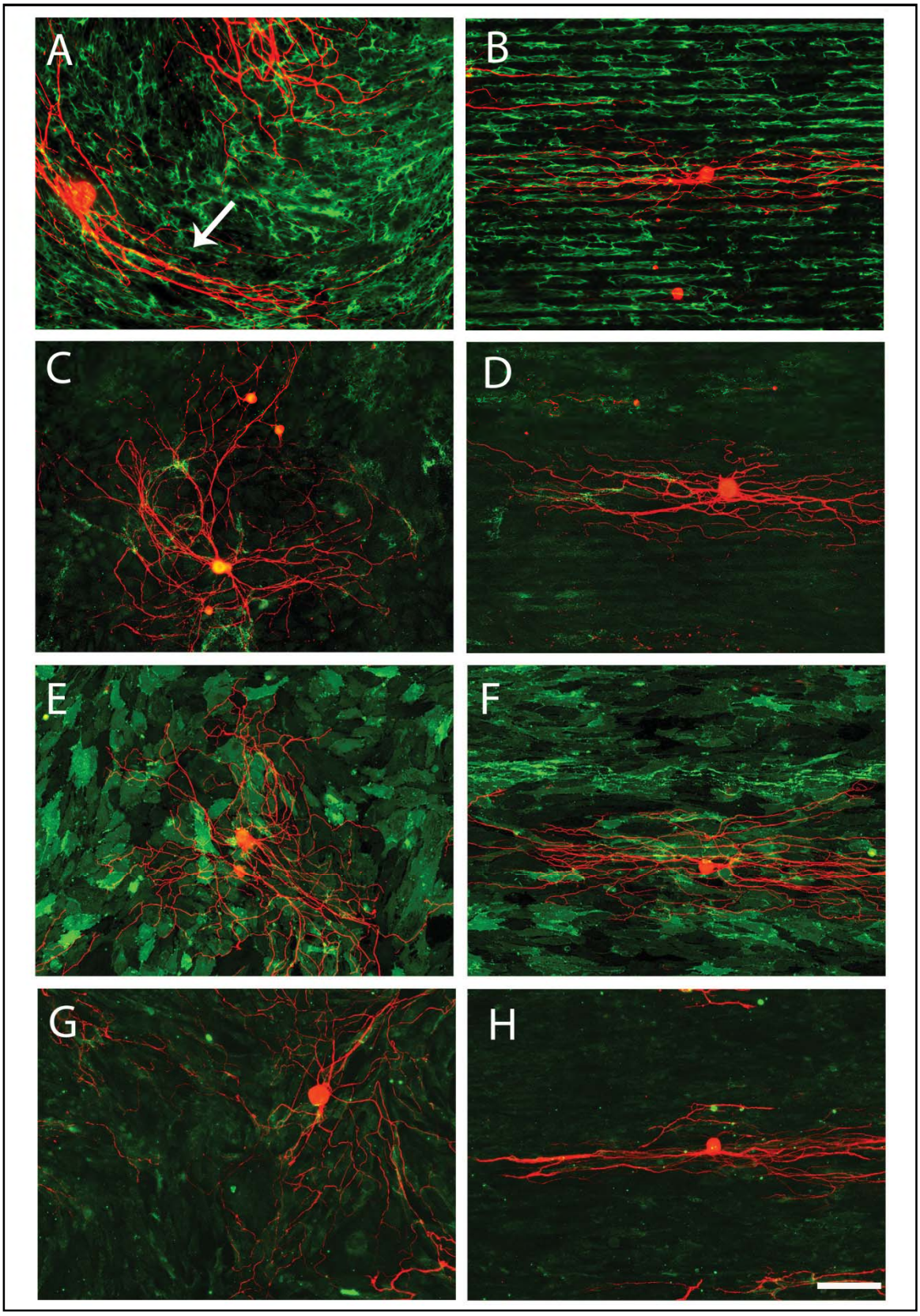
A
B
C
D
E
F
G
H

by the CSPG distribution and the neurites were found to extend through areas of both high and low levels of CSPG expression (Fig. 2-6:D). This phenomenon was also seen with neurites grown on random astrocytes cultures (Fig. 2-6:C), suggesting CSPG derived from astrocytes in our culture conditions might have a weak inhibitory effect on neurite outgrowth that could be overwhelmed by other permissive guidance cues. The expression patterns of randomly organized astrocytes derived NCAM and LN showed no preferred directionality (Fig. 2-6:E and G). The fact that neurites were found to be following with linear arrays of FN expressed on the oriented astrocytes as well as on the random astrocytes when these bundles oriented locally suggested a principal role of astrocyte derived FN in guiding neuronal pathfinding

2.3.5 FN as Guiding Ligand

Among all astrocyte derived insoluble ligands investigated, the anisotropic nature of FN suggests it might act as the most distinct path guiding ligand as revealed by indirect immunohistochemical reactions. Thus, we decided to examine what role that FN plays in interactions with DRG neurite outgrowth. DRG neurons were cultured on fixed oriented astrocyte cultures with or without anti-FN antisera treatment. There were more than 82% of neurites oriented within 20° of the long axis of the underlying LN lanes on untreated fixed oriented astrocyte monolayers (Fig. 2-7:A), whereas following anti-FN antisera treatment, the number of neurites oriented within 20° dropped to 46% (Fig. 2-7:B). There was a statistical difference between untreated and treated groups (Chi Square Test for Independence, $p<0.05$). This result suggested that astrocyte derived FN

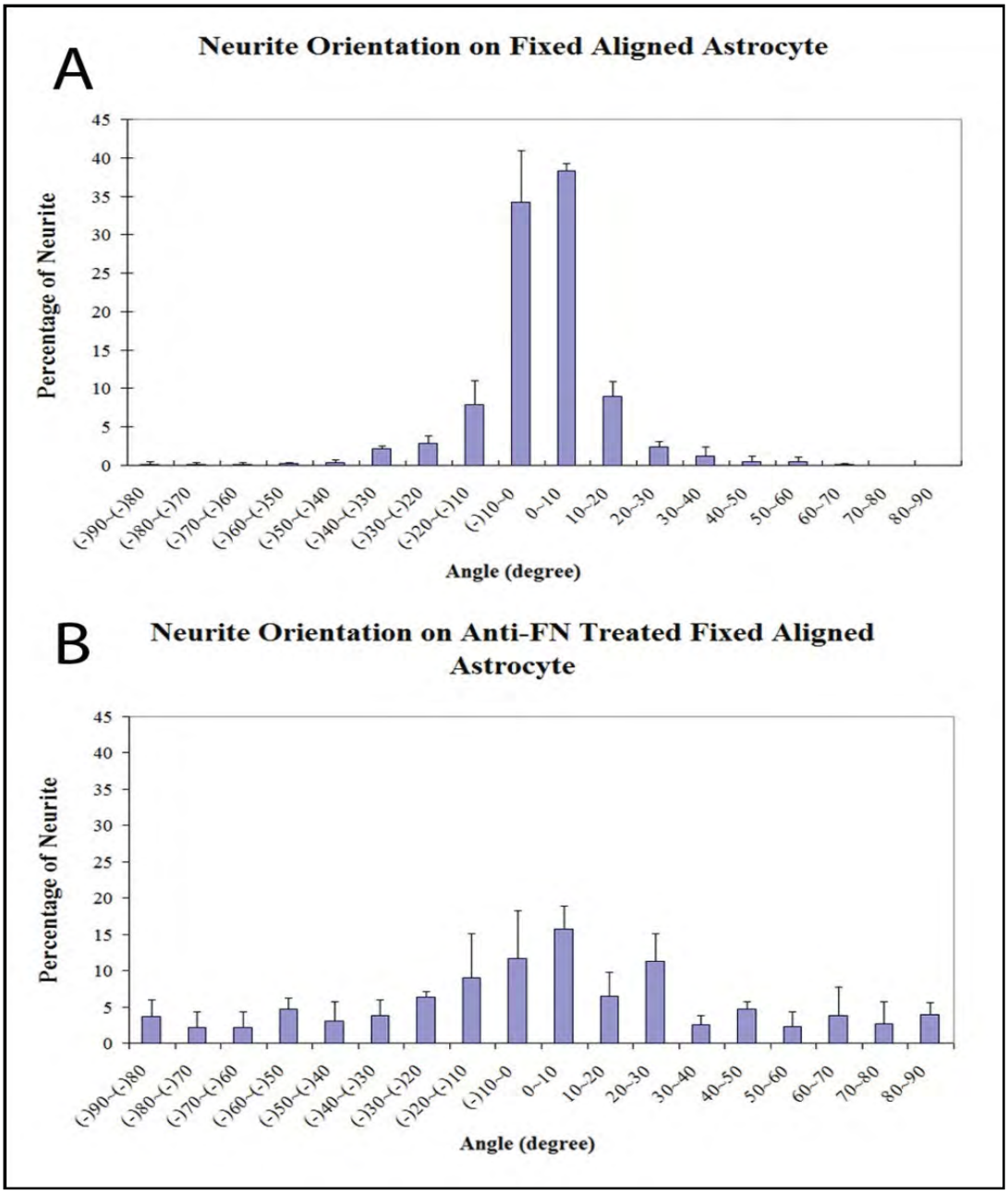

Fig. 2-7: Antibodies to astrocyte derived FN attenuated the directed outgrowth of DRGs on aligned astrocytes monolayers. (A) More than 80% of DRG neurite outgrowth on untreated, fixed oriented astrocyte monolayers was observed growing within 20^{o} of the long axis of the orientation of the underlying stamped LN lanes. (B) Following anti-FN antisera treatment, the percentage of neurites within 20^{o} dropped to 46% that was significantly different using the Chi Square Test for Independence at$p<0.05$.

is a potent guiding ligand for DRG neuronal pathfinding.

2.3.6 Surface Cues Influence Tissue Organization

Following the first astrocyte layer reached confluence on either isotropically (LN field) or anisotropically patterned surface (LN lane pattern), additional astrocyte seedings were applied on top of the first layer and so on to investigate if the first aligned astrocyte monolayer was capable of transmitting the directional cues to subsequent cell layers and manipulate the organization of the overlying cell layer organization. Astrocyte derived FN was used as an indicator for cellular orientation as it was shown that the anisotropy of FN on aligned astrocyte monolayers was most conspicuous parallel to astrocyte alignment (Fig. 2-6:B). Both random and aligned, multilayered astrocyte cultures were mechanically separated from the coverslips using forceps. No preferred spatial organization of FN of randomly organized, multilayered astrocyte cultures was observed (Fig. 2-8:A). On the contrary, the cellular alignment was preserved when astrocytes were repeatedly seeded on the aligned astrocyte monolayers (Fig. 2-8:B). The orientation distribution of FN within the randomly organized, multilayered astrocytes maintained unbiased (Fig. 2-8:C) whereas the FN distribution of aligned, multilayered astrocytes peaked around 90° (Fig. 2-8:D, parallel to the printed LN lanes). The anisotropy index further demonstrated the preserved anisotropy of the aligned, multilayered astrocyte cultures (Fig. 2-8:E). DAPI staining showed the multilayered structure of astrocyte cultures following multiple seedings (Fig. 2-8:F). Reconstructed 3D confocal images also confirmed that the anisotropic organization of FN was distributed throughout the thick

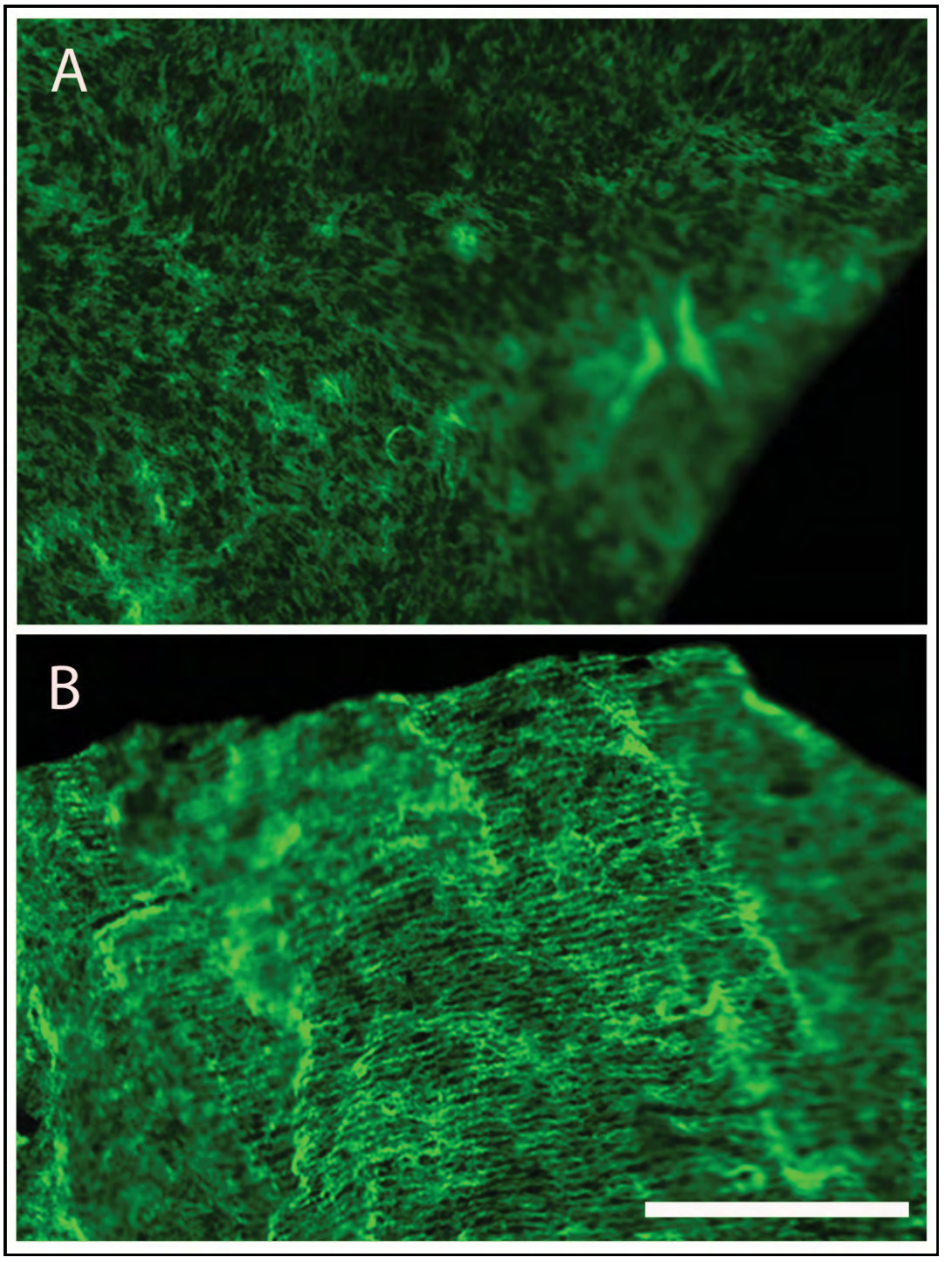

Fig.2-8: The orientation of stamped LN is transferred through multiple cell layers to determine the overall organization of a multilayered astrocyte cell construct. Representative low magnification confocal stacked fluorescent images showing the spatial distribution of FN expressed within a multilayered astrocyte construct gown on a homogeneously stamped LN substrate (A) and on a patterned LN substrate (B) that was mechanically harvested.

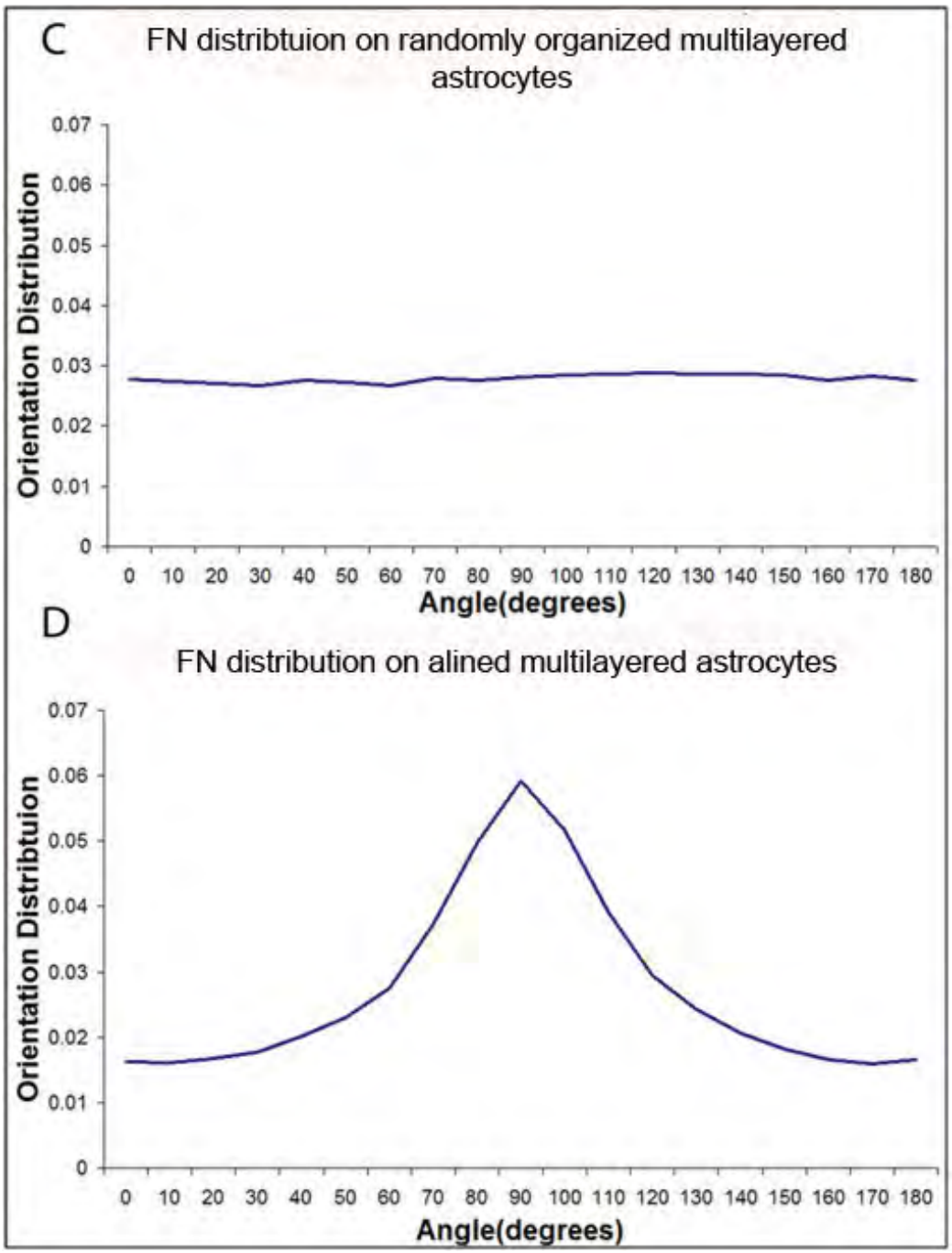

Fig. 2-8 continued: A 2D FFT analysis on both z-stack confocal images showed that FN orientation distribution on the randomly organized, multilayered astrocyte cultures remained unbiased (C) whereas FN distribution on the aligned, multilayered astrocyte cell constructs peaked around 90^{o}, parallel to the long axis of stamped LN lane pattern (D). Two-tailed student t-Test, $p < 0.05$.

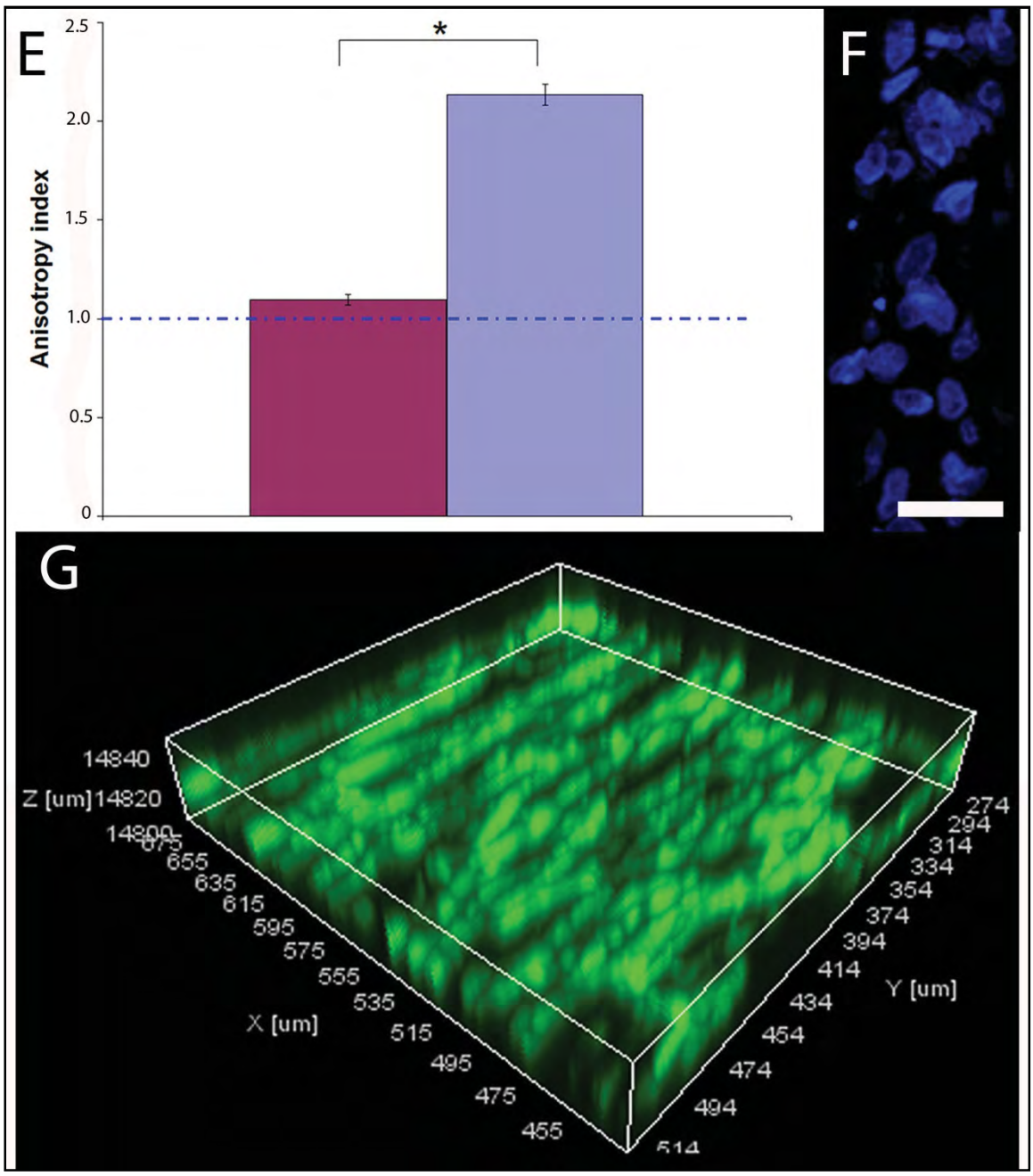

Fig. 2-8 continued:(E) An anisotropy index showed that cellular alignment was maintained within the aligned multilayered, astrocyte cell construct (Two-Tailed Student t-Test $p < 0.05$). (F) Representative cross-sectional view of the DAPI stained astrocyte nuclei showing the thickness of the cell construct. (G) Representative 3D reconstructed confocal image showing that the spatial distribution of FN remained aligned throughout the thickness of the astrocyte cell construct grown on a stamped LN substrate. FN was visualized with IHC and is depicted in green in (A, B, G). Scale bar=500 µm in (A, B);=20 µm in (F)

multilayered astrocyte structure (Fig. 2-8:G). This result demonstrated that surface guidance cues can be transmitted to overlying cell layers via the directional information carried by the spatial distribution of ligands present on an apical surface of the previous cell layer.

2.4 Discussion

Findings of this study demonstrated that the alignment of cultured astrocytes can be controlled by the anisotropic orientation of biomaterial surface ligands that are only a few nanometers in height. Further, spatially oriented astrocytes are capable of directing neuronal outgrowth from their apical surfaces, as well as controlling the orientation of multiple astrocyte cell layers that are orders of magnitude larger than the initial templating ligands. This approach provides an opportunity to investigate the molecular mechanism by which astrocytes guide neuronal pathfinding in the absence of other interfering cues, such as topographical undulations as introduced by grooved guidance substrates [25, 26, 29].

We also demonstrated that the spatial organization of astrocyte derived insoluble factors is sufficient to direct neurite outgrowth grown on featureless surfaces showing that purely biological mechanisms are sufficient to guide tissue level organization. Our immunohistochemical analysis further suggested the involvement of linear arrays of astrocyte associated FN as a principal organizational mechanism. Together, these *in vitro* studies suggest an approach to create a multilayered-tissue construct with oriented morphology that could be useful in regenerative medicine.

Astrocytes, as a major glial cell type in the CNS, have been recognized as supportive substrates for neuronal growth through the secretion of diffusible neurotrophic factors and the expression of such insoluble permissive factors as ECM proteins, cell adhesion and cell surface ligands [11, 12, 14, 33]. Studies have demonstrated that axons tend to follow the orientation of surrounding astroglial cells [7-11] and suggest that the formation of glial cell based tracts or boundaries precedes and guides neuronal pathfinding during CNS development [1-7, 17-19].

However, following CNS injury, along with upregulation of a variety of inhibitory molecules [34-38, 60,] the disrupted extracellular milieu is accompanied by the formation of a disorganized glial scar that is also recognized as a major impediment to axonal regeneration [20-22]. Recently, the beneficial roles of reactive astrocytes after CNS injury have been revealed where they are involved in functional recovery and modulation of inflammatory cells [39]. Therefore, strategies that maintain such positive contributions of reactive astrocytes while also providing directional information to constrain axonal regeneration trajectory may be useful clinically.

In our studies, the alignment of astrocytes was achieved by patterning nanometer level LN molecules as surface guidance cues on otherwise planar substrates. Patterned substrates have been shown to control cell orientation and function [40, 41] and ECM proteins patterned in different shapes can affect the polarization of cell internal organization and future cell division axis [42, 43]. The observed elongated morphology of astrocytes might be manifested through the

interaction between the chemisorbed LN lanes and such ECM receptors as dystroglycan (DG) and integrin β1 that are found on astrocytes. Each of these receptors has been shown to regulate astrocyte attachment and actin organization in response to LN [44, 45].

Previously several groups have shown that aligned astrocytes can direct neurite outgrowth. These approaches used grooved substrate topography on the order of hundreds of nanometers to hundreds of microns [25, 26, 29]. Thus, in these studies it is unclear whether neurite outgrowth was affected by the surface undulations of the grooved substrates [30]. Previously, we reported that when the R.M.S roughness of the substrate is below 45 nm, grooved substrates failed to direct astrocyte orientation [25]. Therefore, the observed alignment of astrocytes on planar surfaces printed with nanometer-level surface cues (5 nm) indicates that the biological aspect of astrocyte orientation alone is sufficient to direct oriented neurite outgrowth in the absence of mechanical cues that could influence neurite trajectories via a different mechanism.

In this study, neurites were found to follow the alignment of underlying astrocytes (live and fixed), indicating that nanometer level surface cues on a planar bridging substrate are sufficient to affect the directional outgrowth of adjacent neural tissue through an intervening astrocyte layer. The astrocyte/meningeal cell interface is thought to be a barrier to axonal regeneration due to the fact that axons tend to stay on top of astrocytes and are unwilling to across the boundary [46]. However, it has been shown that oriented meningeal cell layers support and enhance directed neurite outgrowth [47].

Therefore it would be interesting to see whether such a regeneration barrier could be overcome by inducing organization to these two major cellular components of the glial scar.

The length of directed neurite outgrowth was found to be a function of both the viability and orientation of underlying astrocytes since DRG neurites grown on fixed astrocyte monolayers lack of the neurotrophic factors released from astrocytes [33] and glial cell alignment has been shown to enhance directed neurite outgrowth [24, 25, 28]. This result suggests that a simple approach with organized, nanometer level surface cues on a CNS implanted bridging device may be used to organize the reactive astrocyte layer that encapsulates the implant, and could be used to affect the trajectory of regenerating axons at the device surface.

The fact that neurites still grow parallel on fixed oriented astrocytes demonstrated that the spatial distribution of ECM proteins and/or cell surface bound ligands derived from astrocytes are sufficient to guide neurite extension. It was proposed by Tessier-Lavigne and colleagues that ECM proteins act as short range cues to guide growth cone extension [48] and a great number of ECM proteins and/or surface bound ligands have been demonstrated to affect neurite outgrowth trajectory [11, 12, 14, 18, 19, 49-51].

Permissive and/or repulsive ligands immobilized on culture substrates in different geometries effectively guide outgrowth [50, 52-54]. Therefore, one potential molecular mechanism by which oriented astrocytes govern the directionality of neuronal pathfinding is through the display of a network of ECM

and/or surface bound ligands that mediate neuron–astrocyte interaction and provide directional information. DRG neurites grown on astrocytes aligned on a planar surface provide an opportunity to investigate the molecular mechanism without the interference of other physical guidance mechanisms. Our results suggest that one could engineer artificial bridging devices through mimicking the spatial arrangement of these insoluble ligands displayed on oriented astrocytes.

DRG neurites were found making direct contact and closely associated with the continuous array of astrocyte derived FN, suggesting the potential role of FN in guiding neurite outgrowth. This close association between neurites and astrocyte associated FN was also observed previously where DRGs were grown on astrocytes aligned by grooved substrates [25]. In the present study, the direct role of astrocyte associated FN in guiding neurite outgrowth was strengthened due to the fact that no other mechanical guidance cues were contributing to the alignment of neurites.

Indeed, FN has been demonstrated to be critical for sensory axonal regeneration in adult rat corpus callosum [11] and to modulate neurite outgrowth [50]. However, DRG neurites were found not always making direct contact with astrocyte associated FN. We speculate that after receiving guidance information, neurites might be able to maintain outgrowth trajectory for a certain amount of time or distance traveled before they acquire new information due to the intrinsic stiffness of the trailing axon [31]. Therefore, while not always making direct contact with FN, neurites maintained parallel outgrowth. Still, this observation does not rule out the involvement of other ligands on the astrocyte surface in

guiding neurite extension, such as NCAM [14]. However, the fact that the majority of neurites were not able to maintain directional outgrowth following anti-FN antisera treatment did demonstrate that astrocyte derived FN is a potent mechanism for guiding neurite outgrowth.

The observation that neurite growth was not affected by the level of CSPG expression can be explained in many ways. For example, the different sulfation pattern of glycosaminoglycan (GAG) chains has been shown to render CSPG distinct properties, either permissive or inhibitory [55, 56]. The other possibility is that in our culture system the CSPG exerted inhibitory signals were overridden by other astrocyte derived permissive molecules [36]. The spatial distribution of astrocytes derived NCAM and LN did not appear to exhibit the same conspicuous anisotropic orientation as observed for FN. Their expression pattern suggested that they might be directing neurite outgrowth in a way different than FN by providing a permissive substrate that neurites prefer to extend on.

It has been suggested that cells lose alignment on patterned surfaces once the thickness of the cell/tissue layers goes beyond 20–40 μm [57]. However, in the current study, we demonstrated that the alignment of astrocytes within a multilayered structure can be maintained for at least 30 μm in thickness in a fixed specimen, which under hydrated conditions is likely much thicker. It will be interesting to see if this behavior is cell type specific. It also will be interesting to investigate how thick of the multilayered structure could become in which alignment is still preserved.

While many studies have demonstrated the repulsive nature of various scar-associated ligands in inhibiting axonal regeneration [34, 58, 59], very few studies have suggested how scar tissue may develop. In the current study, we demonstrate that astrocyte alignment can be transmitted through multiple cell layers to control the organization of a tissue construct, potentially via the directional cues carried by a network of spatially organized, astrocyte associated cell surface receptors and ECM ligands. Likewise our data suggest that disorganized astrocytes likely transmit their lack of organization, which likely contributes to the development of the dense inhibitory scar tissue that inhibits regeneration *in vivo* following injury.

2.5 Conclusions

Our studies performed totally *in vitro* show that the manner in which biomaterial bound surface ligands are presented affects the spatial organization of a population of cells at a biomaterial surface. Moreover, such organized patterns of surface ligands can strongly influence the directional outgrowth of neurons interacting with the surface of an organized astrocyte cell layer, as well as being transmitted through multiple cell layers to control the organization of a tissue construct. The results suggest that axonal regeneration can be facilitated following injuries if an organized glial framework is provided at a biomaterial surface. The results of our *in vitro* studies also suggest a biological mechanism by which a disorganized glial framework can develop into inhibitory scar tissue following injury, and conversely how an organized astrocyte framework could be engineered for use in spinal cord injury repair.

2.6 Acknowledgement

The authors thank Elena Budko, M.D., for assistance and thoughtful discussion. We also thank Brian Baker for his help for fabricating microprinting device. We acknowledge funding support from NIH 5R01NS57144.

2.7 References

1. Cummings DM, Malun D, Brunjes PC. Development of the anterior commissure in the opossum: midline extracellular space and glia coincide with early axon decussation. J Neurobiol 1997;32:403-414.

2. Silver J, Edwards MA, Levitt P. Immunocytochemical demonstration of early appearing astroglial structures that form boundaries and pathways along axon tracts in the fetal brain. J Comp Neurol 1993;328:415-436.

3. Silver J, Lorenz SE, Wahlsten D, Coughlin J. Axonal guidance during development of the great cerebral commissures: descriptive and experimental studies, *in vivo*, on the role of preformed glial pathways. J Comp Neurol 1982;210:10-29.

4. Silver J, Rutishauser U. Guidance of optic axons *in vivo* by a preformed adhesive pathway on neuroepithelial endfeet. Dev Biol 1984;106:485-499.

5. Sajin B, Steindler DA. Cells on the edge: boundary astrocytes and neurons. Perspect Dev Neurobiol 1994;2:275-289.

6. Voigt T. Development of glial cells in the cerebral wall of ferrets: direct tracing of their transformation from radial glia into astrocytes. J Comp Neurol 1989;289:74-88.

7. Brook GA, Plate D, Franzen R, Martin D, Moonen G, Schoenen J, et al. Spontaneous longitudinally orientated axonal regeneration is associated with the schwann cell framework within the lesion site following spinal cord compression injury of the rat. J Neurosci Res 1998;53:51-65.

8. Davies SJ, Fitch MT, Memberg SP, Hall AK, Raisman G, Silver J. Regeneration of adult axons in white matter tracts of the central nervous system. Nature 1997;390:680-683.

9. Davies JE, Huang C, Proschel C, Noble M, Mayer-Proschel M, Davies SJ. Astrocytes derived from glial-restricted precursors promote spinal cord repair. J Biol 2006;5:7.

10. Leavitt BR, Hernit-Grant CS, Macklis JD. Mature astrocytes transform into transitional radial glia within adult mouse neocortex that supports directed migration of transplanted immature neurons. Exp Neurol 1999;157:43-57.

11. Tom VJ, Doller CM, Malouf AT, Silver J. Astrocyte-associated fibronectin is critical for axonal regeneration in adult white matter. J Neurosci 2004;24:9282-9290.

12. Costa S, Planchenault T, Charriere-Bertrand C, Mouchel Y, Fages C, Juliano S, et al. Astroglial permissivity for neuritic outgrowth in neuron-astrocyte cocultures depends on regulation of laminin bioavailability. Glia 2002;37:105-113.

13. Fallon JR. Preferential outgrowth of central nervous system neurites on astrocytes and Schwann cells as compared with nonglial cells *in vitro*. J Cell Biol 1985;100:198-207.

14. Neugebauer KM, Tomaselli KJ, Lilien J, Reichardt LF. N-cadherin, NCAM, and integrins promote retinal neurite outgrowth on astrocytes *in vitro*. J Cell Biol 1988;107:1177-1187.

15. Smith GM, Rutishauser U, Silver J, Miller RH. Maturation of astrocytes *in vitro* alters the extent and molecular basis of neurite outgrowth. Dev Biol 1990;138:377-390.

16. Tomaselli KJ, Neugebauer KM, Bixby JL, Lilien J, Reichardt LF. N-cadherin and integrins: Two receptor systems that mediate neuronal process outgrowth on astrocyte surfaces. Neuron 1988;1:33-43.

17. Meiners S, Powell EM, Geller HM. A distinct subset of tenascin/CS-6-PG-rich astrocytes restricts neuronal growth *in vitro*. J Neurosci 1995;15:8096-8108.

18. Snow DM, Lemmon V, Carrino DA, Caplan AI, Silver J. Sulfated proteoglycans in astroglial barriers inhibit neurite outgrowth *in vitro*. Exp Neurol 1990;109:111-130.

19. Snow DM, Watanabe M, Letourneau PC, Silver J. A chondroitin sulfate proteoglycan may influence the direction of retinal ganglion cell outgrowth. Development 1991;113:1473-1485.

20. Fawcett JW, Asher RA. The glial scar and central nervous system repair. Brain Res Bull 1999;49:377-391.

21. Rhodes KE, Moon LD, Fawcett JW. Inhibiting cell proliferation during formation of the glial scar: effects on axon regeneration in the CNS. Neuroscience 2003;120:41-56.

22. Silver J, Miller JH. Regeneration beyond the glial scar. Nat Rev Neurosci 2004;5:146-156.

23. Teng YD, Lavik EB, Qu X, Park KI, Ourednik J, Zurakowski D, et al. Functional recovery following traumatic spinal cord injury mediated by a unique polymer scaffold seeded with neural stem cells. Proc Natl Acad Sci USA 2002;99:3024-3029.

24. Alexander K, Fuss B, Colello RJ. Electric field-induced astrocyte alignment directs neurite outgrowth. Neuron Glia Biol 2006;2:93-103.

25. Biran R, Noble MD, Tresco PA. Directed nerve outgrowth is enhanced by engineered glial substrates. Exp Neurol 2003;184:141-152.

26. Sørensen A, Alekseeva T, Katechia K, Robertson M, Riehle MO, Barnett SC. Long-term neurite orientation on astrocyte monolayers aligned by microtopography. Biomaterials 2007;28:5498-5508.

27. Thompson DM, Buettner HM. Neurite outgrowth is directed by Schwann cell alignment in the absence of other guidance cues. Ann Biomed Eng 2006;34:161–168.

28. Deumens R, Koopmans GC, Den Bakker CG, Maquet V, Blache S, Honig WM, et al. Alignment of glial cells stimulates directional neurite growth of CNS neurons *in vitro*. Neuroscience 2004;125:591-604.

29. Recknor JB, Recknor JC, Sakaguchi DS, Mallapragada SK. Oriented astroglial cell growth on micropatterned polystyrene substrates. Biomaterials 2003;25:2753-2767.

30. Rajnicek A, Britland S, McCaig C. Contact guidance of CNS neurites on grooved quartz: influence of groove dimensions, neuronal age and cell type. J Cell Sci 1997;110:2905-2913.

31. Smeal RM, Rabbitt R, Biran R, Tresco PA. Substrate curvature influences the direction of nerve outgrowth. Ann Biomed Eng 2005;33:376-382.

32. McCarthy KD, de Vellis J. Preparation of separate astroglial and oligodendroglial cell cultures from rat cerebral tissue. J Cell Biol 1980;85:890-902.

33. Müller HW, Junghans U, Kappler J. Astroglial neurotrophic and neuritepromoting factors. Pharmacol Ther 1995;65:1-18.

34. Chen MS, Huber AB, van der Haar ME, Frank M, Schnell L, Spillmann AA, et al. Nogo-A is a myelin-associated neurite outgrowth inhibitor and an antigen for monoclonal antibody IN-1. Nature 2000;403:434-439.

35. Fibrin MT. Myelin-associated inhibitors of axonal regeneration in the adult mammalian CNS. Nat Rev Neurosci 2003;4:703-713.

36. Jones LL, Sajed D, Tuszynski MH. Axonal regeneration through regions of chondroitin sulfate proteoglycan deposition after spinal cord injury: a balance of permissiveness and inhibition. J Neurosci 2003;23:9276-9288.

37. McKeon RJ, Jurynec MJ, Buck CR. The chondroitin sulfate proteoglycans neurocan and phosphacan are expressed by reactive astrocytes in the chronic CNS glial scar. J Neurosci 1999;19:10778–10788.

38. Spencer T, Domeniconi M, Cao Z, Filbin MT. New roles for old proteins in adult CNS axonal regeneration. Curr Opin Neurobiol 2003;13:133-139.

39. Okada S, Nakamura M, Katoh H, Miyao T, Shimazaki T, Ishii K, et al. Conditional ablation of Stat3 or Socs3 discloses a dual role for reactive astrocytes after spinal cord injury. Nat Med 2006;12:829-834.

40. Chen CS, Mrksich M, Huang S, Whitesides GM, Inber DE. Geometric control of cell life and death. Science 1997;276:1425-1428.

41. Clark P, Britland S, Connolly P. Growth cone guidance and neuron morphology on micropatterned laminin surfaces. J Cell Sci 1993;105:203-212.

42. Théry M, Racine V, Pépin A, Piel M, Chen Y, Sibarita JB, et al. The extracellular matrix guides the orientation of the cell division axis. Nat Cell Biol 2005;10:947-953.

43. Théry M, Racine V, Piel M, Pépin A, Dimitrov A, Chen Y, et al. Anisotropy of cell adhesive microenvironment governs cell internal organization and orientation of polarity. Proc Natl Acad Sci USA 2006;103:19771-19776.

44. Ervasti JM, Campbell KP. A role for the dystrophin-glycoprotein complex as a transmembrane linker between laminin and actin. J Cell Biol 1993;122:809-823.

45. Hall DE, Reichardt LF, Crowley E, Holley B, Moezzi H, Sonnenberg A, et al.The alpha 1/beta 1 and alpha 6/beta 1 integrin heterodimers mediate cell attachment to distinct sites on laminin. J Cell Biol 1990;110:2175-2184.

46. Shearer MC, Fawcett JW. The astrocyte/meningeal cell interface--a barrier to successful nerve regeneration? Cell Tissue Res 2001;305:267-273.

47. Walsh JF, Manwaring ME, Tresco PA. Directional neurite outgrowth is enhanced by engineered meningeal cell-coated substrates. Tissue Eng 2005;11:1085-1094.

48. Tessier-Lavigne M, Goodman CS. The molecular biology of axon guidance. Science 1996;274:1123-1133.

49. Ard MD, Bunge RP. Heparan sulfate proteoglycan and laminin immunoreactivity on cultured astrocytes: relationship to differentiation and neurite growth. J Neurosci 1988;8:2844-2858.

50. Biran R, Webb K, Noble MD, Tresco PA. Surfactant-immobilized fibronectin enhances bioactivity and regulates sensory neurite outgrowth. J Biomed Mater Res 2001;55:1-12.

51 Zacharias U, Rauch U. Competition and cooperation between tenascin-R, lecticans and contactin 1 regulate neurite growth and morphology. J Cell Sci 2006;119:3456-3466.

52. Hodgkinson GN, Tresco PA, Hlady V. The differential influence of colocalized and segregated dual protein signals on neurite outgrowth on surfaces. Biomaterials 2007;28:2590-2602.

53. Kam L, Shain W, Turner JN, Bizios R. Axonal outgrowth of hippocampal neurons on micro-scale networks of polylysine-conjugated laminin. Biomaterials 2001;22:1049-1054.

54. Yeung CK, Lauer L, Offenhäusser A, Knoll W. Modulation of the growth and guidance of rat brain stem neurons using patterned extracellular matrix proteins. Neurosci Lett 2001;301:147-150.

55. Gama CI, Tully SE, Sotogaku N, Clark PM, Rawat M, Vaidehi N, et al. Sulfation patterns of glycosaminoglycans encode molecular recognition and activity. Nat Chem Biol 2006;2:467-473.

56. Tully SE, Mabon R, Gama CI, Tsai SM, Liu X, Hsieh-Wilson LC. A chondroitin sulfate small molecule that stimulates neuronal growth. J Am Chem Soc 2004;126:7736-7737.

57. Pietak A, McGregor A, Gauthier S, Oleschuk R, Waldman SD. Are micropatterned substrates for directed cell organization an effective method to create ordered 3D tissue constructs? J Tissue Eng Regen Med 2008;2:450-453.

58. Schnell L, Schwab ME. Axonal regeneration in the rat spinal cord produced by an antibody against myelin-associated neurite growth inhibitors. Nature 1990;343:269-272.

59. Bradbury EJ, Moon LD, Popat RJ, King VR, Bennett GS, Patel PN, et al. Chondroitinase ABC promotes functional recovery after spinal cord injury. Nature 2002; 416:636-640.

60. McKerracher L, David S, Jackson DL, Kottis V, Dunn RJ, Braun PE. Identification of myelin-associated glycoprotein as a major myelin-derived inhibitor of neurite growth. Neuron 1994;13:805–811.

61. Williams C, Xie AW, Yamato M, Okano T, Wong JY. Stacking of aligned cell sheets for layer-by-layer control of complex tissue structure. Biomaterials 2011;32:5625-5632.

CHAPTER 3

ORIENTED ASTROCYTE BASED BIOMATERIAL CONSTRUCTS FOR SPINAL CORD INJURY REPAIR

3.1 Introduction

In the spinal cord, longitudinally aligned astrocytes are found to arrange their processes along the fiber tracts parallel to the trajectories of nerve fibers [1-4]. Following spinal cord injury (SCI), this oriented glial cell framework is interrupted at the injury site accompanied by the formation of disorganized glial scar tissues and accumulation of various scar associated inhibitory ligands [5-9]. While many researchers have been investigating strategies to mitigate the repulsive effects of these inhibitory molecules to facilitate axonal regeneration [10-12], very few have looked at how much the inhibitory nature of the glial scar is contributed by its disorganized cellular structure and ligand distribution.

Cell transplantation studies have suggested the positive correlation between the organized astrocyte framework and efficacy of axonal regeneration following SCI [4, 6, 13, 14]. Transplanted DRG neurons have been found to send out lengthy axonal processes along injured white matter tracts of adult rats, being closely associated with aligned host astrocytic processes [4, 6]. In addition, astrocytes derived from glial restricted precursors have been shown to guide and promote regenerating axons across the lesion site by reorganizing host scar

Forming reactive astrocyte processes toward the lesion center [13,14]. Similar rearrangement of host glial cells, which then guide trajectories of regenerating sensory fibers across the injured dorsal root entry zone has also been documented following olfactory ensheathing cell (OEC) transplantation [15,16].

Unlike mammalian animals whose central nervous system (CNS) axons regenerate following injury but only to a limited extent, the regenerating CNS axons of nonmammalian vertebrates can penetrate through the glial scar [17-19]. The ability of the neuroepithelial cells residing in the nonmammalian vertebrate spinal cord to reform the organized pathway following injury has been suggested to be at least partially attributed to the observed successful axonal regeneration.

These observations lead to the hypothesis that reconstructing an organized glial cell framework at the injury site following SCI could be beneficial for axonal regeneration.

It has been demonstrated that alignment of astrocyte monolayers can be manipulated by various approaches *in vitro*, including physical surface undulation [20-23] and external electric field [24]. In particular, our lab used nanometer-level surface cues to induce astrocyte monolayer organization [55]. We have further shown that organizational cues provided by the first oriented astrocyte monolayer can be transmitted through several overlying astrocyte cell layers to induce orientation of the entire construct morphologically and with regard to its secreted matrix proteins, suggesting the possibility of using such structure to induce glial scar organization during its maturation. Although oriented astrocyte frameworks

have been successfully engineered in these 2D culture systems, it is unclear whether such organized structure could be transferred for *in vivo* applications.

The aim of the present study was to build on our previous work and develop implantable, organized astrocyte constructs *in vitro*, such that its therapeutic potential for SCI repair could be evaluated *in vivo*. Indirect immunohistochemical reactions were applied to investigate the cellular orientation as well as the spatial organization of matrix proteins within recovered astrocyte constructs. DRG outgrowth assay was then used to evaluate the ability of astrocyte constructs to guide axonal regeneration *in vitro*. The feasibility of recovered astrocyte constructs to be manipulated into different geometries for implantation to different injury sites was examined. The possibility of harvesting oriented astrocyte derived acellular ECM constructs was also explored. Last, the ability of acellular, oriented astrocyte derived ECM constructs to support and guide DRG outgrowth was tested *in vitro*.

3.2. Materials and Methods

3.2.1 Micropatterning Device Fabrication

Microcontact printing devices were designed and fabricated as previously described [55]. Briefly, polydimethylsiloxane (PDMS, R-2615, Nusil) microcontact printing devices were designed using L-Edit software and fabricated in the University of Utah Microfibrication laboratory. PDMS two component kit was mixed in a 1:10 ratio, vacuumed treated to remove bubbles, poured into a mold and then cured for 30 mins at 100^{o}C. The cured PDMS stamps were peeled off against the mold and cut into approximately 1 x 1.5 cm^{2} blocks. PDMS stamps

with the isotropic pattern were designed to have flat surfaces whereas stamps with the anisotropic pattern were designed to have continuous lanes (15 μm wide) interspersed with continuous grooves (15 μm wide).

3.2.2 Microcontact Printing

Round glass coverslips (18mm diameter) were cleaned by rinsing with acetone, isopropanol followed by double distilled deionized (DD) water, then sonicated for 20 mins and autoclaved. Nine μl laminin (LN, 400 μg/ml, Sigma) was applied to PDMS printing devices and coverslipped to spread protein solution over the entire device surface for 25 mins. After adsorption, stamps were rinsed with sterile DD water and briefly dried under a nitrogen stream. LN adsorbed stamps with either flat surface or alternating 15 μm wide lanes and grooves were brought into contact with clean coverslips and then removed.

3.2.3 Astrocyte and DRG Isolation and Preparation

Purified primary rat neonatal cortical astrocytes were isolated as previously described [48]. Briefly, cerebral cortices of postnatal Day 1 (P1) Sprague-Dawley rats were dissected with meninges removed. Dissected rat cortical tissue was minced and digested (1.33% collagenase, 30 mins, Worthington Biochemical) followed by 0.25% trypsin treatment (30 mins, Worthington Biochemical). The cells were then triturated and suspended in DMEM/F12 medium (Invitrogen) with 10% fetal bovine serum (FBS, Sigma). Dissected cells were plated in 75 cm^2 flasks. After 1 week, purified astrocytes were obtained by overnight shake-off at 175 rpm.

Dorsal root ganglion neurons (DRG) were isolated from P1 rats as previously described [21]. Ganglion neurons were dissected out from both sides of the spinal column. Nerve roots and attached connective tissue were removed and the ganglia neurons were trypsin/collagenase treated (0.25%/0.33%) for 30 mins. Digested DRGs were triturated and the resulting cell suspension was centrifuged and placed in 1 ml DMEM/F12 plus 50 µl of DNase. Isolated DRG neurons were washed by centrifugation, and ready for seeding.

3.2.4 Engineering 3D Astrocyte Constructs and DRG Culture

Purified rat cortical astrocytes were seeded on patterned (anisotropic) and unpatterned (isotropic) surfaces at a density of 52,000 cells/cm^2 with serum free medium (SATO-) over the first 4-6 hrs and then switched to 10% FBS supplemented with 50 µg/ml ascorbic acid (Sigma) and 150 µg/ml ascorbate-2-phosphate (Sigma) for 2 days to create the first confluent, oriented and randomly organized astrocyte monolayers, respectively. Ascorbic acid and ascorbate supplementation has been shown to increase cell ECM production [30]. Then, subsequent seeding was applied on the previous confluent cell layers at the same density every other day for multiple times. Half of the culture medium in each well was replaced with fresh medium the day following cell seeding starting the 3rd cell seeding process. After 10-14 days of culture, hydrophilic membranes (CellSeed) were put atop the apical surface of dense astrocyte constructs and astrocyte constructs were harvested from the coverslips by peeling off the membranes with forceps. Excess culture medium was used to separate the membranes from harvested constructs. Recovered constructs were then fixed

with 4% paraformaldehyde for 15 mins. Prior DRG neuron seeding, fixed astrocyte constructs were rinsed with sterile PBS several times.

Dissociated DRG neurons were seeded at 1500 neurons/50 µl 10% FBS supplemented with 10 ng/ml NGF (Sigma) per fixed astrocyte construct and let sit for 1 hr to attach. Then, the culture medium supplemented with NGF (10 ng/ml) was added. DRG neurons were cultured for 2 days and then fixed with 4% paraformaldehyde.

3.2.5 Decellularization of Oriented Astrocyte Constructs and DRG Culture

Recovered oriented astrocyte constructs with attached membranes were placed in hypotonic Tris-HCl buffer (10 mM, pH 8.0) containing 0.1% EDTA and 10 KIU/ml aprotinin (Sigma) for 1-2 hrs at room temperature (R.T.) to weaken integrin-ECM interactions and deactivate released proteases due to cell body rupture. Hydrophilic membranes were then removed and oriented constructs were immersed in 0.1% sodium dodecyl sulfate (SDS,10 mM Tris-HCl, pH 8.0) on a rocker at 100 rpm at R.T. overnight to solubilize lipid membranes. Following detergent treatment, oriented constructs were rinsed three times, 30 mins each, in sterile PBS on a rocker. Last, oriented constructs were treated with Tri-HCl buffer (50 mM, pH 7.5) containing RNase (1 U/ml, Sigma) and DNase (50 U/ml, Sigma) on a rocker at 37^{o}C for 3 hrs, followed by rinsing with sterile PBS three times, 30 mins each, on a rocker.

Acellular, oriented astrocyte derived ECM constructs were first air-dried in the center of the glass-bottom petridishes (World Precision Instrument).

Dissociated DRG neurons were cultured on the acellular ECM constructs at a density of 1500 neurons/50 µl 10% FBS supplemented with 10 ng/ml NGF. DRG neurons were seeded and let sit for 1hr to attach. Then, the rest of the 10% FBS supplemented with NGF (10 ng/ml) was added. DRG neurons were cultured for 2 days and then fixed with 4% paraformaldehyde.

3.2.6 Multistacked Astrocyte Constructs and Astrocyte Tube Fabrication

To engineer multistacked, astrocyte constructs, the first harvested astrocyte construct was put atop the second astrocyte construct and incubated for 20 mins with 50-100 µl of culture medium added atop the hydrophilic membrane to keep constructs hydrated. The double-stacked constructs were harvested by gently peeling off the membrane with forceps and then separated from the membrane by adding excess culture medium. After being released from the membranes, double-stacked constructs were fixed with 4% paraformaldehyde for 15 mins.

Agar powder (Gibco) was dissolved into warm D.I. water to make a final concentration of 2.5% agar solution. Agar solution was injected into a laboratory tubing (Dow Corning) of 0.51 mm inner diameter and let cool down to solidify. A syringe was used to push out the solidified agar rod from the plastic tubing. An astrocyte construct was wrapped around an agar rod using forceps under a dissecting microscope to make a tubular astrocyte construct and then incubated for another 30 mins. The cylindrical astrocyte construct was then fixed with 4% paraformaldehyde for 15 mins.

Recovered astrocyte constructs were wrapped around laboratory tubings (Dow Corning) with hand hold forceps and cultured for another week in culture medium supplemented with ascorbic acid (50 µg/ml) and ascorbate-2-phosphate (150 µg/ml). After 1 week, self-supporting astrocyte tubes with open lumens were removed from plastic tubings, fixed with 4% paraformaldehyde for 30 mins then followed by lyophilization. Acellular astrocyte ECM tubes were prepared by decellularizing self-supporting astrocyte tubes with plastic tubings attached following the procedures described in section 2.5. After lyophilization, plastic tubing was removed from the acellular astrocyte ECM tube.

3.2.7 Cryostat Sectioning

Agar powder (Gibco) was dissolved into warm D.I. water to make a final concentration of 0.8% agar solution. Single, double-stacked astrocyte constructs and tubular astrocyte constructs were placed in a square mold and warm 0.8% agar solution was slowly poured into the mold to cover the samples and let them cool down. Solidified 0.8% agar cubes with embedded samples were removed from the mold and left in 30% sucrose solution overnight. Agar cubes were then put on cryostat specimen holders in the desired orientation. Tissue freezing medium (Triangle Biomedical Science) was added to cover the agar cubes and the specimens were then placed in the cryostat at -20^{o}C. Specimens were cut transversely into 15 µm thick sections.

3.2.8 Immunohistochemical Staining

For intracellular antigens, fixed samples were treated with 0.05% Triton X-100 in PBS for 15 mins and rinsed with PBS. No Triton was applied for the extracellular matrix molecular immunohistochemical detection. When intracellular ligands were co-stained with extracellular ligands, extracellular ligands were always processed first, followed by Triton treatment and immunohistochemical reactions for intracellular ligands. Prior indirect immunohistochemical reactions, cryostat sections were rinsed with PBS to remove tissue freezing medium. Samples were blocked with 4% goat serum and 0.1% sodium azide in PBS for 1 hr and incubated with primary antisera against glial fibrillary acidic protein (GFAP, DAKO, 1:1000), neurofilament 160 (NF-160, Sigma, 1:500), laminin (LN, Sigma, 1:500), cellular fibronectin (FN, Sigma, 1:500), chondroitin sulfate proteoglycan (CS-56, Sigma, 1:500), Neural cell adhesion molecule (NCAM, Sigma, 1:500) and Type-1 collagen (Coll, Sigma, 1:500). Fluorescent dye conjugated secondary antibodies (Molecular Probes) were applied at dilution of 1:500 except for GFAP (1:1000). All antibodies were diluted in 4% goat serum and 0.1% azide and applied for 24 hrs at room temperature. Three washes with 30 mins each were applied between applications of primary and secondary antisera. DAPI (10 μM; Molecular Probes) was used for all cell nuclei visualization. Tissue sections were mounted on microscope slides covered with Fluormount-G (Southern Biotech), and coverslipped. Images were acquired using a Nikon epifluorescence microscope equipped with a CCD camera (ImagePro, Media Cybernetics) or using an Olympus FVX laser scanning confocal microscope when noted.

3.3 Results

3.3.1 Engineering 3D Astrocyte Constructs

To engineer 3D astrocyte constructs with either unorganized or organized cellular orientation, micropatterning was used to transfer isotropic (LN field) or anisotropic (LN lanes) protein patterns to glass coverslips as previously described [55]. The LN field stamped surface and LN lanes patterned surface will be referred to as unpatterned and patterned surfaces, respectively, throughout the manuscript. The 3D astrocyte construct culturing and harvesting procedure is schematically illustrated in Figure. 3-1. Primary rat cortical astrocytes were seeded on top of both unpatterned and patterned surfaces in SATO- medium over the first 4-6 hrs to facilitate attachment and then switched to 10% FBS supplemented with ascorbic acid and ascorbate. In 2 days, the first astrocyte layer was observed to reach confluence on both surfaces. The seeding process was then repeated every other day with the same cell density. The elongated morphology of subsequent astrocyte layers cultured on the first oriented astrocyte monolayer induced by the patterned surface was preserved throughout the culture period via microscopic bright field observation. This alignment was not observed for astrocytes cultured on unpatterned surfaces.

After 5-7 seedings, a dense astrocyte construct was formed atop the coverslip and ready to be harvested with a hydrophilic membrane. The recovered construct was then separated from the membrane by adding excess medium to the composite. The hydrophilic membranes prevented shrinkage of recovered astrocyte constructs. Generally, constructs harvested from unpatterned surfaces

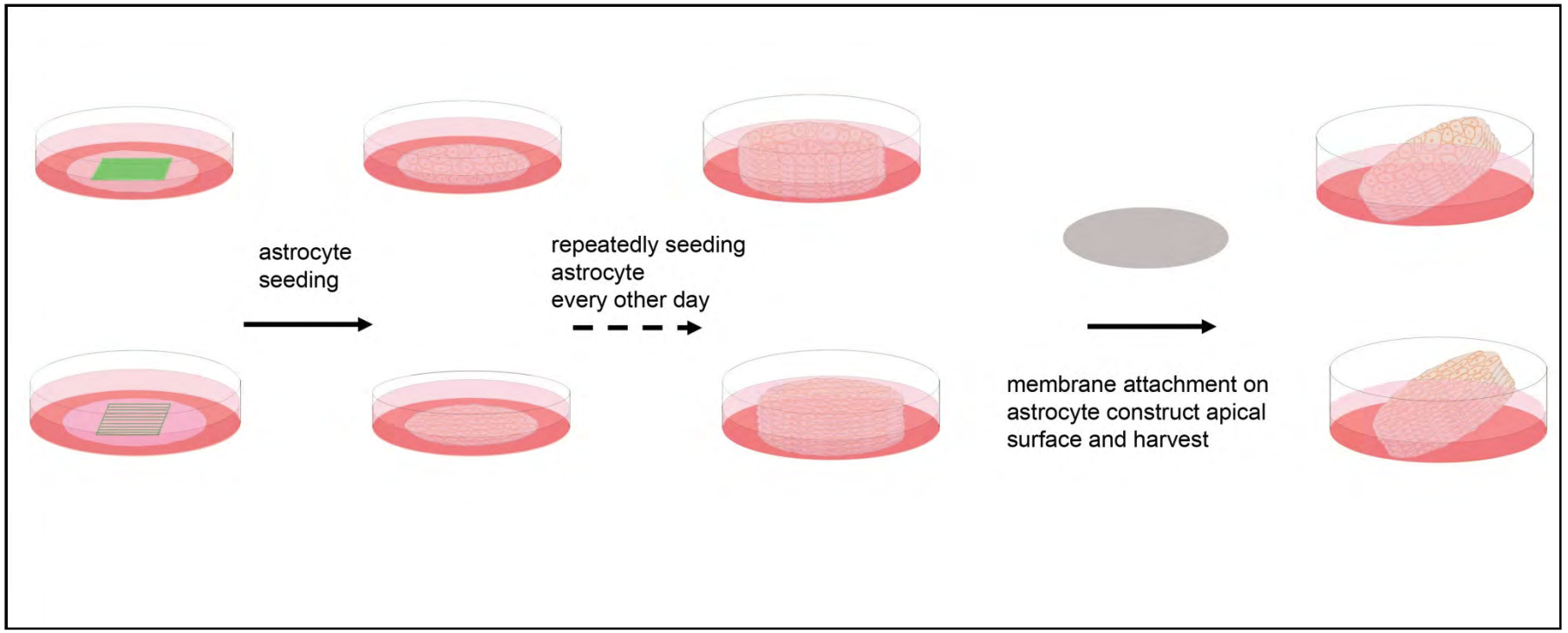

Fig. 3-1 Schematic illustration of engineering and harvesting 3D astrocyte constructs from unpatterned or patterned culture substrates. Primary astrocytes were first seeded on patterned (LN lanes) and unpatterned (homogeneous LN field) surfaces. After the first layers reached confluence on both surfaces, another astrocyte seeding was applied. The seeding process was repeatedly applied every other day for 5-7 times and dense astrocyte constructs were formed a top of culture substrates. Hydrophilic membranes were then applied on the apical surface of the constructs and the constructs were harvested by peeling off the membrane against the culture substrates.

shrank about 50% isotropically without the application of membranes, whereas constructs recovered from the patterned surfaces shrank anisotropically more in the direction parallel to the long axis of printed LN lanes (data not shown). Harvested astrocyte constructs were mechanically stable floating in the medium (Fig. 3-2:A) and a piece of sheet-like material was obtained following lyophilization (Fig. 3-2:B).

3.3.2 Characterization of Engineered Astrocyte Constructs

Astrocyte constructs were cryostat-sectioned transversely. The multilayered structure within the constructs was clearly seen with the DAPI+ astrocyte nuclei staining (Fig. 3-3). The thickness of both randomly organized

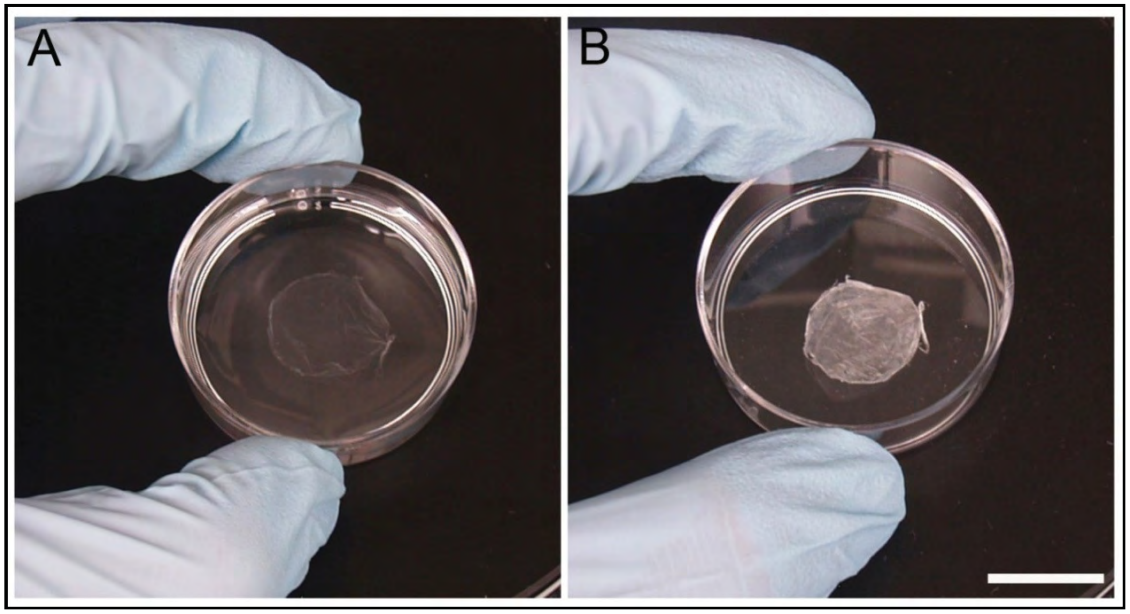

Fig. 3-2 Representative macroscopic image of recovered astrocyte constructs. (A) Recovered astrocyte constructs were mechanically stable to float in the medium. (B) After lyophilization, astrocyte constructs became a piece of sheet-like material. Scale bar = 15 mm.

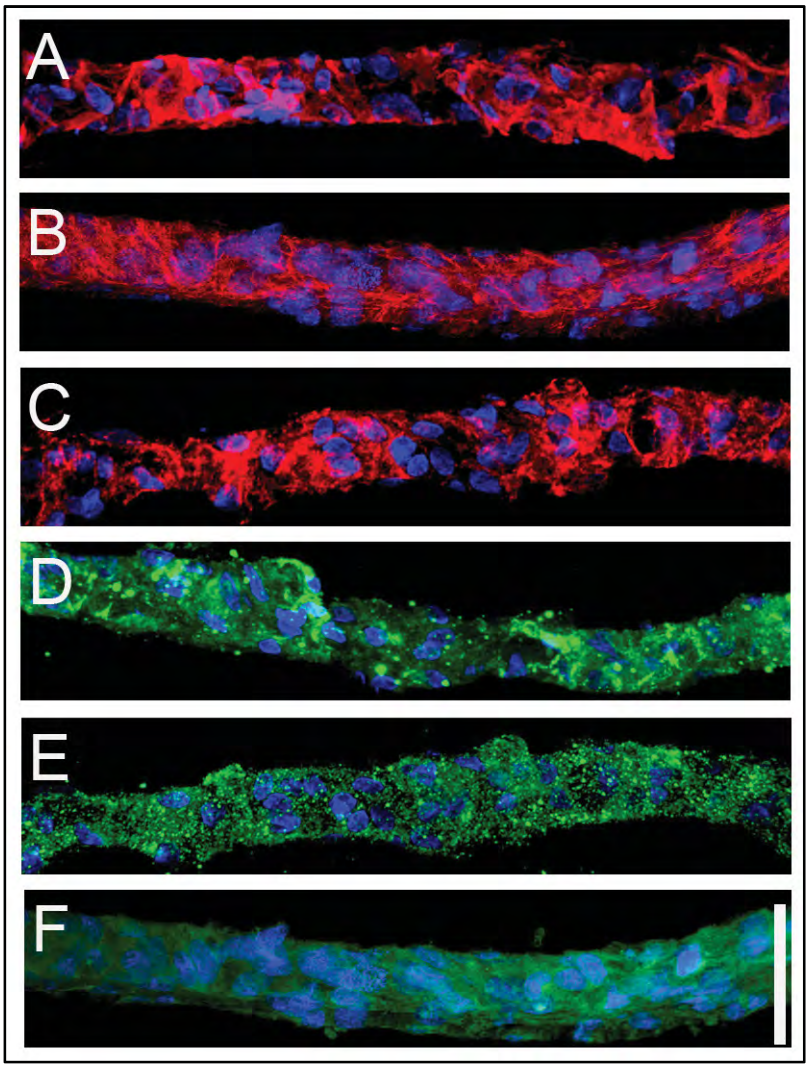

Fig. 3-3 Representative cross-sectional images of the recovered, 5 seedings astrocyte constructs. The harvested construct was primarily composed of astrocytes visualized by the immunofluorescent GFAP staining (A, in red). Astrocyte associated ligands, FN (B, in red), NCAM (C, in red), LN (D, in green) and CSPG (E, in green), were distributed throughout the entire construct. In particular, ascorbic acid and ascorbate treatment resulted in positive type-1 collagen detection (F, in green). The multilayered structure of the constructs was demonstrated by DAPI+ astrocyte nuclei. Scale bar = 50 µm

and oriented constructs was about 30 μm after 5 seedings when they were dehydrated and mounted, suggesting the thickness of the constructs would increase in the hydration state. The cross-sectional views showed that astrocyte associated ECMs such as FN, LN, CSPG and a membrane bound ligand NCAM were distributed throughout the entire constructs (Fig. 3-3:B, C, D and E). In particular, ascorbic acid and ascorbate supplementation resulted in positive type-1 collagen detection within the astrocyte constructs (Fig. 3-3:F)

Confocal microscopic images further demonstrated a strong bias of the orientation of astrocyte associated ligands. Intracellular cytoskeletal protein GFAP and astrocyte derived ECM protein FN also showed anisotropic distribution throughout the aligned astrocyte constructs that were recovered from patterned coverslip surface/s (Fig. 3-4:B, B1 and B2),whereas unorganized distribution of GFAP and FN was seen in randomly organized astrocyte constructs harvested from unpatterned surfaces (Fig. 3-4:A, A1 and A2). FN was expressed in a fibrillar structure in both culture conditions (Fig. 3-4:A2 and B2). Similar to FN, the spatial organization of CSPG also had a biased orientation in aligned astrocyte constructs (Fig. 3-4:D and D1). On the other hand, CSPG distribution in randomly organized constructs was unbiased (Fig. 3-4:C and C1). Astrocyte derived LN also exhibited anisotropy at a certain degree (Fig. 3-4:D and D2) in aligned constructs but not in randomly organized constructs (Fig. 3-4:C and C2). However, the anisotropic nature of LN was not as conspicuous as

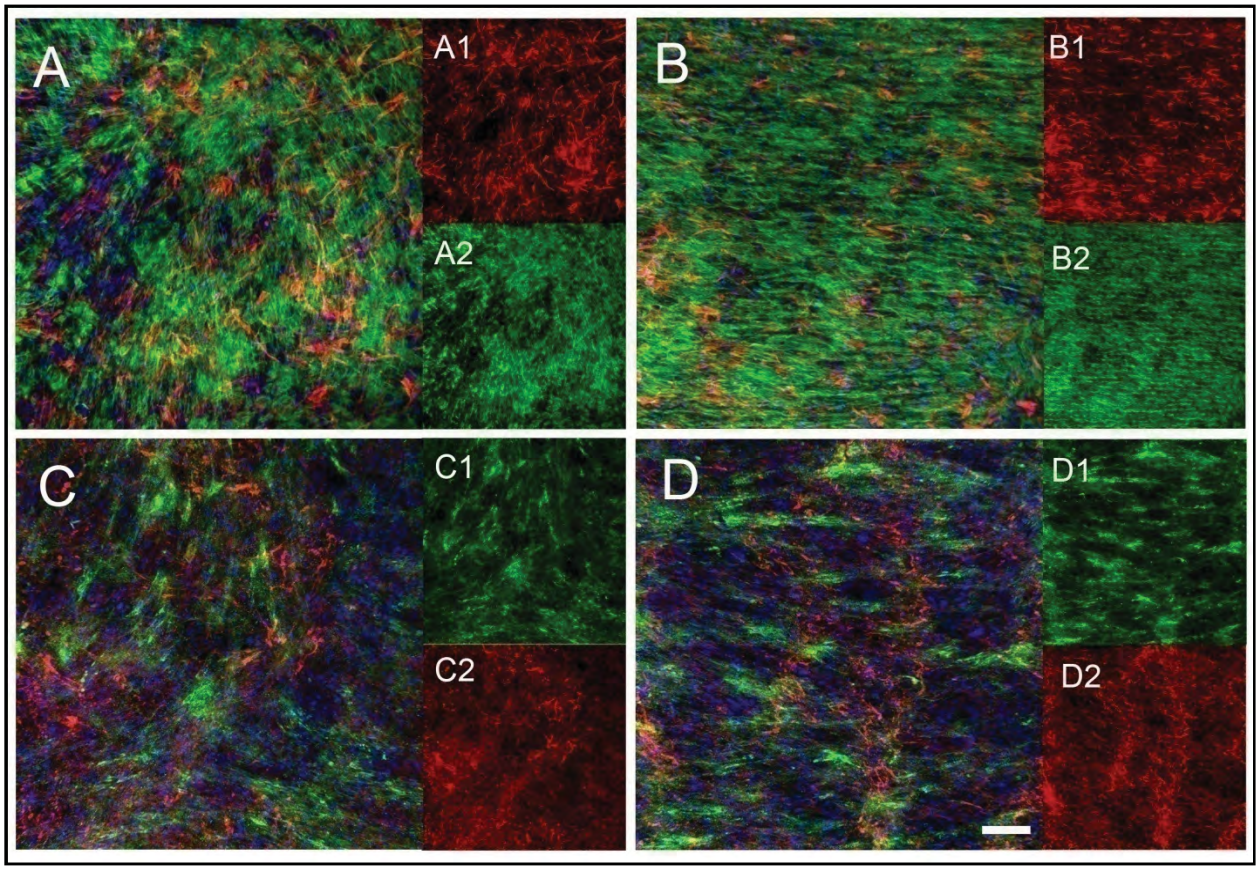

Fig. 3-4 Representative z-stacked confocal images demonstrating the spatial organization of various astrocyte associated ligands within either randomly organized or aligned astrocyte constructs that were engineered by chemisorbed ligand patterns. (A) No preferred orientation of astrocyte specific interfilament marker, GFAP (A1, in red) and extracellular ligand, FN (A2, in green), was observed in randomly organized astrocyte constructs. (B) In sharp contrast, a strong bias of the orientation of GFAP (B1, in red) and FN (B2, in green) within the entire aligned astrocyte constructs was seen. Astrocyte derived FN appeared to have a fibrillar structure in both culture conditions (A2 and B2, in green). (C) Similarly, the spatial organization of CSPG (C1, in green) and LN (C2, in red) in the randomly organized astrocyte constructs appeared disorganized. Whereas spatially organized CSPG (D1, in green) and LN (D2, in red) distributions were noticed within the aligned astrocyte constructs. A1 and B1 represent the GFAP channel from (A) and (B), respectively. A2 and B2 represent the FN channel from (A) and (B), respectively. C1 and D1 represent CSPG channel from (C) and (D), respectively. C2 and D2 represent the LN channel from (C) and (D), respectively. Scale bar= 100 µm.

FN and CSPG. The anisotropic distribution of NCAM and type-1 collagen was also only observed in oriented astrocyte constructs (data not shown).

3.3.3 DRG Outgrowth on Engineered Astrocyte Constructs

Isolated primary P1 DRG neurons were seeded on either fixed randomly organized or fixed oriented astrocyte constructs, respectively, to investigate their ability to support and guide neuronal outgrowth. While DRG neurons were found to extend processes on both random and aligned constructs, directed DRG neurite outgrowth (i.e., neurite extension in a preferred direction) parallel to the spatial organization of astrocyte derived ECM ligands was only observed on fixed aligned constructs (Fig. 3-5).

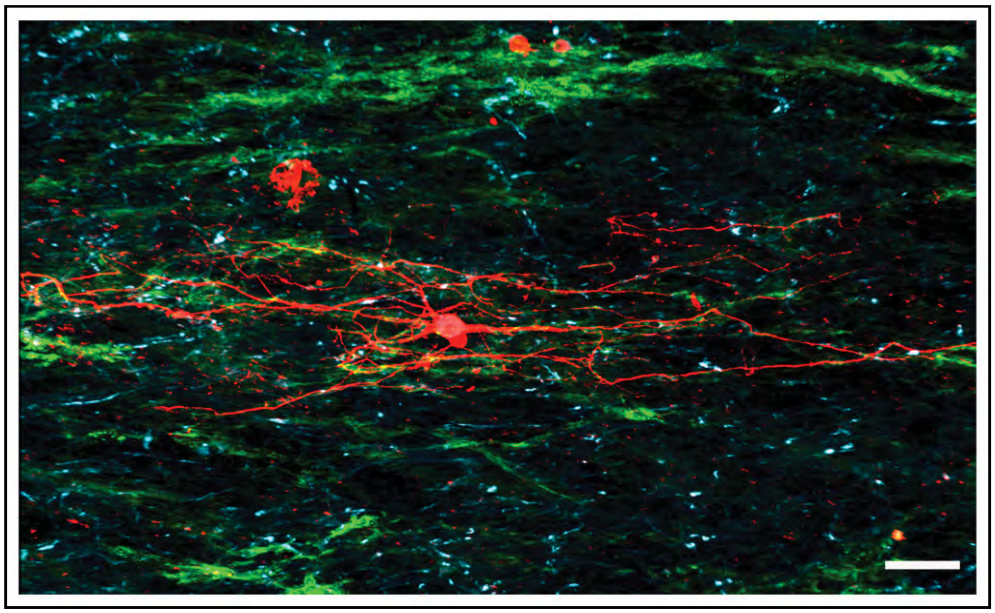

Fig. 3-5: Representative DRG outgrowth behavior on engineered aligned astrocyte constructs. DRG neurites (in red) were found to extend in a preferred direction parallel the spatial organization of oriented astrocyte constructs associated ligands, CSPG (in green) and LN (in blue).This directed outgrowth behavior is similar to what we observed previously on the 2D astrocyte monolayer model [55].Scale bar=100 µm.

3.3.4 Manipulation of Engineered Astrocyte Constructs

Both randomly organized and oriented constructs were mechanically stable and manipulatable. Immediately after being peeled off from coverslips, one construct was stacked atop a second construct and incubated for 20-30 mins at 37^{o}C to engineer a double-stacked astrocyte construct. DAPI+ astrocyte nuclei staining clearly demonstrated that the number of cell layers as well as the thickness of a double-stacked construct increased (Fig. 3-6:A and B) when compared to a single construct in Figure. 3-3. All astrocyte associated ligands investigated (e.g., FN, NCAM) were distributed throughout the double-stacked constructs in a way similar to single constructs (Fig. 3-6:A and B).

Astrocyte constructs were also wrapped around agar rods using hand-hold forceps to form tubular astrocyte constructs of length on the level of millimeters (Fig. 3-6C). Cross-sections of a cylindrical astrocyte constructs showed that the tubular structure around the agar rod was formed by several layers of an astrocyte construct, visualized by GFAP and astrocyte derived FN (Fig. 3-6:D). In addition, recovered astrocyte constructs were also wrapped around plastic tubings and then cultured for another week. After 1 week in culture, the layers of the astrocyte construct around the tubings fused and a self-holing astrocyte tube with an open lumen was formed following removal of the tubing (Fig. 3-6:E and F).

3.3.5 Decellularization of Oriented Astrocyte Constructs

As we found that no ECM materials can be collected when the oriented astrocyte constructs were engineered in the regular astrocyte culture medium,

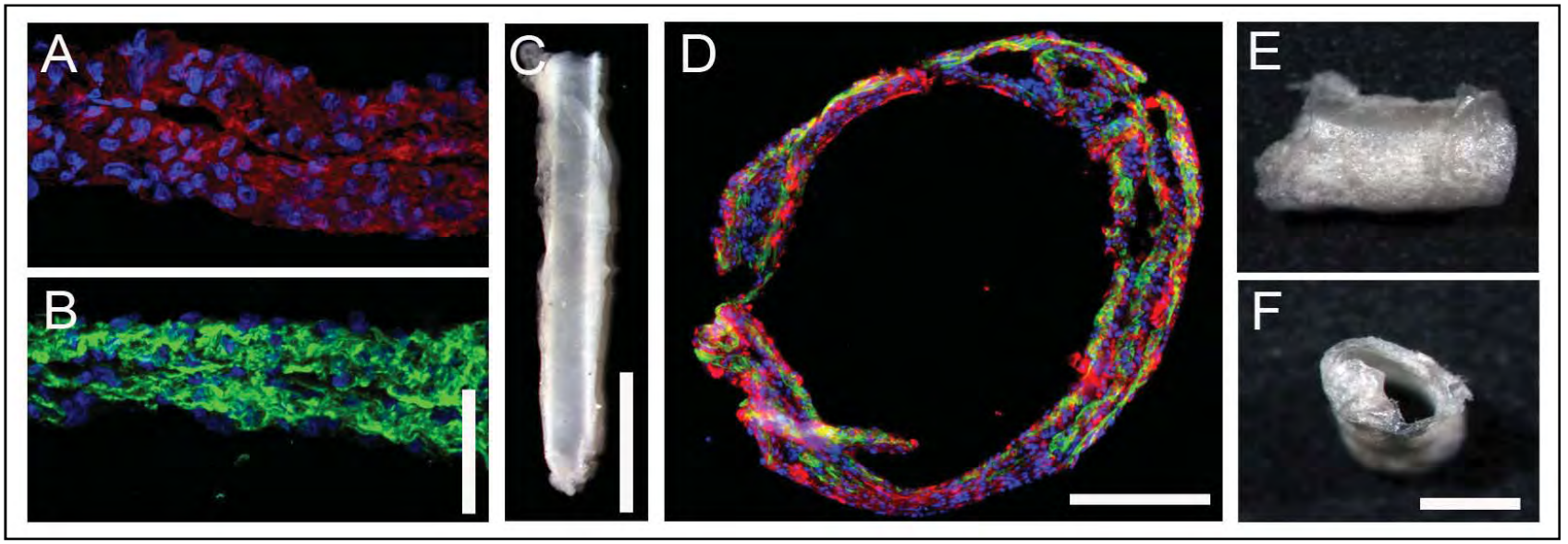

Fig.3-6: Engineered astrocyte constructs are manipulable. Engineered astrocyte constructs were stacked atop each other to create double-stacked astrocyte constructs. Representative cross-sectional images showing that, similar to single astrocyte constructs, the distributions of astrocyte associated membrane ligand NCAM (A, in red), and extracellular protein FN (B, in green), were throughout the entire double-stacked constructs (data of LN and CSPG not shown). The number of DAPI+ astrocyte nuclei has increased in the double-stacked constructs in the vertical direction in (A, B) when compared with single constructs in Fig. 3-3. (C) Representative macroscopic image showing a cylindrical astrocyte tube formed by wrapping an astrocyte construct around an agar rod. (D) Representative cross-sectional view of the astrocyte tube. The tubular structure of the construct was confirmed immunofluorescently by GFAP (in red), FN (in green) and DAPI (in blue) staining. (E, F) A self-holding astrocyte tube with open lumen was engineered by wrapping a recovered astrocyte construct around plastic tubings and cultured for another week. Following 1week, layers of an astrocyte construct around the plastic tubings fused and a self-holding astrocyte tube with an open lumen formed. Images were taken after lyophilization Scale bar= 50 µm in (A), (B); =0.2 cm in (C); =250 µm in (D); 1 mm in (E, F)

ascorbic acid and ascorbate-2-phosphate were then supplemented in the culture medium to boost ECM deposition of astrocytes. Following recovery, oriented astrocyte constructs were decellularized to remove cellular components and nuclear materials. Confocal microscopic images demonstrated that the decellularization process was effective such that little to no immuofluorescent signals of intracellular components and nuclear materials (Fig. 3-7:E, i.e., GFAP and astrocyte nuclei) as well as a membrane bound ligand (Fig. 3-7:F, i.e., NCAM) were observed. On the other hand, a network of astrocyte derived ECM proteins was preserved (Fig. 3-7:A, B, C and D). Similarly, positive type-1 Coll detection within oriented astrocyte derived ECM constructs was observed following decellularization (Fig. 3-7:A). In addition, even with ascorbic acid and ascorbate supplementation, mechanically stable, acellular, oriented astrocyte derived ECM constructs were only collectable when primary astrocytes after passage 2 or 3were used to engineer the cellularized constructs at the first place. The organized fibrillar structure of Coll and FN were found to be maintained in the acellular, oriented astrocyte derived ECM constructs (Fig. 3-7:A and B). The organized spatial arrangement of LN and CSPG in the oriented astrocyte derived ECM constructs was less obvious (Fig. 3-7:C and D).

3.3.6 DRG Outgrowth on Oriented Astrocyte ECM Constructs

Dissociated DRG neurons were seeded on acellular, oriented astrocyte derived ECM constructs to investigate whether simply the presence of a network of organized ECM proteins (i.e., FN and Coll) without the involvement of astrocyte membrane bound ligands is sufficient to guide neuronal pathfinding.

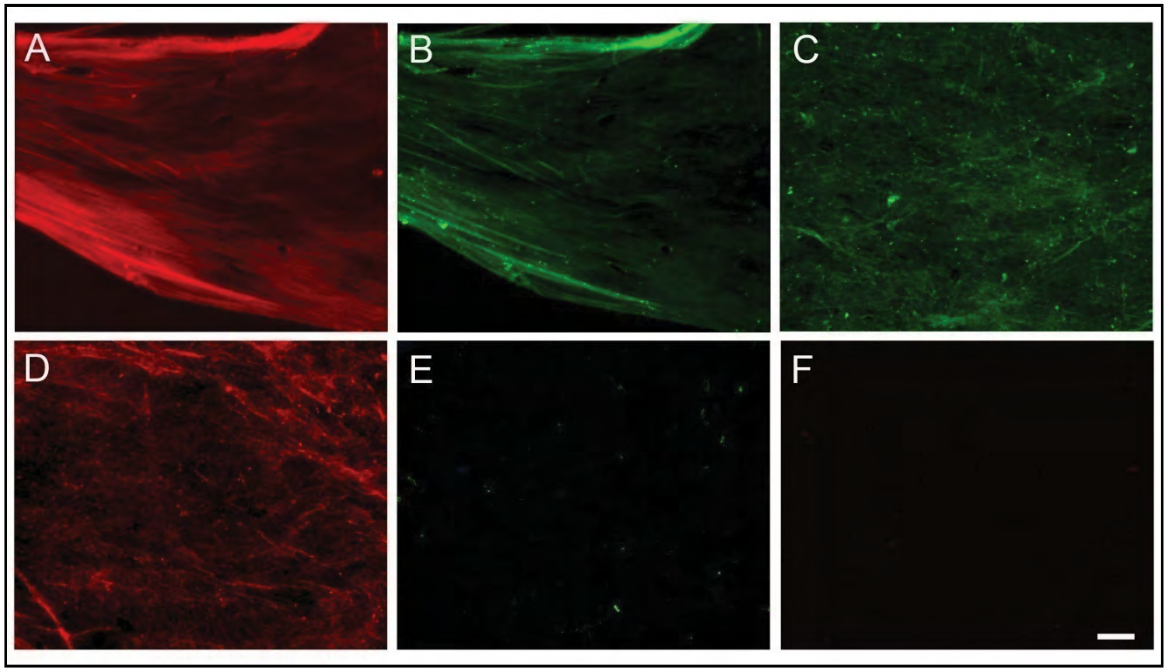

Fig.3-7: Representative ECM protein organization of acellular, oriented astrocyte derived ECM constructs. Organized fibrillar structure of type-1 Coll (A, in red) and FN (B, in green) were displayed in the ECM constructs following the decellularization. The anisotropic organization of CSPG (C, in green) and LN (D, in red) in the acellular ECM constructs was less obvious. (E). Little to no immunofluorescent signals of DAPI+ astrocyte nuclei (in blue) and astrocyte specific interfilament, GFAP (in green), were observed in the ECM constructs. (F) Decellularization effectively removed an astrocyte membrane bound ligand, NCAM (in red). Scale bar=100 µm

After 2 days in culture, we observed that DRG neurite trajectories were generally extended in a preferred direction in a way similar to their outgrowth pattern on cellularized, aligned astrocyte constructs (Fig. 3-8:A). It should be noted that the presence of Schwann cells (Fig. 3-8:A, dark, slender shaped cell bodies) was always observed in our DRG preparation due to the limitation of our isolation technique, which might also contribute to providing guidance information to regenerating neurites. However, we found that the Schwann cells also generally showed biased orientation morphologically parallel to the long axis of the oriented astrocytes derived ECM constructs (i.e., parallel to the long axis of originally printed LN lane pattern, Fig. 3-8:A, arrows), suggesting that the organized ECM construct is capable of influencing the orientation of adjacent migrating and proliferating glial cells.

3.3.7 Acellular, Astrocyte Derived ECM Tubular Constructs

After the recovered astrocyte constructs were wrapped around plastic tubings and cultured for another week, the composite was decellularized to develop tubular astrocyte ECM constructs. Decellularization was performed while the plastic tubing was still attached. Following treatment, tubular ECM constructs with open lumens were obtained by removing the plastic tubings after lyophilization (Fig. 3-8:B and C). In contrast to the self-holding astrocyte tubes, the lumens of the tubular ECM constructs collapsed during rehydration, possibly due to the fact that there was not enough material present holding the wall structure (i.e., each acellular ECM tube was derived from an astrocyte construct recovered from a 18 mm coverslip).

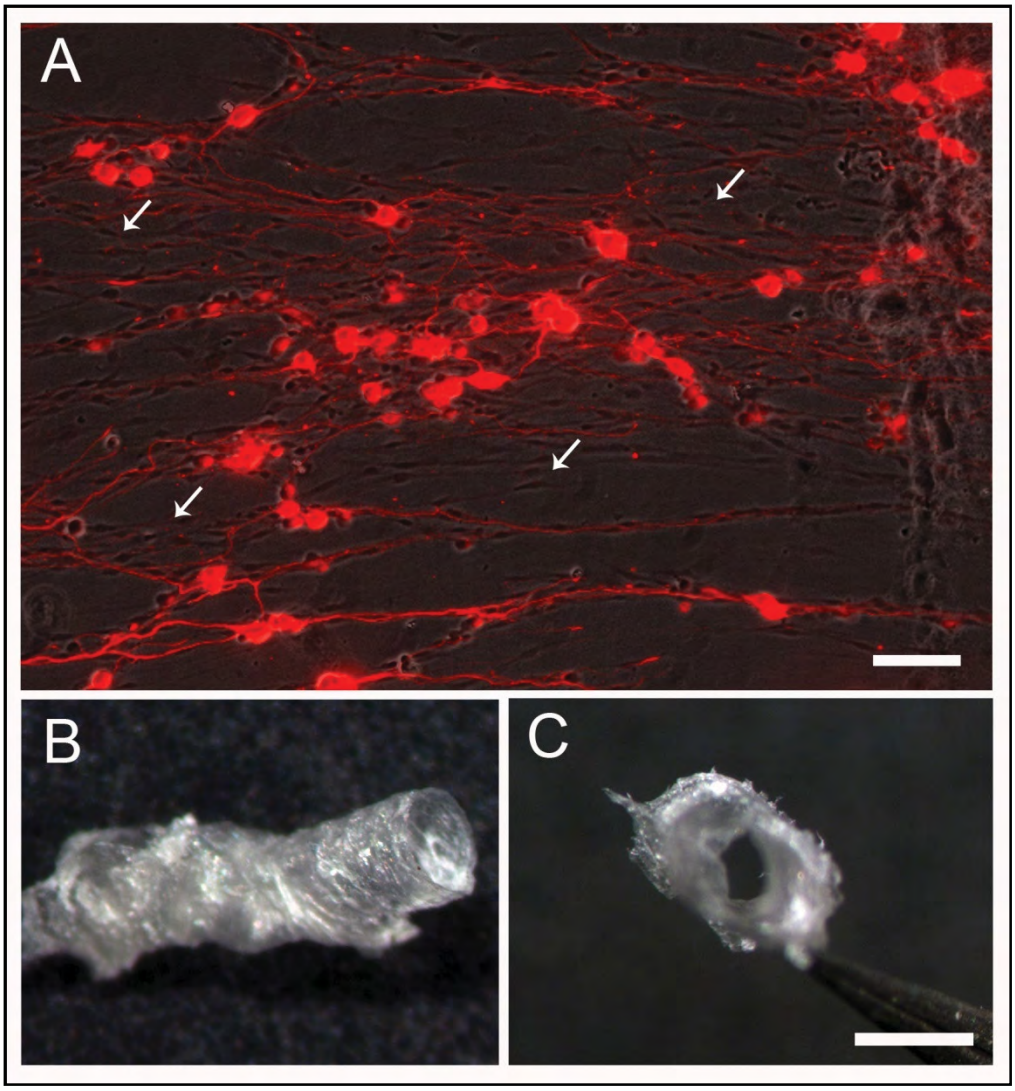

Fig. 3-8: Representative images of DRG outgrowth behavior on oriented astrocyte derived acellular ECM constructs and engineered tubular astrocyte ECM constructs. (A) DRG neurite trajectories (shown in red) were found to generally extend in a preferred direction when cultured on the acellular, oriented astrocyte derived ECM constructs. The ECM construct was air dried on a coverslip and shown in the bright field. It should be noted that due to the limitation of our isolation technique, the presence of Schwann cells (dark, slender cell bodies indicated by arrows) in the DRG culture was always observed, which might also guide neurite outgrowth. However, the morphology of Schwann cells was also found to be generally aligned on the oriented astrocyte derived ECM constructs (i.e., parallel to the long axis of originally printed LN lane pattern), suggesting the organized ECM construct is capable of influencing the orientation of adjacent migrating and proliferating glial cells (B,C) Tubular astrocyte ECM constructs were prepared by decellularizing cellularized self-holding astrocyte tubes. Scale bar=100 µm in (A); =1 mm in (B,C).

3.4. Discussion

Glial scar formation and inflammation-mediated cystic cavities are the hallmark cellular and molecular responses following SCI [26, 27], which interrupt the organized nerve fiber tracts at the injury site [1-4] and are manifested as major obstacles for axonal regeneration [4,6]. Various strategies including synthetic biomaterials [29], cell therapy [13-16] or combinational approaches [28] have been applied in an attempt to facilitate and guide axonal regeneration such that regenerating axons can reinnervate appropriate targets.

Astroglial cells are the most abundant cell type in the CNS and appear as promising candidates for guiding neurite outgrowth utilizing biological mechanisms. Astroglial cells have been suggested to crosstalk with pioneering axons temporally and spatially by arranging into organized glial frameworks and extending their processes parallel to the presumptive fiber tracts at specific periods during development [35-39] or acting as guidepost cells to guide axonal trajectories [40]. Astrocytes have also been shown to serve as supportive substrates for various types of neuronal cell outgrowth *in vitro* [43,44]. Cell transplantation studies have also demonstrated the beneficial roles of young astrocytes in promoting SCI repair [32-34].

Moreover, organized glial structures have been found to effectively facilitate and guide regenerating axonal trajectories following injury in both mammalian and nonmammalian animal SCI models [2,4,6,13,15-19,24,25,45]. While these observations led to a number of studies where astrocyte monolayer alignment was successfully induced to guide and support neuronal trajectories *in*

vitro [20-24, 55], it is unclear if such organized astrocyte structures could be transferred for *in vivo* applications.

In the current study, we developed 3D astrocyte constructs, either randomly organized or aligned, that are mechanically stable and implantable to address such issues. The astrocyte constructs were engineered simply by repeatedly seeding cells atop previous cell layers. In particular, our *in vitro* results showed that the orientation of overlying migrating and proliferating astrocytes can be organized by a previously established oriented astrocyte structure, suggesting such constructs are potentially capable of organizing the disorganized glial scar tissue during its maturation *in vivo*.

Thermo-responsive polymer, poly(N-isopropylacrylamide) (PIPAAM), treated surfaces have been the culture substrates of choice for engineering continuous cell sheets and protein patterning as well as grafted polymer brushes onto PIPAAM surfaces has been applied to induce the organized structure of cell sheets [57, 60]. In the current study, we demonstrated that plain coverslips are also suitable substrates for harvesting multilayered cellular constructs, with or without morphological alignment. This is advantageous as the cost of purchasing PIPAAM grafted substrates and the potential undesired cell sheet detachment due to ambient temperature drop during cell seeding can be avoided.

The aligned astrocyte constructs hold several advantages over traditional cell therapy approaches. First, the desired astrocyte orientation can be engineered within the aligned constructs, which has been suggested to facilitate axonal regeneration [2,4,6,13,15,16,24,25,45] whereas there is little to no control

to the overall cellular orientation via injection of cell suspensions. Second, the astrocyte constructs were harvested along with deposited ECM ligands which have been shown to play an important role in mediating neurite outgrowth during development as well as following injury [25,41,42,55]. Tessier-Lavigne and colleagues [46] first proposed that extracellular matrix molecules could act as short range guidance cues for directing neurite outgrowth. Therefore, having an organized ECM network upon implantation should be advantageous as guidance cues can be readily available for regenerating axons. It has been reported that the axonal regeneration is observed as early as 6 hrs following injury [49]. Moreover, a transplantation study has demonstrated that implantation of ECM-associated cellular grafts resulted in superior regeneration outcome to injection of cell-only suspensions [47].

In addition, oriented astrocyte constructs can be decellularized to reduce the undesired immunogenic response associated with allogeneic or xenogeneic cellularized materials upon implantation [54]. Cell-deposited ECM materials are generally considered to be immunologically tolerable between species and have been used as an alternate to cell therapy for various regenerative medicine applications [30,31,50,53]. Following decellularization, acellular, oriented astrocyte derived ECM constructs were obtained and positively stained for various ECM proteins whereas little to no signals of either intracellular components or cell membrane-bound ligands were seen immunofluorescently, demonstrating the effectiveness of decellularization.

Interestingly, we found that ascorbic acid and ascorbate treatment was needed for astrocytes to deposit enough matrix materials so that acellular ECM constructs can be collected following decellularization. This observation could be explained by the positive type-1 collagen detection within the cellularized and acellular astrocyte constructs following ascorbic acid and ascorbate supplementation, which would contribute to the mechanical properties of the ECM materials. The association between primary astrocytes and type-1 collagen has been previously reported in the literature [59]. In addition to the ascorbic acid and ascorbate supplementation, using primary astrocytes after passage 2 or 3 were also required for acellular ECM constructs collection following decellularization, suggesting that astrocytes might secrete more collagen as they mature *in vitro*. This hypothesis is supported by our finding that no stable ECM materials can be collected from young astrocytes (e.g., no passage) even in the presence of ascorbic acid and ascorbate treatment.

In particular, the spatial organization of type-1 Coll and FN within the acellular ECM constructs maintained an organized fibrillar structure, suggesting that the oriented ECM constructs would still preserve the ability to guide neurite trajectories since we have previously shown that astrocyte associated FN plays an important role in guiding neuronal pathfinding *in vitro* [55].

Indeed, both cellularized, aligned astrocyte constructs and acellular, oriented ECM constructs directed regenerating DRG outgrowth *in vitro*. As indirect immunohistochemical reactions demonstrated the successful removal of astrocyte membrane bound ligands following decellularization, this result

suggests that the directional information carried by the organized ECM matrices alone is sufficient to guide neuronal pathfinding. In the present study the presence of Schwann cells was always observed in our DRG preparation due to the limitation of our isolation technique, which might also contribute to providing guidance for DRG neurite outgrowth. However, the fact that Schwann cells on the decellularized aligned ECM constructs were also observed to generally exhibit oriented morphology *in vitro* further strengthens our hypothesis that the oriented astrocyte derived ECM constructs could potentially influence and organize the orientation of adjacent proliferating and invading glial cells at injury sites *in vivo*.

ECM is also known to serve as reservoirs for cell secreted growth factors [59] and astrocytes have been shown to secret a variety of neurotrophic factors such as NGF, FGF, and IGF [52]. Thus upon construct degradation, these growth factors could be potentially released and acted as inductive cues to modulate surrounding cell functions. Moreover, acellular ECM based biomaterials have been shown to result in superior regeneration outcome when compared to cellularized biomaterials [53]. In contrast to the predominantly M1 inflammatory macrophage phenotype seen at the implantation site induced by the cellular grafts, acellular ECM grafts resulted in a primarily M2 antiinflammatory macrophage phenotype and organized connective tissue remodeling [53]. It has been demonstrated that M1 inflammatory macrophages predominate the lesion site starting 14 days following contusive SCI and cause neurotoxicity to regenerating sensory axons *in vitro* whereas M2 antiinflammatory macrophages

promote axonal outgrowth on inhibitory substrates *in vitro* [58].Thus, implantation of astrocyte derived acellular ECM constructs following SCI could potentially increase the M2/M1 macrophage ratio at the injury site.

In addition, presenting tissue specific biological cues to tissue type matched cell types have been shown to be important for maintaining appropriately differentiated cellular characteristics [49,56]. Thus, it might be potentially advantageous using biomaterials derived from neural cells in the CNS for regenerative medicine applications in the CNS due to the fact that they would carry neural tissue specific biological cues

3.5. Conclusions

Both cellularized and acellular oriented astrocyte based biomaterial constructs were engineered *in vitro* in the present study. As oriented astrocyte based biomaterials are capable of organizing proliferating glial cell orientation and guiding neuronal pathfinding and might carry a network of neural tissue specific biological cues, these *in vitro* results suggest the possible therapeutic applications of these oriented astrocyte based biomaterials as novel tissue engineered bridging device for SCI repair.

3.6 Acknowledgement

The authors thank Elena Budko, M.D., for assistance and thoughtful discussion. We also thank Brian Baker for his help for fabricating microprinting devices. We acknowledge funding support from NIH 5R01NS57144.

3.7References

1. Suzuki M, Raisman G. The glial framework of central white matter tracts: Segmented rows of contiguous interfascicular oligodendrocytes and solitary astrocytes give rise to a continuous meshwork of transverse and longitudinal processes in the adult rat fimbria. Glia 1992;6:222-235.

2. Davies SJ, Field PM, Raisman G. Long interfascicular axon growth from embryonic neurons transplanted into adult myelinated tracts. J Neurosci 1994;14:1596-1612.

3. Suzuki M, Raisman G. Multifocal pattern of postnatal development of the macroglial framework of the rat fimbria. Glia 1994;12:294-308.

4. Davies SJ, Fitch MT, Memberg SP, Hall AK, Raisman G, Silver J. Regeneration of adult axons in white matter tracts of the central nervous system. Nature 1997;390:680-683.

5. McKeon RJ, Schreiber RC, Rudge JS, Silver J. Reduction of neurite outgrowth in a model of glial scarring following CNS injury is correlated with the expression of inhibitory molecules on reactive astrocytes. J Neurosci 1991; 11:3398-3411.

6. Davies SJ, Goucher DR, Doller C, Silver J. Robust regeneration of adult sensory axons in degenerating white matter of the adult rat spinal cord. J Neurosci 1999;19:5810-5822.

7. Rudge JS, Silver J. Inhibition of neurite outgrowth on astroglial scars *in vitro*. JNeurosci 1990;10:3594-3603.

8. McKeon RJ, Höke A, Silver J. Injury-Induced proteoglycans inhibit the potential for laminin-mediated axon growth on astrocytic scars. Exp Neurol 1995; 136:32-43.

9. Lochter A, Vaughan L, Kaplony A, Prochiantz A, Schachner M, Faissner A. J1/tenascin in substrate-bound and soluble form displays contrary effects on neurite outgrowth. J Cell Biol 1991;113:1159-1171.

10. Schnell L, Schwab ME. Axonal regeneration in the rat spinal cord produced by an antibody against myelin-associated neurite growth inhibitors. Nature 1990; 343:269-272.

11. Bradbury EJ, Moon LD, Popat RJ, King VR, Bennett GS, Patel PN, et al. Chondroitinase ABC promotes functional recovery after spinal cord injury. Nature 2002;416:636-640.

12. Chen MS, Huber AB, van der Haar ME, Frank M, Schnell L, Spillmann AA, et al. Nogo-A is a myelin-associated neurite outgrowth inhibitor and an antigen for monoclonal antibody IN-1. Nature 2000;403:434-439.

13. Davies JE, Huang C, Proschel C, Noble M, Mayer-Proschel M, Davies SJ. Astrocytes derived from glial-restricted precursors promote spinal cord repair. J Biol 2006;5:7.

14. Davies JE, Pröschel C, Zhang N, Noble M, Mayer-Pröschel M, Davies SJ. Transplanted astrocytes derived from BMP- or CNTF-treated glial-restricted precursors have opposite effects on recovery and allodynia after spinal cord injury. J Biol 2008;7:24.

15. Li Y, Field PM, Raisman G. Regeneration of Adult Rat Corticospinal Axons Induced by Transplanted Olfactory Ensheathing Cells. J Neurosci 1998;18: 10514-10524.

16. Li Y, Carlstedt T, Berthold CH, Raisman G. Interaction of transplanted olfactory-ensheathing cells and host astrocytic processes provides a bridge for axons to regenerate across the dorsal root entry zone. Exp Neurol 2004;188: 300-308.

17. Reier PJ. Penetration of grafted astrocytic scars by regenerating optic nerve axons in xenopus tadpoles. Brain Res 1979;164:61-68.

18. Singer M, Nordlander RH, Egar M. Axonal guidance during embryogenesis and regeneration in the spinal cord of the newt: The blueprint hypothesis of neuronal pathway patterning. J Comp Neurol 1979;185:1-21.

19. Zukor KA, Kent DT, Odelberg SJ. Meningeal cells and glia establish a permissive environment for axon regeneration after spinal cord injury in newts. Neural Dev2011;6:1.

20. Recknor JB, Recknor JC, Sakaguchi DS, Mallapragada SK. Oriented astroglial cell growth on micropatterned polystyrene substrates. Biomaterials 2004; 25:2753-2767.

21. Biran R, Noble MD, Tresco PA. Directed nerve outgrowth is enhanced by engineered glial substrates. Exp. Neurol 2003;184:141-152.

22. Sørensen A, Alekseeva T, Katechia K, Robertson M, Riehle MO, Barnett SC. Long-term neurite orientation on astrocyte monolayers aligned by microtopography. Biomaterials 2007;28:5498-5508.

23. Deumens R, Koopmans GC, Den Bakker CG, Maquet V, Blacher S, Honig WM, et al. Alignment of glial cells stimulates directional neurite growth of CNS neurons *in vitro*. Neurosci 2004;125:591-604.

24. Alexander JK, Fuss B, Colello RJ. Electric field-induced astrocyte alignment directs neurite outgrowth. Neuron Glia Biol 2006;2:93-103.

25. Tom VJ, Doller CM, Malouf AT, Silver J. Astrocyte-associated fibronectin is critical for axonal regeneration in adult white matter. J Neurosci 2004;24:9282-9290.

26. Dusart I, Schwab ME. Secondary cell death and the inflammatory reaction after dorsal hemisection of the Rat spinal cord. Eur J Neurosci 1994;6:712-724.

27. Fitch MT, Doller C, Combs CK, Landreth GE, Silver J. Cellular and molecular mechanisms of glial scarring and progressive cavitation: *in vivo* and *in vitro* analysis of inflammation-induced secondary injury after CNS trauma. J Neurosci 1999;19:8182-8198.

28. Teng YD, Lavik EB, Qu X, Park KI, Ourednik J, Zurakowski D, et al. Functional recovery following traumatic spinal cord injury mediated by a unique polymer scaffold seeded with neural stem cells. Proc Natl Acad Sci USA 2001;99: 3024-3029.

29. Hurtado A, Cregg JM, Wang HB, Wendell DF, Oudega M, Gilbert RJ, et al . Robust CNS regeneration after complete spinal cord transection using aligned poly-l-lactic acid microfibers. Biomaterials 2011;32:6068-6079.

30. Lu H, Hoshiba T, Kawazoe N, Chen G Autologous extracellular matrix scaffolds for tissue engineering. Biomaterials 2011; 32(10):2489-2499.

31. Hudson TW, Zawko S, Deister C, Lundy S, Hu CY, Lee K, Schmidt CE. Optimized acellular nerve graft is immunologically tolerated and supports regeneration. Tissue Eng 2004;10(11-12):1641-1651.

32. Wang JJ, Chuah MI, Yew DT, Leung PC, Tsang DS. Effects of astrocyte implantation into the hemisected adult rat spinal cord. Neurosci 1995;65:973-981.

33. Wunderlich G, Stichel CC, Schroeder WO, Müller HW. Transplants of immature astrocytes promote axonal regeneration in the adult rat brain. Glia 1994;10:49-58.

34. Kliot M, Smith GM, Siegal JD, Silver J. Astrocyte-polymer implants promote regeneration of dorsal root fibers into the adult mammalian spinal cord. Exp Neurol 1990;109:57-69.

35. Misson JP, Edwards MA, Yamamoto M, Caviness VS Jr. Identification of radial glial cells within the developing murine central nervous system: studies based upon a new immunohistochemical marker. Brain Res Dev Brain Res 1988;44:95-108.

36. Voigt T. Development of glial cells in the cerebral wall of ferrets: Direct tracing of their transformation from radial glia into astrocytes. J Comp Neurol 1989;289:74-88.

37. Silver J, Lorenz SE, Wahlsten D, Coughlin J. Axonal guidance during development of the great cerebral commissures: Descriptive and experimental studies, *in vivo*, on the role of preformed glial pathways. J Comp Neurol 1982; 210:10-29.

38. Silver J, Edwards MA, Levitt P. Immunocytochemical demonstration of early appearing astroglial structures that form boundaries and pathways along axon tracts in the fetal brain. J Comp Neurol 1993; 328(3): 415-436.

39. Silver J, Rutishauser U. Guidance of optic axons *in vivo* by a preformed adhesive pathway on neuroepithelial endfeet. Dev Biol 1984;106:485-499.

40. Cummings DM, Malun D, Brunjes PC. Development of the anterior commissure in the opossum: Midline extracellular space and glia coincide with early axon decussation. J Neurobiol 1997;32:403-414.

41. Liesi P, Silver J. Is astrocyte laminin involved in axon guidance in the mammalian CNS? Dev Biol 1988;130:774-785.

42. Neugebauer KM, Tomaselli KJ, Lilien J, Reichardt LF. N-cadherin, NCAM, and integrins promote retinal neurite outgrowth on astrocytes *in vitro*. J Cell Biol 1988;107:1177-1187.

43. Fallon JR. Preferential outgrowth of central nervous system neurites on astrocytes and Schwann cells as compared with nonglial cells *in vitro*. J Cell Biol 1985;100:198- 207.

44. Smith GM, Rutishauser U, Silver J, Miller RH. Maturation of astrocytes *in vitro* alters the extent and molecular basis of neurite outgrowth. Dev Biol 1990; 138:377-390.

45. Brook GA, Plate D, Franzen R, Martin D, Moonen G, Schoenen J, et al.. Spontaneous longitudinally orientated axonal regeneration is associated with the Schwann cell framework within the lesion site following spinal cord compression injury of the rat. J Neurosci Res 1998; 53:51-65.

46. Tessier-Lavigne M, Goodman CS. The molecular biology of axon guidance.Science 1996;274:1123-1133.

47. Li Y, Decherchi P, Raisman G. Transplantation of olfactory ensheathing cells into spinal cord lesions restores breathing and climbing. J Neurosci 2003; 23:727-731.

48. McCarthy KD, de Vellis J. Preparation of separate astroglial and oligodendroglial cell cultures from rat cerebral tissue. J Cell Biol 1980;85:890-902.

49. Kerschensteiner M, Schwab ME, Lichtman JW, Misgeld T. *In vivo* imaging of axonal degeneration and regeneration in the injured spinal cord.Nat Med 2005;11:572-577.

50. Badylak SF, Obermiller J, Geddes L, Matheny R. Extracellular matrix for myocardial repair. Heart Surg Forum 2002;6:E20–26.

51. Taipale J, Keski-Oja J. Growth factors in the extracellular matrix. FASEB J 1997;11:51-59.

52. . Müller HW, Junghans U, Kappler J. Astroglial neurotrophic and neurite-promoting factors.Pharmacol Ther 1995;65:1-18.

53. Brown BN, Valentin JE, Stewart-Akers AM, McCabe GP, Badylak SF. Macrophage phenotype and remodeling outcomes in response to biologic scaffolds with and without a cellular component.Biomaterials 2009;30:1482-1491.

54. Badylak SF, Gilbert TW. Immune response to biologic scaffold materials.Semin Immunol 2008;20:109-116.

55. Meng F, Hlady V, Tresco PA. Inducing alignment in astrocyte tissue constructs by surface ligands patterned on biomaterials. Biomaterials2012 ;33:1323-1335.

56. Zhang Y, He Y, Bharadwaj S, Hammam N, Carnagey K, Myers R, et al. Tissue-specific extracellular matrix coatings for the promotion of cell proliferation and maintenance of cell phenotype. Biomaterials 2009;30:4021-4028.

57. Takahashi H, Nakayama M, Shimizu T, Yamato M, Okano T. Anisotropic cell sheets for constructing three-dimensional tissue with well-organized cell orientation. Biomaterials 2011;32:8830-8838.

58 Kigerl KA, Gensel JC, Ankeny DP, Alexander JK, Donnelly DJ, Popovich PG. Identification of two distinct macrophage subsets with divergent effects causing either neurotoxicity or regeneration in the injured mouse spinal cord.J Neurosci 2009. 29:13435-44.

[59] Heck N, Garwood J, Schütte K, Fawcett J, Faissner A. Astrocytes in culture express fibrillar collagen. Glia 2003. 41:382-392.

[60] Williams C,Tsuda Y, Isenberg BC, Yamato M, Shimizu T, Okano T, et al. Aligned cell sheets grown on thermo-responsive substrates with microcontact printed protein patterns. Adv Mater 2009. 21:2161-2164.

CHAPTER 4

MENINGEAL FIBROBLAST-BASED BIOMATERIALS FOR DURAL REGENERATION

4.1 Introduction

4.1.1 Dural Defect

Dura mater is the outermost layer of the meninge tissue and dural defects often occur as a result of trauma resection and other surgical procedures [1-3]. The consequence of such injury is the exposure of underlying isolated central nervous system (CNS) tissue, which increases the possibility of further infections. Thus, it is the general surgical practice to repair dural defects to restore normal tissue homeostasis and barrier functions

On the other hand, a different opinion, based on both experimental and clinical works, supports the idea that dural defect repairs itself without the need of a surrogate replacement [4, 5]. Similar to standard wound healing scenario found in other tissues, inflammatory cell infiltration is observed to first arrive the lesion site, followed by fibroblast proliferation and migration, and new connective tissue deposition becomes the major healing process 1 week following injury [6]. Trotter and colleagues first demonstrated in a clinical study that the dural defect was completely repaired by itself in a few weeks after a partial excision and regenerated dural tissue was not distinguishable from surrounding normal dura

[5]. The same conclusion is also supported by others based on their study on dogs [4].

Although some researchers hold the idea that dural defects self-repair and it is unnecessary to replace the defect area with foreign materials, serious complications associated with dural defects have been reported in the literature. Meningocerebral adhesion is one common dural defect associated complication. It occurs due to the formation of adhesions between exposed brain tissue and overlying skull lining connective tissue layer [7] and this adhesion formation is involved in inducing posttraumatic epilepsy [7, 8]. Cerebral fungus is another complication associated with dural defects [9], which increases the tendency of brain tissue herniation through the wounded site. The craniocerebral erosion is a rather rare pathological condition related to dural defects where skull erosions are observed in areas corresponding to underlying dural defects [10] The most serious pathological complication accompanying dural defects are meningitis and/or extradural abscess, which occur as a result of bacterial infection from the cerebrospinal fluid (CSF) leakage induced secondary contamination[11].

Due to the occurrence of the above mentioned complications, replacing dural defects with grafting materials appears the dominant opinion among neurosurgeons. It was stated by Teng and Feign that “The chief purpose of using a dural substitute in neurosurgery is to prevent adhesions between the exposed brain and the overlying soft tissues rather than to fill the defect in the severed dura mater.“ [12]

Ideal materials as dural substitutes were sought beginning in the early 19th century and a variety of biomaterials have been evaluated for suitability to repair such defects.

4.1.2 Non-Natural Materials as Dural Substitutes

4.1.2.1 Inorganic materials as dural substitutes. Different inorganic metallic foils were first explored as potential dural substitutes because they are thin, soft and have smooth surfaces [7, 8, 13-17]. Gold foil was the first metallic material proposed as dural substitutes to prevent the formation of meningocerebral adhesions that causes postoperative epilepsy and the surgical procedure was performed in a patient [13]. However, the patient was readmitted due to the returned convulsion. This recurrence of convulsion following gold foil implantation has also been reported by others [14]. Silver foil was shortly pursued by neurosurgeons as dural surrogates for the same purpose. In a study, the patient was released after duraplasty and remained healthy for at least 1 year [7]. Tantalum foils were studied in the 1940s as potential dural surrogates [15, 16]. Although a dense fibrous encapsulation around the tantalum foil was observed in dogs, a clinical study showed only fine and thin fibrous envelope enclosing the graft, which made the authors advocate the use of tantalum foils for dural defect repair in humans [16]. A comprehensive study was done by Chao and colleagues where the performance of a number of metallic materials as dural substitutes was compared, including aluminium, silver, nickel and stainless steel foils [8]. It was found that although meningocerebral adhesions are avoided following implantation, these metallic foils generally induce a strong tissue

response, including dense connective tissue envelopes, presence of foreign body giant cells and cerebral scar tissue formation. While metallic foils were popular materials in the early 19th century for preventing postoperative adhesions, their use was soon discontinued due to the strong foreign body responses.

4.1.2.2 Synthetic materials as dural substitutes. Rubber tissue was the first synthetic material investigated for dural repair to prevent meningocerebral adhesions and epilepsy [18, 19]. While Abbe and colleagues reported a dense development of granulation tissue around the implant, which eventually broke the rubber and enclosed the fragments, Haynes and colleagues used similar rubber material to repair defects after a spinal cord tumor removal and reported that the patient were recovered uneventfully [19]. Polyethylene (PE) films were explored as dural substitutes as it was suggested that a versatile material would be needed for different duraplastic surgery situations [20]. The material was applied on dogs and monkeys where only nonadherent, neomembranes were found around the grafts and no foreign body giant cells were observed. It was also successfully applied in humans [20].

The synthetic acrylic fiber Orlon has also been evaluated as dural surrogates on monkeys [21]. The Orlon was found loosely adherent to the skull without fibrous encapsulation and foreign body giant cell presence. However, Orlon was found firmly attached to the bone 15 months after surgery. Clinically, a patient who received an Orlon implant was reported to remain healthy for at least 3 months. In addition, Vinyon N was tested as dural substitutes on monkeys with either intact or injured brain tissues [12]. The authors reported that no

meningocerebral adhesions or convulsions were found following implantation even in animals with injured cortical tissues and the materials could be easily separated from the cortex.

Expanded polytetrafluoroethylene (ePTFE) is a nonabsorbable material extensively studied both experimentally and clinically for repairing dural defects [22-24]. In one clinical study with 34 patients, ePTFE dural substitutes were sutured to the defect site and later on easily detached from the overlying connective tissue layer during reoperation. Microscopically, ePTFE was found to be encapsulated by a thin sheet of connective tissue and in associations with minimal adhesions [24]. Recently, the feasibility of a modified version of ePTFE dural substitutes, GORE PRECLUDE® MVP®, was examined [25]. One side of the modified ePTFE is engineered to facilitate fibroblast migration and proliferation while the other surface limits cell/tissue adhesion. The material was used as “underlay” graft in 59 patients with at least 4 months follow-up and good recovery outcome was reported for all patients. However, a higher rate of wound related complications was noticed, which the authors claimed can be avoided by close positioning of the graft to the overlying dural tissue.

Hydrogels made of poly-hydroxyethylmethacrylate (poly-HEMA) as dural surrogates have also been investigated [26]. HEMA hydrogels were used as overlay dural repairing materials without suturing in rats with damaged brain tissues. Neither adhesion formation nor CSF leakage was observed in animals that received hydrogel implantation whereas mild to severe brain herniation was seen in sham operated animals.

The performance of biosynthetic cellulose for dural defects repair hasalso been evaluated and reported [27]. Biosynthetic cellulose was found to effectively prevent meningocerebral adhesions and convulsions even when underlying brain tissues were damaged. However, moderate fibrosis enclosing the graft was observed, which caused the cellulose graft adherent to the bone.

Recently, Xie and colleagues investigated the therapeutic potential of radially aligned poly (ε-caprolactone) nanofibers for repairing dural defects[28]. They showed that radially aligned nanofibers facilitated dural cell migration to the graft center *in vitro*; however, no *in vivo* data were reported. Kurpinski and Patel studied both random and aligned nanofibrous dural substitutes and reported that neither adhesions nor inflammatory response adjacent to or at the implantation sites was found in all groups except along the suture line where the graft was sutured [29]. In particular, the authors found that aligned nanofibrous dural substitutes induced a more consistent and thicker connective tissue deposition than random substitutes across the durotomy site.

Synthetic, biodegradable polymers have been studied as dural substitutes to avoid the chronic inflammatory response commonly associated with non-absorbable materials. Vicryl (polyglactin 910) was found to be significantly absorbed 40 days following implantation in dogs with little meningocerebral adhesions and modest inflammatory response noticed [30]. The graft zone was completely replaced by fibrous tissue deposition and no chronic inflammatory response was observed. Gelfoam, a gelatin based natural biodegradable

material, was also evaluated in the same study and appeared to elicit a similar but greater inflammatory reaction [30].

Synthetic dural substitutes made of GM972 (i.e., composite material composed of 50% polylactic acid/50% caprolactone and polyglycolide acid nonwoven fabric) was found to be completely absorbed within24 weeks with no adhesions noticed. In addition, the authors reported that no inflammatory response associated with graft degradation was observed [31]. Clinically, no patients were reported to suffer from infection following GM972 implantation and CT scan showed no abnormal signs surrounding implantation site during a 2-12-month follow-up [32]. However, it was shown in a separate clinical study that some patients experienced subcutaneous CSF accumulation, hemorrhage or tumor recurrence and needed reoperation [33].

4.1.2.3 Complications associated with synthetic dural substitutes. While synthetic materials are widely used for duraplasty, there are still concerns regarding their safety. In 1983, Adegbite and colleagues reported a case of post-operative complication in association with silastic dural substitutes that were implanted to repair dural defects generated due to meningioma removal [34]. The patient was experiencing headaches, mental deterioration and confusion. The symptoms were attributed to the hematoma formation in the neomembrane enclosing the silastic dural substitute. Similar pathologies associated with the use of silastic material for dural reconstruction have also been reported by other studies [35-37]. Since the loosely adherent neomembrane is often observed around silastic dural substitutes, it is proposed that the formation of hematoma is

due to the breakage of vessels in the neomembrane, caused by relative movement between the surrounding connective tissue and the silastic material [38]. Hematoma formation has also been observed in one patient who received Dura Film (i.e., silicone-coated Dacron) to repair a defect after tumor removal [39]. In a separate case, the development of thick connective sheath associated with silastic substitutes was postulated to stimulate recurrent tumor 4 years after the patient's first surgery for tumor removal [39]. Recurrence of meningioma has also been reported due to progressive compression to the brain tissue generated by the growing fibrous tissue 20 years after a patient received Marlex mesh (i.e., crystalline polypropylene and high-density polyethylene) following tumor removal [40]

Although Neuropatch®(i.e., purified polyester-urethane)has been reported to be a suitable material for dural defect repair in a clinical study [41], it has also been documented in the literature that it causes a higher incidence of wound site infection than pericranium grafts [42]. Despite the fact that the higher infection rate is not significant, Neuropatch is reported to be in association with a significantly higher CSF leakage rate [42]. Additionally, Neuropatch has been reported to be associated with either tumor recurrence or intense inflammatory reactions due to bacterial contamination [43]. Recently, Huang and colleagues reported that, instead of inducing a higher rate of wound site infection and CSF leakage, Neuropatch increases the chance of hematoma formation [44].

4.1.3 Natural Materials as Dural Substitutes

4.1.3.1 Animal membranes as dural substitutes. In 1938, Glaser and Thienes studied the possibility of using either heteroplastic or autoplastic membranes as dural substitutes [45]. The authors reported that the inflammatory reaction associated with both types of membranes was still evident after 9 months and both materials were then incorporated by 12 months. Only slight adhesion formation was seen when the underlying brain tissue was damaged. Chao and colleagues compared a series of animal membranes for dural defect replacement on cats with injured pia mater [8]. Among all materials tested, they recommended the use of aminotic membranes for human clinical studies based on their observations that aminotic membranes induced the least adhesion formation and were incorporated to form new dural tissue. Carglie membranes, on the other hand, were found to stimulate dense adhesion formation when the underlying pia mater was damaged [8]. Contrary to Chao's observation, Pudenz and Odom reported that, instead of preventing adhesions, different types of aminotic membranes(i.e., viable, fixed, attenuated) actually stimulated adhesion formation [17]. Their conclusions were supported by another study [46].

Lyophilized human cadaveric dura was a popular dural surrogate in the 1960s [47-50]. In general, inflammatory response is found in association with the lyophilized dura for the first few weeks, then the material is infiltrated by fibroblasts along the natural pores of the graft and gradually replaced by fibrous tissue in several months [47, 48]. The application of such materials has been

reported to have low incidence of infection, low CSF leakage rate and minimal foreign body response in clinical studies [49, 50].

The usefulness of acellular dermal graft from human cadaveric skin as dural substitutes has also been explored [51-53]. Faster incorporation of acellular dermal grafts by native dural tissue has been observed when compared to autologous pericranium grafts in minipigs [51]. Histologically, acellular dermal grafts have been reported to result in deposition of organized, fibrous structure similar to the native dura whereas autologous pericranial tissue leads to disorganized collagen fiber deposition. When tested clinically, the material has been reported to be associated with similar infection rate as autologous tissue and low incidence of CSF leakage was noted [52].

Based on the successful applications of small intestinal submucosa (SIS) in repairing soft tissues, SIS has been examined as dural substitutes [54, 55]. SIS has been found to induce significantly more vascularization following implantation compared to control sites where dural defects were left open [54, 55]. The predominant cell type seen populating the grafted area following SIS resorption has been shown to be spindle shaped, mesenchymal cells [54].

Glutaraldehyde fixed porcine peritoneum has been reported to facilitate water tight closure when used for dural repair in dogs [56]. No meningocerebral adhesions were observed following implantation. However, the peritoneal membrane was found to form adhesions to the overlying temporal muscle layer. Fibrous encapsulation and neovascularization around the implant were also noticed and, in some animals, chronic inflammatory response was seen.

Although glutaraldehyde fixed porcine peritoneum was shown to be suitable for dural closure in animal studies, the glutaraldehyde fixation process has been found to cause the hyperthermic reaction in humans [56]. However, apart from this side effect, patients were reported to experience uncomplicated recovery up to five years.

In addition to porcine peritoneum, pericardium of either porcine or bovine origin are also of interest [50, 57]. The pericardial membrane has been found to undergo similar tissue reactions as the peritoneal graft when applied as dural substitutes in rabbits [57]. In a clinical study, no patients were reported to experience antigenic response following implantation. The autopsy showed fibroblast migration through interstitial pores within the graft with neocollagen deposition and only a small piece of the material was seen after 24 months [50].

While earlier clinical studies showed that autologous fascial grafts were applicable for dural defect repair [58], Tachibana and colleagues evaluated the healing process of the dural tissue following fascial graft implantation experimentally [59]. In particularly, they studied the effect of overlying subcutaneous tissue on facilitating dural regeneration. When compared to ePTFE, defect sites reconstructed by fascial graft held significant higher intracranial pressure. The fascial graft was first encapsulated by dense connective tissues that connected the graft to the surrounding dura mater and then being incorporated. They also observed faster dural tissue regeneration with the presence of overlying subcutaneous tissue; however, dural tissue regeneration without subcutaneous tissue was, although slower, similar.

4.1.3.2 Collagen based products as dural substitutes. Acellular, collagen based materials that are either chemically processed or modified have drawn a lot of attention in the field of duraplasty because they possess several advantages over cellularized animal membranes and cadaveric dura. Collagen is generally considered to be immunologically tolerable between species and its structure acts as scaffolds that support cell migration, proliferation and deposition of new connective tissue. Moreover, they can be easily stored and are relatively inexpensive. These collagen based products also avoid the potential disease transmission that has been reported in association with both cellularized animal membranes and cadaveric dura [71, 72, 74].

Processed collagen films and laminates as dural substitutes were first evaluated by Kline and Jannetta [60, 61]. In both studies, the authors reported that collagen laminates appeared to result in a more intensive fibrosis encapsulation when compared to collagen films and the laminate structure also induced more meningocerebral adhesions. Either collagen films or laminates were found fully degraded following implantation; however, the collagen laminate has been shown to have a slower degradation rate. Foreign body response (FBR) has also been noted in different studies when collagen film laminates were used as dural substitutes [62, 63].

Narotam and colleagues conducted comprehensive studies on using collagen sponge as dural substitutes and described a serious of cellular events following collagen sponge implantation [64, 65]. Microscopically, they observed blood cells and early fibroblastic activities in the sponge and neomembrane

formation during the first 2 weeks. The fibroblast activity and neovascularization were well established by 30 days, which were then followed by collagen sponge resorption and complete incorporation of the material by native dural tissue after 6 months. Similar responses have also been reported in an animal study [64].

Dura-guard®, Duragen® and Durepair® are three commercially available, collagen based dural substitutes of bovine origin [66]. Among these three products, only Durepair® is not chemically crosslinked. Depending on the nature of the original tissues, Duragen® has the largest interstitial pore size (100 μm), followed by Durepair® (10-20 μm) and Dura-guard® (5 μm). When tested in dogs, the interstitial pore size was found to play an important role in affecting substitute degradation where Duragen® degraded the fastest (1 month), followed by Durepair® (6 months) and Dura-guard remained largely intact even after 6 months. Similarly, Dura-guard® has been shown to remain intact after 6 months in rabbits with strong fibrosis encapsulation, which was suggested to cause compression to the rabbit brain tissue [67].

Tissudura® is another commercially available collagen based dural substitute that is transparent and primarily composed of uncrosslinked equine type I collagen. It has been applied both in experimental animals and human subjects [68-70]. In sheep, Tissudura® has been shown to induce an intensive acute inflammatory response, followed by graft degradation and the continuity between the native dura mater and newly deposited collagen matrices was well established after 8 weeks [68]. In clinical studies, CT scan and MRI were used to detect CSF leakages, signs of infection and graft rejection in patients who

received Tissudura®[69, 70]. Parlato and colleagues reported no such complications were found during a 1-year follow-up [70] whereas several cases of CSF leakage were reported by Gazzari and colleagues as early as 7 days postsurgery [69].

4.1.3.3 Complications and limitations associated with natural dural substitutes. While lyophilized, cadaveric dura has been applied as dural substitutes with low incidence of postoperative complications [47-50], its association with the Creutzfedlt-Jacob disease (CJD), which causes infected brain tissue developing holes and turning into sponge-like structure, has been reported [71, 72]. In addition, immunogenic reactions developed in patients against the implanted cadaveric dura has also been documented [73]. Moreover, the preparation and storage of such material are time consuming and expensive.

Autologous grafts, such as fascia lata, temporalis fascia and pericardium, have the advantage over xenografts and allografts as they are nonimmunogenic. However, the availability of autologous grafts is limited and may be insufficient when the dural defect area is large. Additionally, a second surgical operation is needed for graft harvesting, which would prolong the surgical and anesthetic time and may lead to painful donor sites.

Cellularized animal membranes, which have abundant availability, have been reported to induce intensive adhesion formation [8, 17]. The possibility of disease transmission or material associated immunogenicity also limits their application [74, 75]. Besides animal membranes, different forms of human aminotic membranes (e.g., viable, defatted, boiled, dry) have also been shown to

induce dense cerebromeningeal adhesions and not recommended for clinical use [17, 46].

Collagen based products generally show satisfactory outcomes when used as dural substitutes. They hold several advantages such as inducing minimal inflammatory response, avoiding chronic FBR due to their resorbable nature and acting as biological scaffolds that support cell proliferation and migration. However, the laminate structure of collagen products has been shown to induce intensive inflammatory reactions, fibrotic encapsulation as well as adhesion formation [60, 61]. Moreover, the natural interstitial pore size within the collagen based dural substitutes also affects the host tissue responses. Among three commercially available collagen products, Dura-guard®, which has the smallest interstitial pore size (5 μm), has been shown to result in fibrosis encapsulation similar to nonresorbable synthetic materials [66].

4.1.4 Advantage of Tissue Specificity in Regenerative Medicine

ECM materials are generally accepted to induce minimal immunogenicity and have been widely applied in regenerative medicine applications [76-78]. Although ECM materials derived from different tissue/organ sources share common protein components, subtle difference still exists, which has been shown to influence cellular functions[79]. Therefore, the idea of using tissue specific ECM that carry appropriate biological cues to facilitate the regeneration of tissues targeted for repair has become increasingly popular [80-84]. Studies have shown that tissue type specific ECM coatings perform superior ability to promote proliferation of tissue type matched cell types and maintain appropriate

differentiated cellular characteristics as the specific ECM coatings better mimic the native extracellular milieu *in vivo*[82, 83]. The importance of the specificity of acellular ECM scaffolds has also been emphasized by a study where implantation of ECM materials derived from a different tissue origin resulted in formation of foreign tissue types at the repair site [85]. It is believed that the foreign tissue formation is due to the presence of inappropriate biological cues introduced by the implanted ECM materials, which fails to provide tissue specific regeneration. It has also been demonstrated previously that myocardial tissue matrices promoted migration of both human coronary endothelial cells and rat aortic smooth muscle cells, two myocardial tissue specific cell types [84].

In addition, implantation of acellular, ECM scaffolds, even of allogeneic or xenogeneic sources, has been shown to lead to constructive tissue remodeling in defect areas with infiltrating macrophages being predominantly antiinflammatory M2 phenotype. On the other hand, cellularized grafts have been found to be accompanied by primarily inflammatory M1 macrophages and lead to dense connective tissue deposition and scar formation [86].

Given this knowledge, in the present study, 3D biological constructs were engineered using postnatal day 1 (P1) rat meningeal fibroblasts, the most abundant cell type residing in the meninges tissue, including the dura mater. The constructs were evaluated for suitability as dural substitutes *in vitro*. Indirect immunohistochemistry was used to compare the extracellular matrix protein expression of the engineered constructs to natural adult rat dural mater. Cell

based assays were used to examine the suitability of the construct to support cell adhesion, proliferation and migration into the construct.

4.2. Materials and Methods

4.2.1 Rat Meningeal Fibroblast and Dural Tissue Isolation

Primary postnatal day 1 (P1) rat meningeal fibroblasts were isolated from the cranial meninges of Sprague-Dawley rats as previously described [87]. Briefly, rat meningeal tissue was peeled from the surface of the cerebral cortices, then digested in collagenase for 30 mins (0.33% w/v), followed by 30 mins trypsin-EDTA treatment (0.25% w/v, Invitrogen) and dissociated by repeated trituration in DNase (0.1% w/v, Worthington Biochemical) through a fire-polished pipette. After trituration, dissected cells were plated in T-75cm^2 tissue culture flask (Greiner) in DMEM/F12 containing 10% fetal bovine serum (FBS, Sigma) and grown to confluence. Adult rat cranial dura mater was also prepared by peeling it from the inner surface of the skull from adult Sprague-Dawley rats separately.

4.2.2 Engineering and Harvesting 3D Meningeal Constructs

Primary rat meningeal fibroblasts were seeded on sterilized glass coverslips at a density of 52,000 cells/cm^2 in 10% FBS supplemented with ascorbate-2-phosphate (150 µg/ml, Sigma) and ascorbic acid (50 µg/ml, Sigma) to promote collagen deposition and maturation. After the first meningeal fibroblast layer reached confluence, subsequent seeding was applied on the confluent cell layer at the same density. This seeding process was repeated every other day for 6-8 times. Starting with the third seeding process, half of the

culture medium was replaced with fresh medium supplemented with ascorbate-2-phosphate (150µg/ml) and ascorbic acid (50µg/ml) the day following cell seeding. Dense 3D meningeal constructs were harvested after 12-16 days of culture. Hydrophilic membranes (Cellseed) were put atop of the apical surface of dense meningeal constructs and the constructs were detached from the coverslips by gently peeling off the membrane with forceps. Excess culture medium was added to separate the membranes from recovered constructs. Harvested meningeal constructs were fixed using 4% paraformaldehyde for 15 mins. Several meningeal constructs were harvested without membranes via gently scratching the coverslips surface using forceps and recovered constructs were again fixed with 4% paraformaldehyde.

4.2.3 Decellularization of Engineered Meningeal Constructs

Harvested meningeal constructs with attached membrane were placed in hypotonic Tris-Hcl buffer (10 mM, pH 8.0) with 0.1% EDTA and 10 KIU/ml aprotinin (Sigma) for 1-2 hrs at room temperature (R.T.) to disrupt integrin-ECM interactions and deactivate proteases that were released due to cell body rupture. Then, samples were immersed in Tris-Hcl buffer containing 0.1% sodium dodecyl sulfate (SDS) (10 mM, pH 8.0) on a rocker at 100 rpm at R.T overnight to dissolve lipid membranes with supporting membranes removed. Following SDS treatment, samples were rinsed three times, 30 mins each, in PBS on a rocker. Last, samples were treated with Tri-Hcl buffer (50 mM, pH 7.5) containing ribonuclease (1 U/ml, Sigma) and deoxyribonuclease (50 U/ml, Sigma) on a

rocker at 37oC for 3 hrs to break down DNA and RNA. Samples were again rinsed with PBS three times, 30 mins each, on a rocker.

4.2.4 Cell Culture on Decellularized Meningeal ECM Constructs

Decellularized meningeal ECM constructs were first air-dried in the center of the 35 mm glass-bottom dish (World Precision Instruments). Allogeneic primary rat meningeal fibroblasts were seeded at 35,000 cells/dish in 2 ml DMEM/F12 with 10% FBS. Allogeneic meningeal fibroblasts were cultured for 2 days and then fixed with 4% paraformaldehyde.

4.2.5 Histological Sectioning

Agar powder (Gibco) was dissolved in warm D.I. water to make a final concentration of 0.8% agar solution. Meningeal constructs were placed in a square mold and warm 0.8% agar solution was slowly poured into the mold to cover the samples. The agar solution was then cooled and solidified. Solidified 0.8% agar cubes were removed from the mold with samples embedded and infiltrated in 30% sucrose solution overnight. Agar cubes were then put on cryostat specimen holders at the desired orientation. Tissue freezing medium (Triangle Biomedical Science) was added to cover the agar cubes, and the specimens were placed in the cryostat at -20^{o}C. Specimens were cut transversely into 15 μm thick sections.

4.2.6 Tissue Thickness Measurements

Adult rat native dura mater, as well as 6 and 8 seeding engineered meningeal constructs, were embedded in the agar gel and cryostat sectioned into

15 µm thick sections as described in section 2.5. Image J software was used to measure the thickness of the cross-sections of each embedded sample with a N = 3 from each group.

4.2.7 Quantification of Meningeal Fibroblast Adhesion and Proliferation on Decellularized Meningeal ECM Constructs

Acellular meningeal ECM constructs were first air-dried on 18mm coverslips. For cell adhesion assay, dried ECM constructs were coated with 4% Bovine serum albumin (BSA) solution for 3 hrs at 37^{o}C to block nonspecific cell-ECM interactions and then rinsed with sterile PBS prior cell seeding. Astrocytes and meningeal fibroblasts were seeded at a density of 52,000 cells/cm^2 in 1 ml DMEM/F12 supplemented with 10% FBS for 90 mins and then fixed with 4% paraformaldehyde. Coverslips coated with 4% BSA were seeded with meningeal fibroblasts at the same density for comparison. All groups were rinsed with sterile PBS once prior to cell fixation. DAPI+ cell nuclei were used as the indicator for cell number quantification. Ten 10X fluorescent images were taken at different locations from each coverslip. A built-in function of ImagePro (Media Cybernetics) was used to count the number of DAPI+ nuclei from each image. There were N=3 for each group for analysis.

For cell proliferation assay, meningeal fibroblasts and astrocytes were seeded on the dried meningeal ECM constructs, respectively, at a density of 52,000 cells/cm^2 in 1 ml DMEM/F12 supplemented with 10% FBS for 4 days. Meningeal fibroblasts were also cultured on 10% FBS coated coverslips for comparison. Prior cell fixation, coverslips from all groups were first rinsed with

sterile PBS once. Half of the coverslips from each group were fixed after 2 days and the other half were fixed after 4 days in culture. DAPI+ cell nuclei were used as the indicator for cell number quantification. Ten 10X fluorescent images were taken at different locations from each coverslip. A built-in function of ImagePro (Media Cybernetics) was used to count the number of DAPI+ nuclei from each image. There were N=3 for each group at each time point.

4.2.8 Immunohistochemical Analysis

For intracellular antigens, samples were treated with 0.05% Triton X-100 in PBS for 15 min and then rinsed with PBS. No Triton was applied for immunohistochemical staining for extracellular matrix ligands. When intracellular ligands were co-stained with extracellular ligands, extracellular ligands were always processed first, followed by Triton treatment and then the immunohistochemical reactions for intracellular ligands were processed. For indirect immunohistochemical reactions, cryostat sections were rinsed with PBS to remove tissue freezing medium. Samples were treated with 4% goat serum and 0.1% sodium azide in PBS for 1 hr and then incubated with primary antisera against laminin (LN; Sigma; 1:500), cellular fibronectin (CFN; Sigma; 1:500), chondroitin sulfate proteoglycan (CS-56; Sigma; 1:500) and type-1 collagen (Coll; Sigma; 1:500). Fluorescent dye conjugated secondary antibodies (Molecular Probes) were applied at dilution of 1:500. All antibodies were diluted in 4% goat serum /0.1% azide and applied for 24 hrs at room temperature. Three washes with 30mins each were applied between applications of primary and secondary antisera. DAPI (10 μM; Molecular Probes) was used for cell nuclei visualization.

Tissue sections were mounted on microscope slides covered with Fluormount-G (Southern Biotech), and coverslipped. Images were acquired using a Nikon epifluorescence microscope equipped with a CCD camera (ImagePro) or using an Olympus FVX laser scanning confocal microscope when noted.

4.2.9 Statistical Analysis

All quantitative data were reported as the mean ± standard deviation. One way ANOVA was used to compare the means. p values < 0.05 were considered statistically significant.

4.3. Results

4.3.1 Characterization of Native Adult Rat Dura Mater

Indirect immunohistochemical reactions demonstrated that harvested native adult rat dura mater were positive for several major ECM proteins including type-1 Collagen (Coll), chondroitin sulfate proteoglycan (CSPG), fibronectin (FN) and laminin (LN) (Fig.4-1:A, B, C and D). In particular, the fibrillar structure of type-1 Coll was clearly seen in the rat dura mater. The thickness of adult rat dura mater was approximately 100 µm (Fig. 4-2) and the vasculature network of the rat dura mater can be clearly seen with the LN staining which runs through the tissue (Fig. 4-1:D and F). The multiple layers of DAPI positive cell nuclei shown in the cross-sectional image demonstrated the multilayered cellular structure of the dura mater (Fig. 4-1:E).

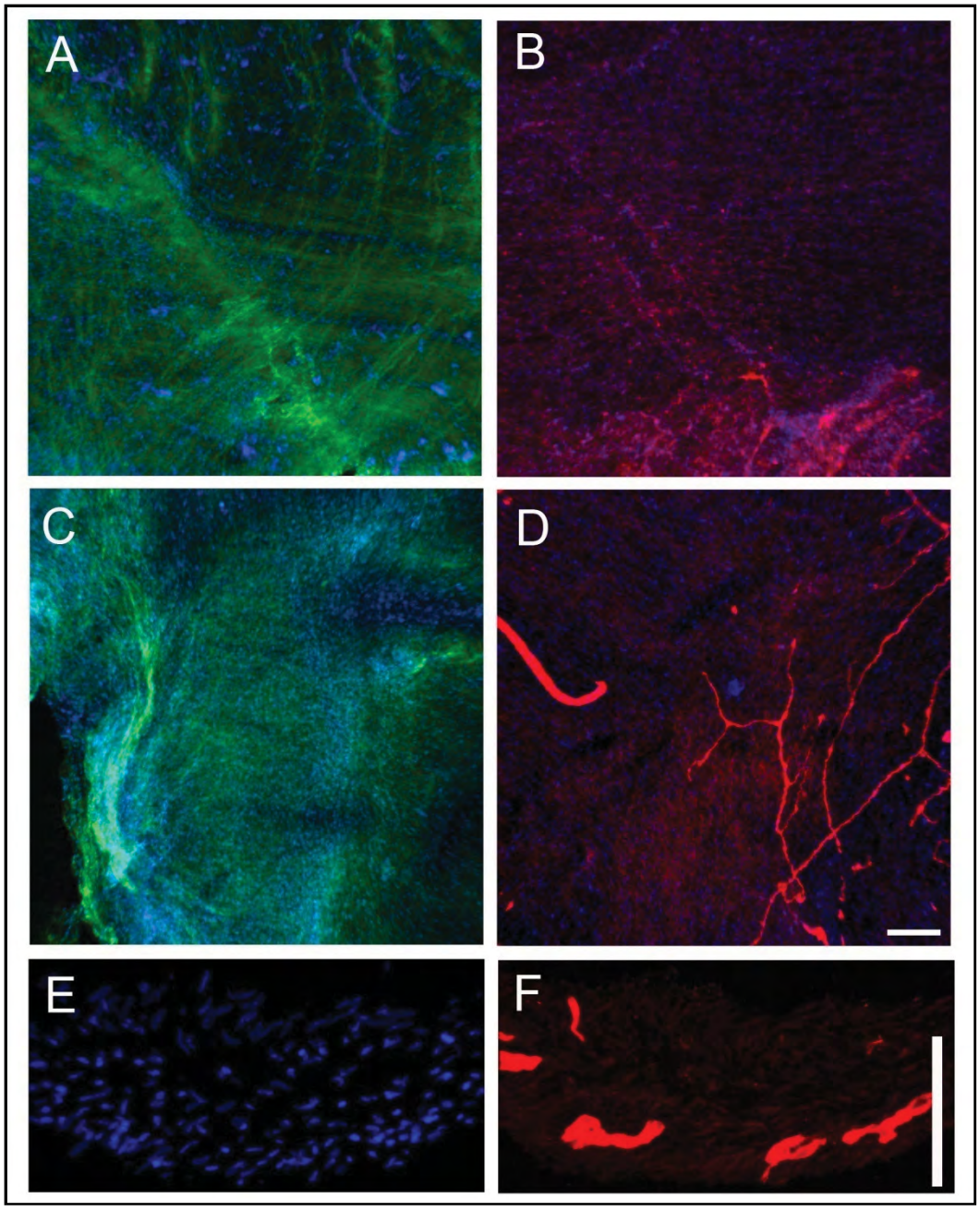

Fig.4-1:Representative extracellular matrix protein profile of native adult rat dural mater, adult rat dural mater was positively reacted with antisera against type-1Coll (A, in green), CSPG (B, in red), FN (C, in green) and LN (D and F, in red). The cross-sectional image of adult rat meninges showed multilayered cellular structure (E). Vasculature network are seen running through in some areas of the dura (D, F). Occasionally, cellular alignment was observed in the dural mater (B, top half of the image). DAPI was used for nuclei observation (A-E, in blue). Scale bar= 100µm in (A-F).

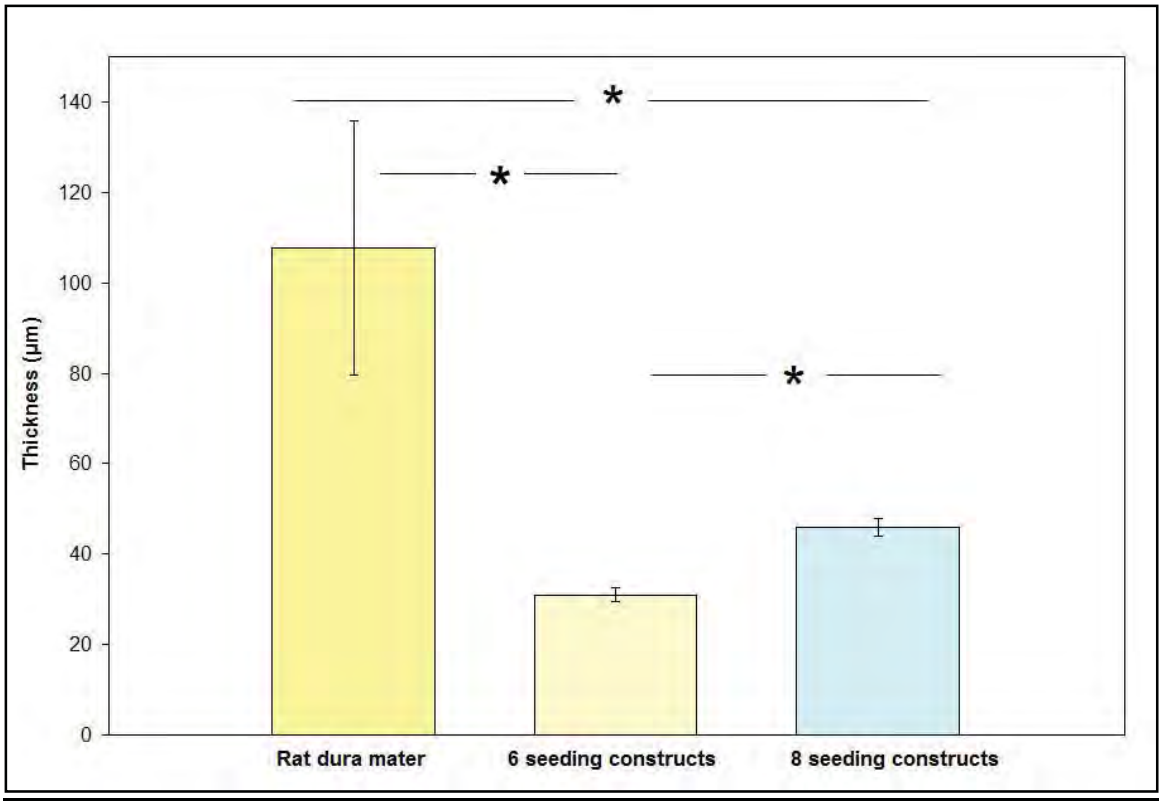

Fig.4-2:Thickness comparison of native adult rat dural mater, 6 seeding and 8 seeding engineered meningeal cell constructs. There was a statistical significant difference in the thickness between any two groups (ANOVA, post hoc, $p<0.05$).

4.3.2 Engineering 3D Multilayered Meningeal Fibroblast Constructs

The procedure of engineering each multilayered meningeal fibroblast construct is illustrated in Fig. 4-3A. Primary rat meningeal fibroblasts were seeded onto clean coverslips in culture medium and the seeding process was repeated every other day for multiple times. The waiting period was determined based on our observation that a confluent cell layer formed on coverslips in 2days at the seeding density used. After 6-8 seedings, a dense cellular construct was established on the coverslip, then a hydrophilic membrane was put on top of the construct and the construct could be separated from the substrate and

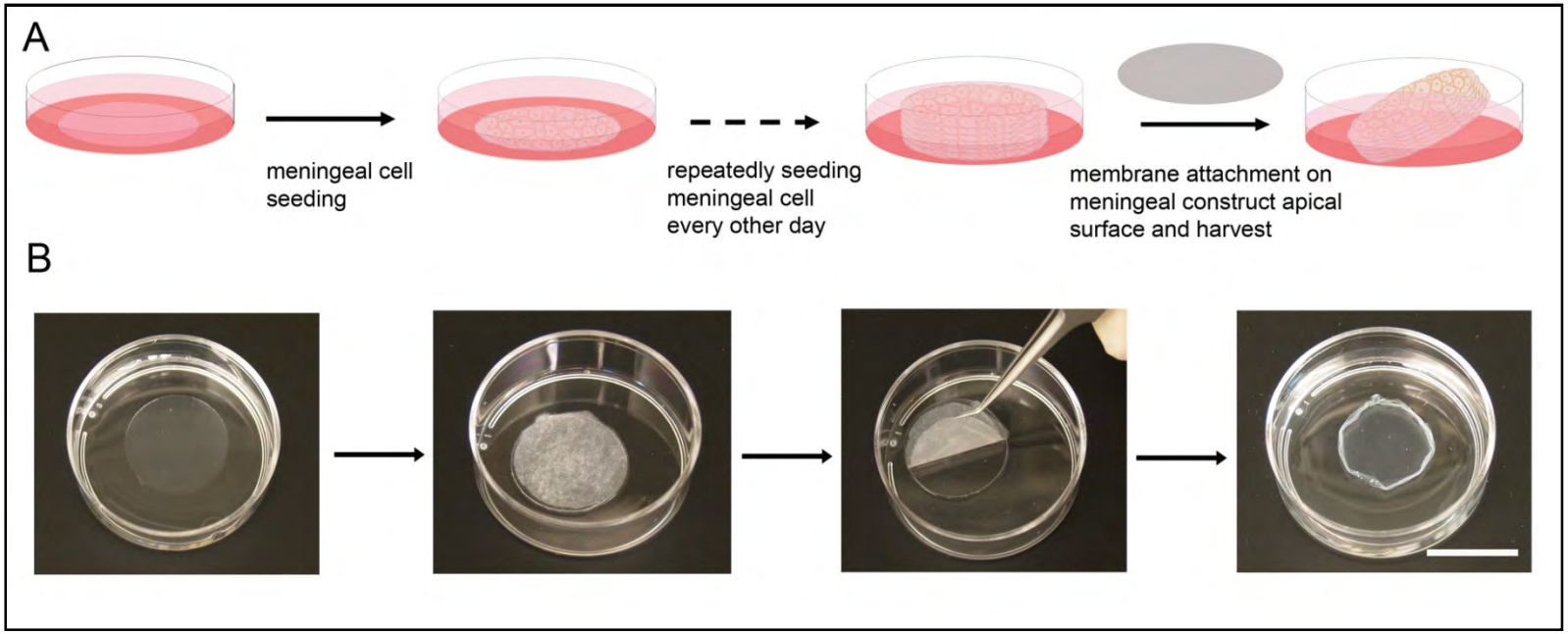

Fig.4-3: Schematic illustration of engineering multilayered, meningeal fibroblast derived constructs. (A) A meningeal fibroblast construct was engineered by repeatedly seeding meningeal fibroblasts on previous cell layers and then recovered with a hydrophilic membrane from a 18mm coverslip. (B) Macroscopic image showing the recovery of a meningeal fibroblast construct from culture substrate with a hydrophilic membrane. Meningeal constructs recovered with hydrophilic membranes maintain the original size without shrinkage. Scale bar=1.5 cm.

harvested by peeling off the membrane against the coverslips with hand-held forceps (Fig. 4-3:B). Meningeal constructs that were recovered with a hydrophilic membrane were able to maintain the size without further shrinkage (Fig. 4-3:B).On the other hand, when the membrane was not applied and the construct were mechanically removed from the coverslips by gently scratching the coverslip surface with forceps, meningeal constructs shrank isotropically (data not shown).

4.3.3 Characterization of Engineered Meningeal Fibroblast Constructs

Engineered meningeal constructs were incubated with immunohistochemical markers for ECM proteins detection. Similar to the ECM protein expression observed in harvested native adult rat meningeal tissue (Fig. 4-1), engineered meningeal constructs also reacted positively with antisera against type-1 Coll, CSPG, FN and LN (Fig. 4-4:A, B, C and D). Cross-sectional images showed the multilayered structure of the engineered meningeal construct and the distribution of ECM proteins throughout the thickness of the construct (Fig. 4-5). The thickness of the engineered constructs increased with the number of cell seedings. There was a significant difference in the thickness between 6 seeding and 8 seeding constructs (Fig. 4-2; ANOVA, post hoc $p<0.05$). There is also a significant difference in the thickness between adult rat dural mater and 6 seeding and 8 seeding constructs, respectively (Fig. 4-2; ANOVA, post hoc $p<0.05$).

.

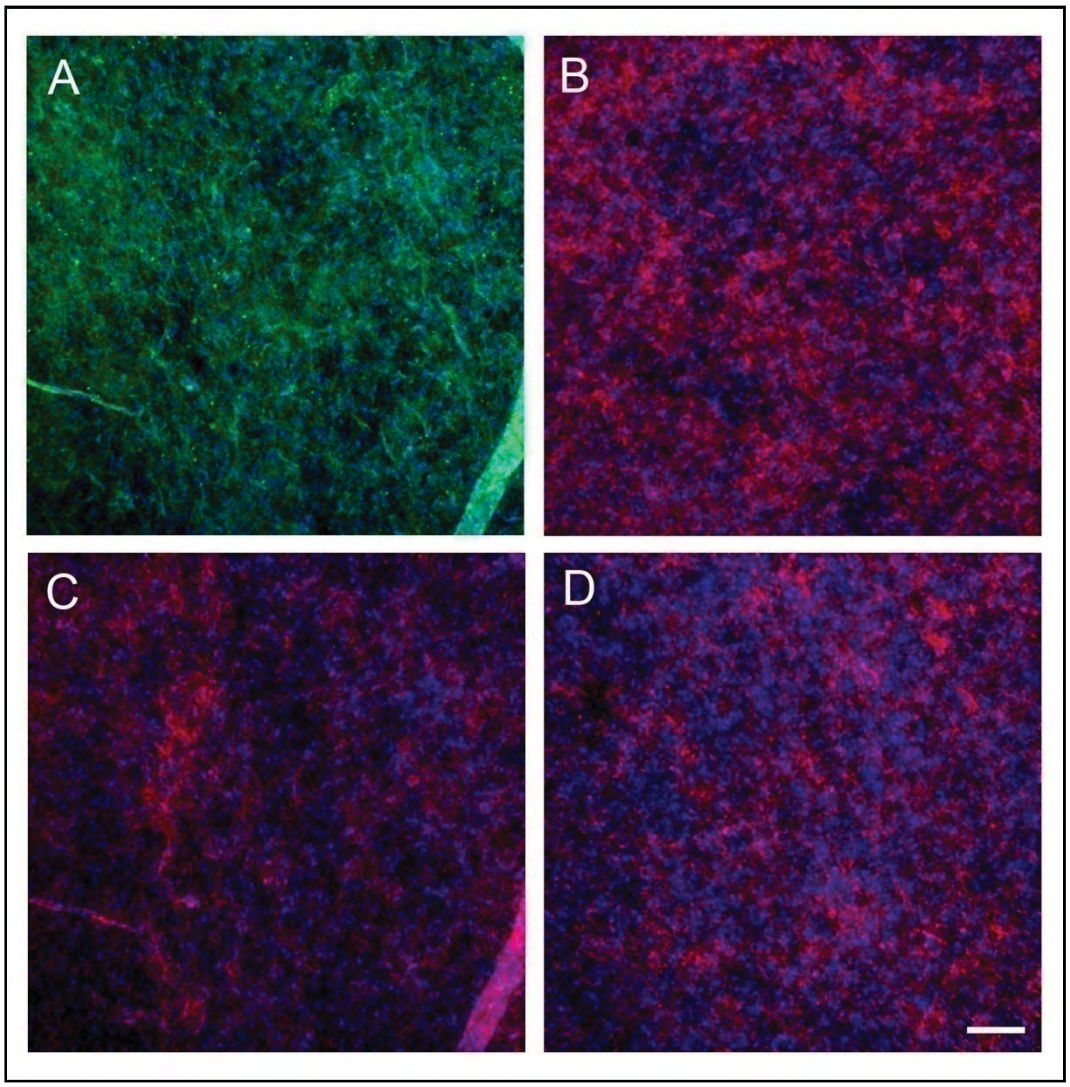

Fig.4-4: Representative extracellular matrix protein profile of engineered meningeal fibroblast constructs. Engineered meningeal constructs had similar expression of major ECM proteins as the natural rat dural mater and were positively reacted with antisera against type-1 Coll (A, in green), CSPG (B, in red), FN (C, in red), LN (D, in red). Scale bar=100 µm.

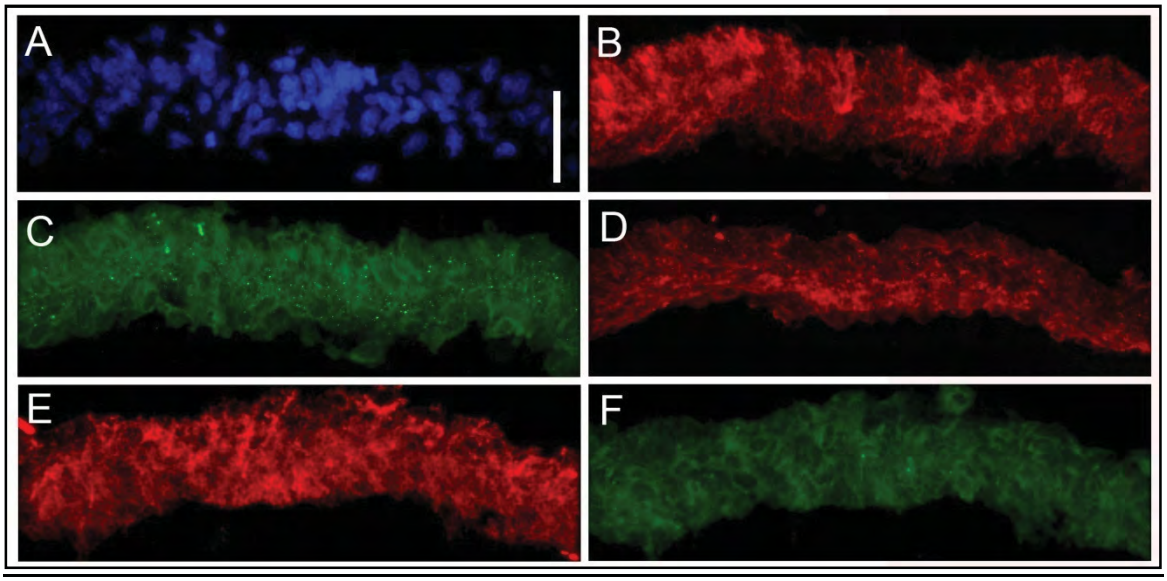

Fig.4-5: Representative cross-sectional images of engineered meningeal fibroblast constructs. Indirect immunohistochemical reactions showed that the examined ECM proteins, FN (B, in red), Coll (C, in green), CSPG (D, in red), LN (E, in red), were distributed throughout the entire engineered constructs. (A) DAPI staining demonstrated the multilayered structure of the engineered constructs. Actin micofilament was used as the cytoskeletal marker for meningeal fibroblasts (F, in green). Scale bar= 50 µm.

4.3.4 Decellularization and Characterization of Acellular Meningeal ECM Constructs

Following harvesting from coverslips with membranes attached, the meningeal constructs were first immersed in hypotonic buffer containing EDTA and protease inhibitors to weaken integrin-ECM interactions and deactivate proteases that were released due to cell body rupture. Then the constructs were treated with 0.1% SDS to remove cellular components, followed by DNase and RNase treatment to break down DNA and RNA. The decellularized meningeal ECM constructs became more transparent following lyophilization when compared with their cellularized counterparts and maintained about the

same size and configuration as the cellular constructs (Fig. 4-6:A and B). All major ECM proteins investigated, including type-1 Coll, CSPG, FN and LN, were preserved within the decellularized meningeal ECM constructs with no positive DAPI+ cell nuclei (Fig. 4-7:A, B, C and D). The presence of actin microfilament, an intracellular cytoskeleton protein, was also investigated to confirm the effectiveness of the decellularization processes. Little to no immunofluorescent signals for actin microfilaments and meningeal fibroblast nuclei were found following decellularization (Fig. 4-7:E) whereas abundant DAPI+ cell nuclei and strong actin filament expression were observed in the cellularized counterparts (Fig. 4-7F).

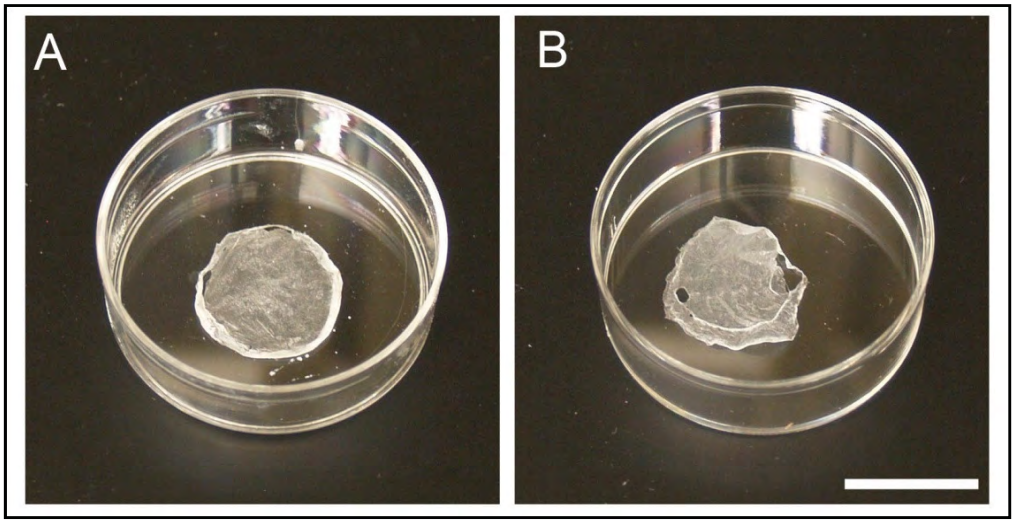

Fig. 4-6: Representative macroscopic images of lyophilized meningeal fibroblast constructs and decellularized, meningeal ECM constructs. (A) A piece of opaque, sheet-like material was obtained following lyophilization of a meningeal cell construct. (B) A lyophilized, acellular meningeal ECM construct maintained a similar size and configuration as the cellularized counterpart; however, appeared to be more transparent. Both biomaterials are mechanically stable and can be handled with hand-hold forceps. Scale bar=1.5 cm

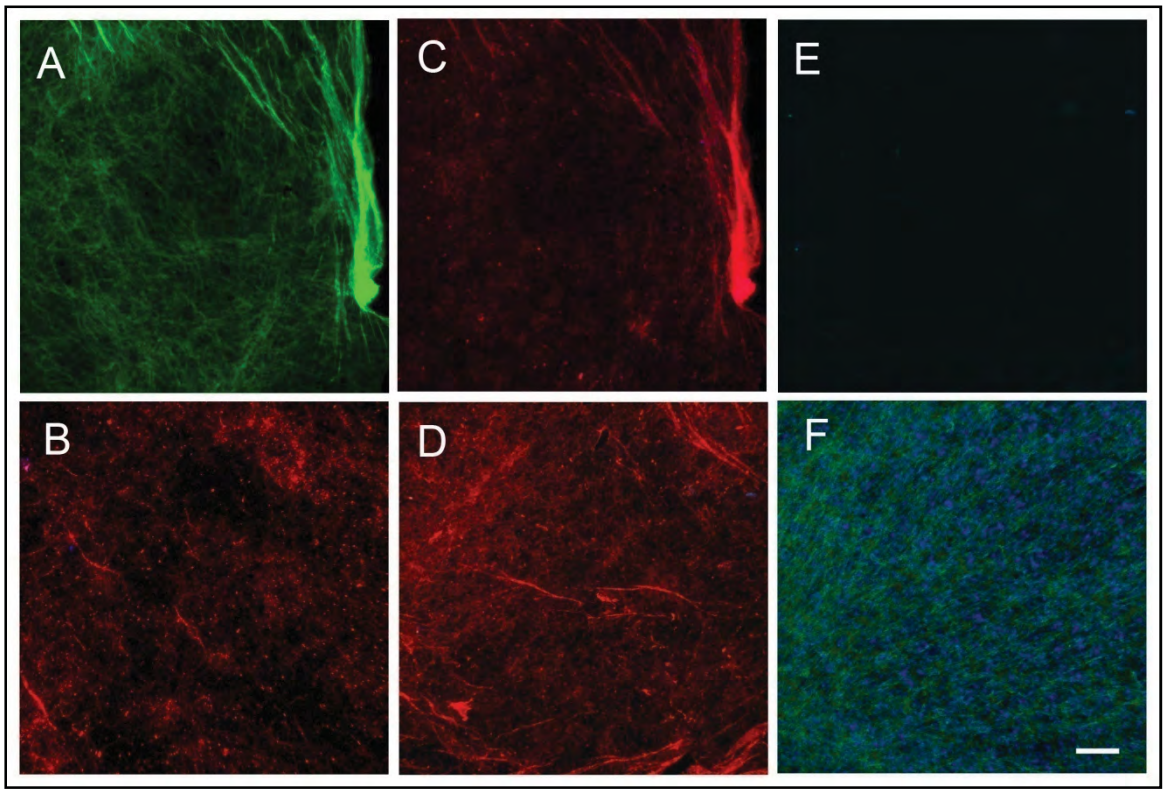

Fig. 4-7: Representative ECM protein profile of decellularized meningeal ECM constructs. Indirect immunohistochemical reactions demonstrated that following decellularization, the acellular ECM constructs were positively stained for type-1 Coll (A, in green), FN (B, in red), CSPG (C, in red) and LN (D, in red), similar to the native adult rat dura mater. In particular, a network of type-1 Coll fibers was clearly seen in the acellular ECM constructs. (E) On the other hand, little to no immunofluorescent signals of actin microfilaments and DAPI+ cell nuclei were observed in the acellular ECM constructs following decellularization. (F) The cellularized meningeal fibroblast constructs were positively stained for intracellular cytoskeletal protein, actin microfilaments (in green) and DAPI+ cell nuclei (in blue),). Scale bar= 100 µm.

4.3.5 Cell Culture on Decellularized Meningeal ECM Constructs

Allogeneic primary rat meningeal fibroblasts were seeded onto decellularized meningeal ECM constructs to investigate whether the materials support cell adhesion and proliferation. Following 2days, meningeal fibroblasts were found to spread out on both ECM constructs and culture medium coated coverslip surfaces (for comparison) as visualized by actin microfilament staining (Fig. 4-8: A and B). In contrast to meningeal fibroblasts grown on culture medium coated coverslips, whose cell bodies flattened and spread out isotropically (Fig. 4-8:A), meningeal fibroblasts cultured on acellular ECM constructs were found to be morphologically elongated, demonstrating that the ligand distribution of the underlying ECM matrices influences cellular morphology (Fig. 4-8:B).When meningeal fibroblasts and astrocytes were plated onto decellularized ECM constructs, no difference in the ability of acellular ECM constructs to support cell adhesion of both cell types was observed (Fig. 4-8:C). However, in a 4-day cell proliferation assay, a significantly higher proliferation rate of allogeneic meningeal fibroblasts over allogeneic astrocytes was found on the decellularized ECM constructs (Fig. 4-8:D; ANOVA, post hoc $p<0.05$).

4.4. Discussion

Dura mater is the outermost meninges tissue that isolates and protects the CNS tissue and it is the general surgical practice to repair dural defects with a biomaterial patch to restore its barrier functions [1, 3]. Various materials ranging from autografts [58, 89], allografts [49-52], xenografts [54-57], degradable and nondegradable polymers [24-32] as well as natural biopolymers [63-68] have

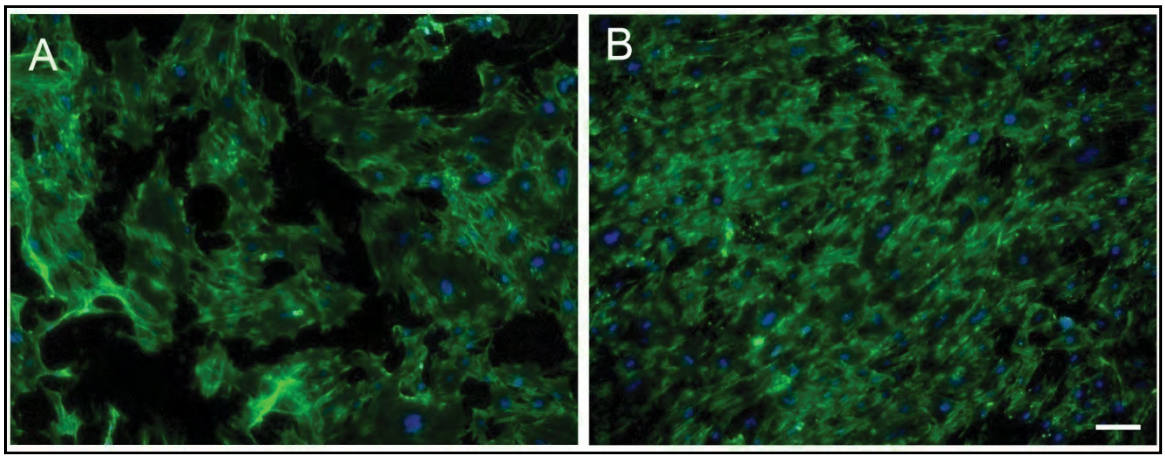

Fig. 4-8: Acellular meningeal ECM constructs support primary meningeal fibroblast adhesion and proliferation. Representative images of the morphology of meningeal fibroblasts cultured on serum-coated coverslip surfaces (A) and acellular ECM constructs (B) following 2 days in culture. In contrast to meningeal fibroblasts which flattened and spread out isotropically on the coverslip surfaces, the meningeal fibroblasts appeared to be morphologically elongated on the ECM constructs, suggesting that the spatial distribution of ECM ligands influenced cellular morphology.

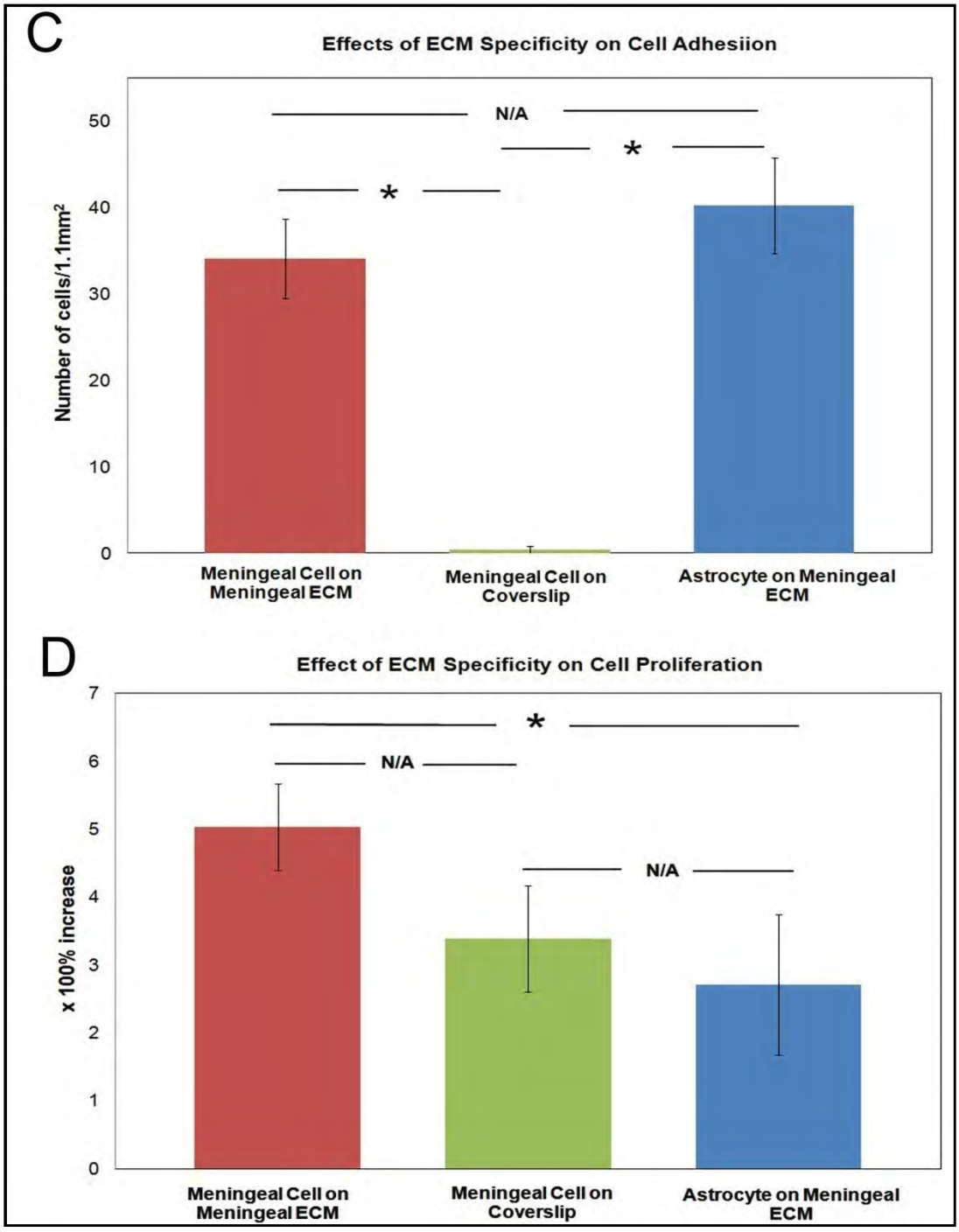

Fig.4-8 continued: (C) No significant difference in the ability of the acellular constructs to support allogeneic meningeal fibroblast or astrocyte adhesion was observed. (D) On the other hand, a significant higher proliferation rate of tissue specific meningeal fibroblasts over astrocytes were found on the ECM constructs ($p < 0.05$, ANOVA). Scale bar= 100µm.

been tested as dural substitutes. However, poor biocompatibility and complications associated with many of these materials, including chronic inflammatory responses and immunogenic reactions, have restricted their wide spread use [35-44, 71-74]. While collagen-based dural repair products are currently widely used by neurosurgeons, the fact that they are derived from tissue sources other than the meningeal dura tissue suggests these biomaterials might not carry appropriate biological cues, which have been suggested to promote tissue type specific regeneration [81-84]. This idea of using tissue type specific ECM materials for targeted tissue repair is supported by a study where foreign tissue formation was observed when ECM scaffolds derived from mismatched tissue types were introduced for myocardial repair [85].

To provide an improved alternative to clinicians, we have developed novel biomaterial constructs that are derived by the meningeal fibroblasts, the major supporting cell type reside with the natural meninges tissue, including the dura mater. Both cellularized and acellular ECM constructs derived by meningeal fibroblasts are mechanically stable and can be handled with hand-hold forceps. Indirect immunohistochemical analysis demonstrated that both types of engineered constructs expressed similar ECM proteins as adult rat cortical dura mater, suggesting the complexity of the ECM matrix was recapitulated in a manner that mimics the natural extracellular milieu *in vivo*. In addition, acellular ECM constructs support allogeneic meningeal fibroblast adhesion and promote their proliferation *in vitro*. Together, these *in vitro* studies suggest that such an

approach may be useful to produce biomaterials that may be used to repair the damaged meningeal tissues of the CNS.

Different approaches have been developed to create 3D cellular constructs *in vitro*, utilizing either temperature-responsive surfaces to facilitate continuous cell sheet detachment [94, 95, 106] or nanometer-sized ECM films to facilitate the formation of multilayered structure [96, 97]. In addition to preclinical animal studies, such multilayered cellular constructs have also been successfully applied in a clinical study on human subjects [94]. In our case, the formation of multilayered meningeal fibroblast constructs was achieved simply by repeating seeding cells in the serum-supplemented culture medium. Our observation was not cell type specific since we have observed the formation of similar multilayered structure with at least 3 different cell types (i.e., meningeal fibroblast, astrocyte and human vocal fold fibroblast) using our approach. Moreover, our simple approach to engineer multilayered cellular constructs is advantageous in a way that avoids the expensive cost of using high concentration ECM protein solutions [96, 97], purchasing special culture substrates or the complex chemistry processes involved in fabricating one [94, 95, 106].

While the allogeneic cellular tissue constructs have been shown to hold therapeutic potential for repairing a variety of damaged tissues in animal models [95, 106], autologous cell sources remain the optimal choice when it comes to patients due to the immunogenic rejections following transplantation [94]. However, it may be time consuming to expand autologous cells in culture in order to acquire enough cells for therapeutic applications. In our study, acellular

meningeal ECM constructs were also developed following decellularization to the cellularized constructs in order to provide an alternative for autologous cell therapy. The decellularized ECM constructs preserved only cell-produced ECM materials, which are generally considered to be immunologically tolerable between species and would elicit minimal inflammatory response [98]. In addition, the acellular ECM biomaterials can be easily sterilized, stored and used as over-the-counter products. Indirect immunohistochemical reactions demonstrated that both cellular and nuclear materials were effectively removed as evidenced by the absence of DAPI+ nuclei and immunofluorescent signals of intracellular actin micofilaments. On the other hand, a similar ECM protein profile to the native rat meningeal dura tissue was preserved, suggesting appropriate biological function of the ECM was maintained. The decellularized meningeal ECM constructs also have a similar ligand organization as the decellularized rat dura mater, particularly a network of intermingled collagen fibers (data not shown).

ECM is also known as the natural carrier of cell-secreted growth factors [99, 100]. Although the content of growth factors within the acellular meningeal ECM constructs in the current study was not investigated, the potential candidates that might be preserved in the matrices include NGF, NT-3 and bFGF [101]. These trophic factors could be released upon ECM construct degradation, which would further modulate cell functions and mediate subsequent tissue remodeling processes [102, 103]. The bioactivity of these growth factors has been shown to remain active even following decellularization or sterilization [105, 107]. In addition, the nature of biological scaffolds has been demonstrated to be

able to affect infiltrating macrophage phenotype and tissue remodeling outcome [86]. In particular, acellular ECM scaffolds have been shown to result in primarily antiinflammatory M2 macrophage phenotype at the implantation site, which then lead to constructive tissue remodeling.

Rat meningeal fibroblasts were seeded atop decellularized meningeal ECM constructs to investigate the ability of ECM constructs to support cell adhesion and proliferation *in vitro*. Although we did not find statistically more allogeneic meningeal fibroblasts than allogeneic astrocytes adhered on the ECM constructs, a significantly higher proliferation rate of meningeal fibroblasts over astrocytes was observed, suggesting the acellular ECM constructs can facilitate dural defect regeneration by promoting host dural meningeal fibroblast proliferation. In addition, it has also been shown that tissue specific ECM attracts migration of tissue-matched cell types [84]. However, in addition to the tissue specificity which has been shown previously to play a role in influencing cell proliferation [82, 83], we cannot rule out the possibility that the significant difference seen in the cell proliferation assay was also contributed by the fact that meningeal fibroblasts inherently proliferate faster than astrocytes *in vitro*.

The meningeal fibroblast constructs and acellular meningeal ECM constructs developed in this study are of sheet-like structure and can be handled with hand-held forceps, demonstrating that both biomaterial constructs can be easily applied as patching materials for injured meningeal dura tissue repair. While meningeal cellular constructs can be directly applied as biological surrogates for dural defect repair when autologous cell source is available,

acellular meningeal ECM constructs can be prepared as an alternative to autografts with either allogeneic or even xenogeneic cell sources.

4.5. Conclusions

Meningeal fibroblast derived biomaterial constructs were developed in the present study. The fact that both cellularized constructs and decellularized ECM constructs were derived by the specific cell type that composes the natural dural tissue suggests these biomaterials might carry appropriate biological cues that could stimulate tissue specific regenerative response. As studies have shown the advantage of introducing tissue type specific ECM for damaged tissue targeted for repair, meningeal fibroblast derived constructs might hold superior therapeutic potential for neurosurgical applications. The ongoing research is investigating the biocompatibility of both meningeal cell derived constructs *in vivo*.

4.6 Acknowledgement

The authors thank Elena Budko, M.D., for assistance and thoughtful discussion. We also thank Brian Baker for his help for fabricating microprinting devices. We acknowledge funding support from NIH 5R01NS57144.

4.7 References

1. Cushing H. A study of a series of wounds involving the brain and its enveloping structures. Brit J Surg 1918;5:558-684.

2. Dandy WE. Treatment of rhinorrhea and otorrhea. Arch Surg Chicago 1944;49:75-85.

3. Cushing H. The establishment of cerebral hernia as a decompressive measure for inaccessible brain tumors; with the description of intermuscular methods of making the bone defect in temporal and occipital regions. Surg Gynec Obstet 1950;1(297-314).

4. Sayad WY, Harvey SC. The regeneration of the meninges: The dura mater. Ann Surg 1923;77:129-141.

5. Trotter W. Sensitivity of the skin in realtion to neurological theory. Lancet 1924;1:1252-1256.

6. Braun JS, Kaissling B, Hir ML, Zenker W. Cellular componentsvof the immune barrier in the spinal meninges and dorsal rootvganglia of the normal rat: immunohistochemical (MHC class II) andvelectron-microscopic observations. Cell Tissue Res 1993;273:209-217.

7. Harris ML. The use of silver foil to prevernt adhesions in brain surgery. JAMA 1904;42:763-765.

8. Chao YC, Humphreys S, Penfield W. A new method of preventing adhesions. The use of amnioplastin after craniotomy. Br Med J 1940;1:517-538.

9. O'Connell JEA. Traumatic cerebral fungus. Br J Surg 1943;30:201-212.

10. Ersahin Y, Gülmen V, Palali I, Mutluer S. Growing skull fractures (craniocerebral erosion). Neurosurg Rev 2000;23:139-144.

11. West CA, Towns G, Bachelor AG, Liddington MI. Reconstruction of skull base and dura using rectus abdominis muscle combined with a vascularised fascial perforator flap. J Plast Reconstr Aesthet Surg 2006;59:631-635.

12. Teng P, Feigin I. Vinyon “N” as a dural aubstitute. an experimental study in the monkey. J Neurosurg 1955;12:591-600.

13. Beach HHA. Gold foil in cerebral surgery. Boston Med Surg J 1897;136:281-282.

14. Woolsey G. Gold foil in trephine opening in the skull. Ann Surg 1897;25:630-632.

15. Delarue NC, Linell EA, Mckenzie KG. An experimental study on the use of tantalum in the sub-dural space. J Neurosurg 1944;1:239-242.

16. Robertson RCL, Peacher WG. The use of tantalum foil in the subdural space. J Neurosurg 1945;2:281-284.

17. Pudenz RH, Odom GL. An experimental study of the effect of human amniotic membrane, amnioplastin, beef allantoic membrane, cargile membrane, tantalum foil and polyvinyl alcohol films. Surgery 1942;12:318-344.

18. Abbe R. Rubber tissue for meningeal adhesions. Trans Amer Surg Ass 1895;13:490-491.

19. Haynes WG. The use of a sterile rubber glove as a covering for the dural defect resulting from the removal of a spinal cord tumor. Case report Am J Surg 1943;59:133-135.

20. Brown MH, Grindlay JH, Craig WM. The use of polythene film as a dural substitute; a preliminary report. J Neurosurg 1947;4:505-507.

21. Huertas J. The use of orlon for dural replacement. J Neurosurg 1955;12:550-554.

22. Yamagatam S, Goto K, Oda Y, Kikuchi H. Clinical experience with expanded polytetrafluoroethylene sheet used as an artificial dura mater. Neurol Med Chir (Tokyo) 1993;33:582-585.

23. Nagata K, Kawamoto S, Sashida J, Abe T, Mukasa A, Imaizumi Y. Mesh-and-glue technique to prevent leakage of cerebrospinal fluid after implantation of expanded polytetrafluoroethylene dura substitute--technical note. Neurol Med Chir (Tokyo) 1999:316-318; discussion 318-319.

24. Viñas FC, Ferris D, Kupsky WJ, Dujovny M. Evaluation of expanded polytetrafluoroethylene (ePTFE) versus polydioxanone (PDS) for the repair of dura mater defects. Neurol Res 1999;21:262-268.

25. Chappell ET, Pare L, Salehpour M, Mathews M, Middlehof C. GORE PRECLUDE MVP dura substitute applied as a nonwatertight "underlay" graft for craniotomies: product and technique evaluation. Surg Neurol 2009;71:126-128; discussion 128-129.

26. Bhatia S, Bergethon PR, Blease S, Kemper T, Rosiello A, Zimbardi GP, et al. A synthetic dural prosthesis constructed from hydroxyethylmethacrylate hydrogels. J Neurosurg 1995;83:897-902.

27. Mello LR, Feltrin LT, Fontes Neto PT, Ferraz FA. Duraplasty with biosynthetic cellulose: an experimental study. J Neurosurg 1997;86:143-150.

28. Xie J, Macewan MR, Ray WZ, Liu W, Siewe DY, Xia Y. Radially aligned, electrospun nanofibers as dural substitutes for wound closure and tissue regeneration applications. ACS Nano 2010;4:5027-5036.

29. Kurpinski K, Patel S. Dura mater regeneration with a novel synthetic, bilayered nanofibrous dural substitute: an experimental study. Nanomedicine (Lond) 2011;6:325-337.

30. Maurer PK, McDonald JV. Vicryl (polyglactin 910) mesh as a dural substitute. J Neurosurg 1985;63:448-452.

31. Yamada K, Miyamoto S, Nagata I, Kikuchi H, Ikada Y, Iwata H, et al. Development of a dural substitute from synthetic bioabsorbable polymers. J Neurosurg 1997;86:1012-1017.

32. Miyamoto S, Yamada K, Nagata I, Ikada Y, Iwata H, Ueno Y, et al. Clinical application of new bioabsorbable artificial dura mater: a preliminary report. J Artif Organs 1998;1:10-14.

33. Yamada K, Miyamoto S, Takayama M, Nagata I, Hashimoto N, Ikada Y, et al. Clinical application of a new bioabsorbable artificial dura mater. J Neurosurg 2002;96:731-735.

34. Adegbite AB, Paine KW, Rozdilsky B. The role of neomembranes in formation of hematoma around Silastic dura substitute Case report. J Neurosurg 1983;58:295-297.

35. Simpson D, Robson A. Recurrent subarachnoid bleeding in association with dural substitute. Report of three cases. J Neurosurg 1984;60:408-409.

36. Siccardi D, Ventimiglia A. Fibrotic-haemorrhagic reaction to synthetic dural substitute. Acta Neurochir (Wien) 1995;132:148-149.

37. Robertson SC, Menezes AH. Hemorrhagic complications in association with silastic dural substitute: pediatric and adult case reports with a review of the literature. Neurosurgery 1997;40:201-205; discussion 205-206.

38. Banerjee T, Meagher JN, Hunt WE. Unusual complications with use of silastic dural substitute. Am Surg 1974;40:434-437.

39. Ongkiko CMJ, Keller JT, Mayfield FH, Dunsker SB. An unusual complication of Dura Film as a dural substitute. J Neurosurg 1984;60:1076-1079.

40. Cohen AR, Aleksic S, Ransohoff J. Inflammatory reaction to synthetic dural substitute. Case report. J Neurosurg 1980;70:633-635.

41. Raul JS, Godard J, Arbez-Gindre F, Czorny A. Use of polyester urethane (Neuro-Patch) as a dural substitute. Prospective study of 70 cases. Neurochirurgie 2003;49:83-89.

42. Malliti M, Page P, Gury C, Chomette E, Nataf F, Roux FX. Comparison of deep wound infection rates using a synthetic dural substitute (neuro-patch) or pericranium graft for dural closure: a clinical review of 1 year. Neurosurgery 2004;54:599-603; discussion 603-604.

43. El Majdoub F, Löhr M, Maarouf M, Brunn A, Stenzel W, Ernestus RI. Transmigration of fibrino-purulent inflammation and malignant cells into an artificial dura substitute (Neuro-Patch): report of two cases. Acta Neurochir (Wien) 2009;151:833-835.

44. Huang YH, Lee TC, Chen WF, Wang YM. Safety of the nonabsorbable dural substitute in decompressive craniectomy for severe traumatic brain injury. J Trauma 2011;71:533-537.

45. Glaser MA, Thienes CH. Dural Defects: How important is their surgical repair: an experimental and clinical study upon heteroplastic and autoplastic dural grafts. Cal West Med 1938;48:163-166.

46. Hicks JD, Trethewie ER, Williams E. Experimental studies in the use of amnioplastin ANZ J Surg 1942;11.:268-272.

47. Sharkey PC, Usher FC, Robertson RC, Pollard CJ. Lyophilized human dura mater as a dural substitute. J Neurosurg 1958;15:192-198.

48. Rosomoff HL. Ethylene oxide sterilized, freeze-dried dura mater for the repair of pachymeningeal defects. J Neurosurg 1959;16:197-208.

49. Abbott WM, Dupree ELJ. Clinical results of lyophilized human cadaver dura transplantation. J Neurosurg 1971;34:770-773.

50. Laun A, Tonn JC, Jerusalem C. Comparative study of lyophilized human dura mater and lyophilized bovine pericardium as dural substitutes in neurosurgery. Acta Neurochir (Wien) 1990;107:16-21.

51. Chaplin JM, Costantino PD, Wolpoe ME, Bederson JB, Griffey ES, Zhang WX. Use of an acellular dermal allograft for dural replacement: an experimental study. Neurosurgery 1999;45:320-327.

52. Warren WL, Medary MB, Dureza CD, Bellotte JB, Flannagan PP, Oh MY, et al. Dural repair using acellular human dermis: experience with 200 cases: technique assessment. Neurosurgery 2000;46:1391-1396.

53. Islam S, Ogane K, Ohkuma H, Suzuki S. Usefulness of acellular dermal graft as a dural substitute in experimental model. Surg Neurol 2004;61:297-302; discussion 303.

54. Cobb MA, Badylak SF, Janas W, Boop FA. Histology after dural grafting with small intestinal submucosa. Surg Neurol 1996;46:389-393; discussion 393-384.

55. Cobb MA, Badylak SF, Janas W, Simmons-Byrd A, Boop FA. Porcine Small Intestinal Submucosa as a Dural Substitute. Surg Neurol 1999;51:99-104.

56. Xu BZ, Pan HX, Li KM, Chen XJ, Tian YD, Li YL, et al. Study and clinical application of a porcine biomembrane for the repair of dural defects. J Neurosurg 1988;69:707-711.

57. Gök A, Zorludemir S, Polat S, Tap O, Kaya M. Experimental evaluation of peritoneum and pericardium as dural substitutes. Res Exp Med (Berl) 1995;195:31-38.

58. Thammavaram KV, Benzel EC, Kesterson L. Fascia lata graft as a dural substitute in neurosurgery. South Med J 1990;83:634-636.

59. Tachibana E, Saito K, Fukuta K, Yoshida J. Evaluation of the healing process after dural reconstruction achieved using a free fascial graft. J Neurosurg 2002;96:280-286.:280-286.

60. Kline DG. Dural replacement with resorbable collagen. Arch Surg 1965;91:924-929.

61. Jannetta PJ, Whayne TFJ. Formaldehyde-treated, regenerated collagen film and film-laminate as a substitute for dura mater. Surg Forum 1965;16:435-437.

62. Lee JF, Odom GL, Tindall GT. Experimental evalation of silicone-coated dacron and collagen fabric-film laminate as dural substitutes. J Neurosurg 1967;27:558-564.

63. Laquerriere A, Yun J, Tiollier J, Hemet J, Tadie M. Experimental evaluation of bilayered human collagen as a dural substitute. J Neurosurg 1993;78:487-491.

64. Narotam PK, Van Dellen JR, Bhoola K, Raidoo D. Experimental evaluation of collagen sponge as a dural graft. Br J Neurosurg 1993;7:635-641.

65. Narotam PK, van Dellen JR, Bhoola KD. A clinicopathological study of collagen sponge as a dural graft in neurosurgery. J Neurosurg 1995;82:401-412.

66. Zerris VA, James KS, Roberts JB, Bell E, Heilman CB. Repair of the dura mater with processed collagen devices. J Biomed Mater Res B Appl Biomater 2007;83:580-588.

67. Barbolt TA, Odin M, Léger M, Kangas L, Hoiste J, Liu SH. Biocompatibility evaluation of dura mater substitutes in an animal model. Neurol Res 2001;23:813-820.

68. Knopp U, Christmann F, Reusche E, Sepehrnia A. A new collagen biomatrix of equine origin versus a cadaveric dura graft for the repair of dural defects--a comparative animal experimental study. Acta Neurochir (Wien) 2005;147:877-887.

69. Gazzeri R, Neroni M, Alfieri A, Galarza M, Faiola A, Esposito S, et al. Transparent equine collagen biomatrix as dural repair. A prospective clinical study. Acta Neurochir (Wien) 2009;151:537-543.

70. Parlato C, di Nuzzo G, Luongo M, Parlato RS, Accardo M, Cuccurullo L, et al. Use of a collagen biomatrix (TissuDura) for dura repair: a long-term neuroradiological and neuropathological evaluation. Acta Neurochir (Wien) 2011;153:142-147.

71. Hoshi K, Yoshino H, Urata J, Nakamura Y, Yanagawa H, Sato T. Creutzfeldt-Jakob disease associated with cadaveric dura mater grafts in Japan. Neurology 2000;55:718-721.

72. Lane KL, Brown P, Howell DN, Crain BJ, Hulette CM, Burger PC, et al. Creutzfeldt-Jakob disease in a pregnant woman with an implanted dura mater graft. . Neurosurgery 1994;34:737-739; discussion 739-740.

73. Alleyne CHJ, Barrow DL. Immune response in hosts with cadaveric dural grafts. Report of two cases. J Neurosurg 1994;81:610-613.

74. Haywood AM. Transmissible spongiform encephalopathies. N Engl J Med 1997;337:1821-1828.

75. Badylak SF, Gilbert TW. Immune response to biologic scaffold materials. Semin Immunol 2008;20:109-116.

76. Boland ED, Matthews JA, Pawlowski KJ, Simpson DG, Wnek GE, Bowlin GL. Electrospinning collagen and elastin: preliminary vascular tissue engineering. Front Biosci 2004;9:1422-1432.

77. Lu H, Hoshiba T, Kawazoe N, Chen G. Autologous extracellular matrix scaffolds for tissue engineering. Biomaterials 2011;32:2489-2499.

78. Eitan Y, Sarig U, Dahan N, Machluf M. Acellular cardiac extracellular matrix as a scaffold for tissue engineering: in vitro cell support, remodeling, and biocompatibility. Tissue Eng Part C Methods 2010;16:671-683.

79. McClelland R, Wauthier E, Uronis J, Reid L. Gradients in the liver's extracellular matrix chemistry from periportal to pericentral zones: influence on human hepatic progenitors. Tissue Eng Part A 2008;14:59-70.

80. Huet C, Pisselet C, Mandon-Pépin B, Monget P, Monniaux D. Extracellular matrix regulates ovine granulosa cell survival, proliferation and steroidogenesis: relationships between cell shape and function. J Endocrinol 2001;169:347-360.

81. Sellaro TL, Ravindra AK, Stolz DB, Badylak SF. Maintenance of hepatic sinusoidal endothelial cell phenotype in vitro using organ-specific extracellular matrix scaffolds. Tissue Eng Part A 2007;13:2301-2310.

82. Zhang Y, He Y, Bharadwaj S, Hammam N, Carnagey K, Myers R, et al. Tissue-specific extracellular matrix coatings for the promotion of cell proliferation and maintenance of cell phenotype. Biomaterials 2009;23-24:4021-4028.

83. Stern MM, Myers RL, Hammam N, Stern KA, Eberli D, Kritchevsky SB, et al. The influence of extracellular matrix derived from skeletal muscle tissue on the proliferation and differentiation of myogenic progenitor cells ex vivo. Biomaterials 2009;30:2393-2399.

84. Singelyn JM, DeQuach JA, Seif-Naraghi SB, Littlefield RB, Schup-Magoffin PJ, Christman KL. Naturally derived myocardial matrix as an injectable scaffold for cardiac tissue engineering. Biomaterials 2009;30:5409-5416.

85. Badylak S, Obermiller J, Geddes L, Matheny R. Extracellular matrix for myocardial repair. Heart Surg Forum 2003;6:E20-E26.

86. Brown BN, Valentin JE, Stewart-Akers AM, McCabe GP, Badylak SF. Macrophage phenotype and remodeling outcomes in response to biologic scaffolds with and without a cellular component. Biomaterials 2009;30:1482-1491.

87. Walsh JF, Manwaring ME, Tresco PA. Directional neurite outgrowth is enhanced by engineered meningeal cell-coated substrates. Tissue Eng 2005;11:1085-1094.

88. Haines DEe. The meninge, in fundamental neuroscience. Churchill Licingston, PA. 1996:p. 99-111.

89. Abuzayed B, Kafadar AM, Oğuzoğlu SA, Canbaz B, Kaynar MY. Duraplasty using autologous fascia lata reenforced by on-site pedicled muscle flap: technical note. J Craniofac Surg 2009;20:435-438.

90. Ma L, Gao C, Mao Z, Zhou J, Shen J, Hu X, et al. Collagen/chitosan porous scaffolds with improved biostability for skin tissue engineering. Biomaterials 2003;24:4833-4841.

91. Wahl DA, Czernuszka JT. Collagen-hydroxyapatite composites for hard tissue repair. Eur Cell Mater 2006;11:43-56.

92. Protasoni M, Sangiorgi S, Cividini A, Culuvaris GT, Tomei G, Dell'Orbo C, et al. The collagenic architecture of human dura mater. J Neurosurg 2011;114:1723-1730.

93. Dobrovol'skii GF. Ultrastructure of the meninge. Neurosci Behav Physiol 1984;14:100-110.

94. Nishida K, Yamato M, Hayashida Y, Watanabe K, Yamamoto K, Adachi E, et al. Corneal reconstruction with tissue-engineered cell sheets composed of autologous oral mucosal epithelium. N Engl J Med 2004;351:1187-1196.

95. Miyahara Y, Nagaya N, Kataoka M, Yanagawa B, Tanaka K, Hao H, et al. Monolayered mesenchymal stem cells repair scarred myocardium after myocardial infarction. Nat Med 2006;12:459-465.

96. Matsusaki M, Kadowaki K, Nakahara Y, Akashi M. Fabrication of cellular multilayers with nanometer-sized extracellular matrix films. Angew Chem Int Ed Engl 2007;46:4689-4692.

97. Nishiguchi A, Yoshida H, Matsusaki M, Akashi M. Rapid construction of three-dimensional multilayered tissues with endothelial tube networks by the cell-accumulation technique. Adv Mater 2011;23:3506-3510.

98. Crapo PM, Gilbert TW, Badylak SF. An overview of tissue and whole organ decellularization processes. Biomaterials 2011;32:3233-3243.

99. Vlodavsky I, Folkman J, Sullivan R, Fridman R, Ishai-Michaeli R, Sasse J. Endothelial cell-derived basic fibroblast growth factor: synthesis and deposition

into subendothelial extracellular matrix. Proc Natl Acad Sci USA 1987;84:2292-2296.

100. Taipale J, Keski-Oja J. Growth factors in the extracellular matrix. FASEB J 1997;11:51-59.

101. Franzen R, Martin D, Daloze A, Moonen G, Schoenen J. Grafts of meningeal fibroblasts in adult rat spinal cord lesion promote axonal regrowth. Neuroreport 1999;10:1551-1556.

102. Streuli C. Extracellular matrix remodelling and cellular differentiation. Curr Opin Cell Bio 1999;11:634-640.

103. Bashkin P, Doctrow S, Klagsbrun M, Svahn CM, Folkman J, Vlodavsky I. Basic fibroblast growth factor binds to subendothelial extracellular matrix and is released by heparitinase and heparin-like molecules. Biochemistry 1989;28:1737-1743.

104. McDevitt CA, Wildey GM, Cutrone RM. Transforming growth factor-beta1 in a sterilized tissue derived from the pig small intestine submucosa. J Biomed Mater Res A 2003;67:637-640.

105. Hodde JP, Ernst DM, Hiles MC. An investigation of the long-term bioactivity of endogenous growth factor in OASIS Wound Matrix. J Wound Care 2005;14:23-25.

106. Ohashi K, Yokoyama T, Yamato M, Kuge H, Kanehiro H, Tsutsumi M, et al. Engineering functional two- and three-dimensional liver systems in vivo using hepatic tissue sheets. Nat Med 2007;13:880-885.

107. McDevitt CA, Wildey GM, Cutrone RM. Transforming growth factor-beta1 in a sterilized tissue derived from the pig small intestine submucosa. J Biomed Mater Res A 2003;67:637-640.

CHAPTER 5

SUMMARY, CONCLUSIONS, AND FUTURE WORK

5.1 Summary and Conclusions

SCI is extremely debilitating to patients and costly to the health care system. With significant SCI attributed mortality and morbidity in the world, various therapeutic strategies, have been investigated, either experimentally and clinically, to improve patients' quality of life. Studies utilizing pharmacological methods to mitigate the inhibitory components of the glial scar and facilitate axonal regeneration following SCI have been the primary approaches in the field. In this research, we aimed to tackle the issue from a novel perspective by developing cell-derived tissue engineered biomaterials that can be used in combination with other therapeutic approaches to improve the efficacy of current treatments.

In Chapter 2, a 2D model of oriented astrocyte monolayers was developed *in vitro* and served as the framework of the engineering approach that was utilized in Chapter 3 to develop implantable, oriented astrocyte based biomaterial constructs. The oriented astrocyte monolayer model clearly demonstrates that it is a purely biological mechanism by which oriented astrocytes guide DRG neurite outgrowth as planar culture substrates were provided. In particular, by culturing DRG neurons atop fixed, oriented astrocyte monolayers, we demonstrated the

spatial distribution of astrocyte associated insoluble ligands play the principal role in guiding neurite trajectories. Antisera experiments further showed that astrocyte associated FN functions as a potent neurite outgrowth guiding ligand. Last, we demonstrated that nanometer level surface guidance cues can be transmitted through multiple cell layers to organize multilayered cellular constructs on the scale of tens of microns thick.

In Chapter 3, 3D astrocyte constructs with either randomly organized or oriented cellular organization were developed in the absence of synthetic scaffolding materials. The recovered astrocyte constructs are mechanically stable and implantable. The confocal microscopy showed that the anisotropic spatial distribution of various astrocyte associated ligands is maintained in the oriented astrocyte constructs whereas no biased orientation distribution of the same ligand profile is observed in randomly organized constructs. Oriented astrocyte constructs maintain the ability to direct regenerating DRG neurite outgrowth in a direction parallel to the spatial distribution of associated ligands *in vitro,* similar to the 2D monolayer model. In addition, recovered astrocyte constructs are manipulatable, which can be engineered into multistacked constructs or self-holding tubular structures. Moreover, the cellular components of the cellularized constructs can be removed to harvest acellular ECM constructs that would elicit the minimal immune response and result in constructive tissue remodeling following implantation. Acellular, oriented astrocytes derived ECM constructs are also able to guide neurite outgrowth and influence the orientation of adjacent proliferating and migrating glial cells *in vitro*.

In Chapter 4, meningeal fibroblast-derived biomaterials were developed using the same engineering approach described in Chapter 3 for dural defect repair. Dural defect reconstruction has been shown to be able to prevent meningeal fibroblast infiltration and collagenous material deposition into SCI lesion center, which benefits the regeneration process of the cord. Indirect immunohistochemical reactions showed that both engineered meningeal constructs and acellular meningeal ECM constructs have similar ECM protein profile as the native adult rat dural mater, suggesting appropriate biological function of the ECM is maintained. The spatial distribution of the ligands within the acellular ECM constructs was found to influence the morphology of overlying proliferating allogeneic meningeal fibroblasts. Although no difference in the ability of meningeal ECM constructs to support either astrocytes or meningeal fibroblast adhesion was observed, we did find a significantly higher proliferation rate of meningeal fibroblasts over astrocytes on the meningeal ECM constructs.

5.2 Future Work

5.2.1 The Effect of Cellular Organization on Overcoming Inhibitory Astrocyte-Meningeal Fibroblast Interface

As outlined in this dissertation, infiltration of meningeal fibroblasts and resulting deposition of collagenous materials are common tissue response scenarios observed following penetration or laceration SCI, leading to the formation of a fibrotic scar [1, 2]. The repulsive effect of meningeal fibroblast infiltration on axonal regeneration has been demonstrated both *in vitro* and *in vivo*[1, 3-5]. Neurite trajectories have been found to grow preferentially on

astrocyte patches and readily cross from the meningeal cell territories to astrocyte territories, but failed to extend in the other direction. It has been shown that pharmacological or neurotrophin treatments can moderately increase the crossing behavior *in vitro*[4, 5].

In Chapter 2, we demonstrated that astrocyte alignment can be engineered using nanochemically printed protein pattern, which led to the development of a network of organized, anisotropically distributed astrocyte associated ligands. It has been proposed that the efficacy of growth cone pathfinding would be more efficient in the organized extracellular milieu as the complex decision making process encountered when exploring the disorganized extracellular territory, involving growth cone adhesion and retraction, is avoided. Therefore, it would be interesting to test *in vitro* if the inhibitory astrocyte/meningeal cell boundary could be overcome by simply manipulating the cellular organization of both cell types at the interface using the anisotropic protein pattern.

5.2.2 Cell-Derived ECM Constructs and Macrophage Polarization

The fact that studies utilizing either transplantation of activated macrophages or depletion of hematogenous macrophages have been shown to promote functional recovery following SCI leads to considerable debate as to whether these inflammatory cells play an adverse or beneficial role on tissue repair and axonal regeneration [6, 7].This controversy has been elucidated by recent studies that shed light on the heterogeneity of activated macrophages/microglia, that mediate different effects on axonal regeneration [8,

9].In particular, M1 inflammatory macrophages have been demonstrated to mediate neurotoxic effects on regenerating axons whereas M2 antiinflammatory macrophages promote axonal regeneration, even on inhibitory substrates *in vitro*. *In vivo*, M1 inflammatory macrophages have been shown to predominate the lesion site starting 14 days following SCI [8].

It has been shown in non-neuronal tissues that implantation of acellular ECM scaffolds lead to a predominantly M2 antiinflammatory macrophage phenotype and constructive tissue remodeling at the implantation site whereas a primarily M1 inflammatory phenotype is observed when cellular grafts are implanted [10]. Therefore, it will be interesting to test if astrocyte derived ECM constructs would shift the polarization of macrophages/microglia at the SCI lesion site toward a predominantly M2 antiinflammatory phenotype, which leads to facilitated axonal regeneration, whereas cellularized astrocyte constructs would induce a primarily M1inflammatory macrophage phenotype, which inhibits regeneration. In addition, implantation of oriented astrocyte derived biomaterial constructs also provides an opportunity to investigate the ability of these biomaterial constructs to organize the orientation of glial scar-forming reactive astrocytes surrounding the lesion site and the effect of cellular organization on axonal regeneration.

This study could provide information regarding whether having an inflammatory macrophage phenotype at the lesion site or the presence of an unorganized pathway is the predominant mediator of failed axonal regeneration and the best approach to improve current SCI treatments. In order to answer

these questions, future studies could be conducted with four experimental groups including implantation of oriented astrocyte-derived biomaterial constructs (cellularized and acellular) as well as randomly organized astrocyte-derived constructs (cellularized and acellular) in a hemisection SCI model as it is relatively easy to generate and reproducible [19].

Although studies have shown that ECM scaffolds result in a predominantly M2 antiinflammatory macrophage phenotype at implantation site, it is still unknown what drives the differentiation of macrophages. As macrophages have been demonstrated to be the primarily mediators of ECM degradation and modification [11], it is possible that macrophage polarization is at least partially mediated by ligands they digest from the matrix and then take up in the cell bodies. The simple approach developed in the thesis work for harvesting cell-derived ECM constructs could potentially be applied to genetically modified cell types that are engineered to upregulate or ablate the secretion of particular types of ECM proteins. Use of genetically modified cell types provides the opportunity to study the effects of ECM components on inducing macrophage polarization. On the other hand, by crosslinking ECM constructs, which has been shown previously to reduce the extent of ECM degradation [12], we could also investigate if degradation of ECM materials plays a role on macrophage polarization. These studies could provide information on engineering ECM materials to induce a primarily antiinflammatory tissue response at the injury site.

In the current study, ECM constructs with or without organized protein ligand distribution were developed, which could serve as unique substrates to

study whether specific macrophage phenotypes would be simply induced by the ligand organization present in ECM constructs *in vitro*. Moreover, if distinct macrophage polarizations were observed on the two different ECM substrates engineered, it would be interesting to investigate how long the polarized state of macrophages could be maintained and if the presentation of organized ligands could overwhelm the effects of different cytokines shown to polarize macrophages to specific phenotypes when added to culture media [13]. This *in vitro* study would provide insights on designing novel biomaterial coatings to improve biocompatibility via engineering ligand presentation.

The spatial distribution of each protein ligand within the ECM constructs engineered (i.e., disorganized and organized) and their relative distributions could be revealed by indirect immunohistochemical reactions against specific protein ligands. The revealed protein distributions could then be converted into digitalized image files and fabricated into different patterns onto PDMS printing devices. The protein patterns could then be printed onto biomaterial surfaces using multiprotein microcontact printing approach such that the relative distribution of multiple protein ligands is preserved [20]. Macrophages could then be seeded on printed protein patterns and the ability of ligand organization on inducing macrophage polarization could be evaluated using cell surface markers or secreted cytokine profiles.

In addition to ligand organization, by comparing the M2/M1 macrophage ratio seen on distinct protein ligand combinations that are printed onto biomaterial surfaces (e.g.,FN + LN vs. FN + CSPG), it is also feasible to evaluate

which ligand(s)'s organization plays the most important role on macrophage polarization.

5.2.3 Injectable Cell Type-Specific ECM Biomaterials

Several rodent SCI models, including complete transection, hemisection and compression/contusion injures, have been developed to study the cellular and molecular response following SCI and test the efficacy of various experimental therapeutic strategies [14-16]. While the transection and hemisection SCI models are relatively easy to generate and reproducible, they are not clinically relevant to the human SCI, where the majority of human SCI is contusion/compression injury [17]. The hallmark of this type of injury is the formation of an oval-shaped cystic cavity in the center of the lesion site with a rim of preserved spinal cord tissue [14]. To prevent causing more damage to the remaining tissue and nerve fibers, therapeutic strategies utilizing minimally invasive techniques such as injectable biomaterials are preferred to fill the cavity.

In this dissertation, a simple approach to prepare cell type-specific ECM matrices was developed. It is interesting to investigate the feasibility to develop an injectable biomaterial from these cell type specific-ECM materials for delivery to sites of interest by minimally invasive techniques and potentially conform to any three-dimensional wounded defects. It has been shown that injectable ECM gels can be prepared from digesting porcine bladder [18]. Moreover, multiple cell types can be applied at the same time during construct fabrication to increase the complexity of the derived ECM scaffolds. This would better mimic the natural *in vivo* tissue environment. It will also be interesting to evaluate the feasibility of

ECM gels to serve as carriers for delivery of live cell suspensions or matrices for controlled release of growth factors and cytokines that would promote cell survival, angiogenesis and guide tissue repair. This study provides information on developing tissue type specific ECM materials, which can be introduced to injury sites through minimally invasive techniques.

An *in vitro* experiment could be first conducted to evaluate the effect of the complexity of ECM gels on various cellular functions, such as cell survivability, proliferation and phenotype expression. ECM constructs (e.g., derived from a single cell type or multiple cell types) could be engineered and decellularized according to methods described in this thesis work, then prepared into gel form as described previously [18].ECM gel derived from natural tissue that contains the same cell types used for engineering ECM constructs could be used for comparison. Cell suspensions could be mixed with different ECM gels and cultured *in vitro*. Cell live/dead assay, proliferation measurement kit and in situ hybridization technique could be used to reveal cellular functions within different ECM gels. For *in vivo* test, a rat myocardial infarction model could be used to test the ability of cell-derived ECM gels (e.g., single cell type or multiple cell types) to promote tissue regeneration [21] and naturally derived myocardial matrix gel could be used for comparison [22].

5.3 References

1. Pasterkamp RJ, Giger RJ, Ruitenberg M-J, D. HAJG, De Wit J, De Winter F, et al. Expression of the gene encoding the chemorepellent semaphoring III is induced in the fibroblast component of neural scar tissue formed following injuries of adult but not neonatal CNS. Mol Cell Neurosci 1999;13:143–166.

2. Hermanns S, Klapka N, Müller HW. The collagneous lesion scar and obstacle for axonal regeneration in brain and spinal cord injury. Restor Neurol Neurosci 2001;19:139-148.

3. Bundesen LQ, Scheel TA, Bregman BS, Kromer LF. Ephrin-B2 and EphB2 regulation of astrocyte-meningeal fibroblast interactions in response to spinal cord lesions in adult rats. J Neurosci 2003;23:7789 - 7800.

4. Shearer MC, Niclou SP, Brown D, Asher R, Holtmaat AJGD, Levine JM, et al. The astrocyte/meningeal cell interface is a barrier to neurite outgrowth which can be overcome by manipulation of inhibitory molecules or axonal signalling pathways. Mol Cell Neurosci 2003;24:913-925.

5. Shearer MC, Fawcett JW. The astrocyte/meningeal cell interface - a barrier to successful nerve regeneration? Cell Tissue Res 2001;305:267-273.

6. Rapalino O, Lazarov-Spiegler O, Agranov E, Velan GJ, Yoles E, Fraidakis M, et al. Implantation of stimulated homologous macrophages results in partial recovery of paraplegic rats. Nat Med 1998;4:814-821.

7. Popovich PG, Guan Z, Wei P, Huitinga I, van Rooijen N, Stokes BT.Depletion of hematogenous macrophages promotes partial hindlimb recovery and neuroanatomical repair after experimental spinal cord injury. Exp Neurol 1999;158:351-365.

8. Kigerl KA, Gensel JC, Ankeny DP, Alexander JK, Donnelly DJ, Popovich PG.Identification of two distinct macrophage subsets with divergent effects causing either neurotoxicity or regeneration in the injured mouse spinal cord. J Neurosci 2009;29:13435-13444.

9. Shechter R, London A, Varol C, Raposo C, Cusimano M, Yovel G, et al. Infiltrating blood-derived macrophages are vital cells playing an anti-inflammatory role in recovery from spinal cord injury in mice. PLoS Med 2009;6:e1000113.

10. Brown BN, Valentin JE, Stewart-Akers AM, McCabe GP, Badylak SF. Macrophage phenotype and remodeling outcomes in response to biologic scaffolds with and without a cellular component. Biomaterials 2009;30:1482-1491.

11. Valentin JE, Stewart-Akers AM, Gilbert TW, Badylak SF. Macrophage participation in the degradation and remodeling of extracellular matrix scaffolds. Tissue Eng Part A 2009;15:1687-1694.

12. Liang HC, Chang Y, Hsu CK, Lee MH, Sung HW. Effects of crosslinking degree of an acellular biological tissue on its tissue regeneration pattern. Biomaterials 2004;25:3541-3552.

13. Stout RD, Jiang C, Matta B, Tietzel I, Watkins SK, Suttles J. Macrophages sequentially change their functional phenotype in response to changes in microenvironmental influences. J Immunol 2005;175:342-349.

14. Beattie MS, Bresnahan JC, Komon J, Tovar CA, Van Meter M, Anderson DK, et al. Endogenous repair after spinal cord contusion injuries in the rat. Exp Neurol 1997;148:453-463.

15. Davies JE, Huang C, Proschel C, Noble M, Mayer-Proschel M, Davies SJ. Astrocytes derived from glial-restricted precursors promote spinal cord repair. J Biol 2006;5(3):7.

16. Hurtado A, Cregg JM, Wang HB, Wendell DF, Oudega M, Gilbert RJ, et al. Robust CNS regeneration after complete spinal cord transection using aligned poly-l-lactic acid microfibers. Biomaterials 2011;32:6068-6879.

17. Fleming JC, Norenberg MD, Ramsay DA, Dekaban GA, Marcillo AE, Saenz AD, et al. The cellular inflammatory response in human spinal cords after injury. Brain 2006;129:3249-3269.

18. Freytes DO, Martin J, Velankar SS, Lee AS, Badylak SF. Preparation and rheological characterization of a gel form of the porcine urinary bladder matrix. Biomaterials 2008;29:1630-1637.

19. Davies JE, Huang C, Proschel C, Noble M, Mayer-Proschel M, Davies SJ. Astrocytes derived from glial-restricted precursors promote spinal cord repair. J Biol 2006;5:7.

20. Eichinger CD, Hsiao TW, Hlady V. Multiprotein microcontact printing with micrometer resolution. Langmuir 2012; 28:2238-2243.

21. Huang NF, Sievers RE, Park JS, Fang Q, Li S, Lee RJ. A rodent model of myocardial infarction for testing the efficacy of cells and polymers for myocardial reconstruction. Nat Protoc 2006;1:1596-1609

22. Singelyn JM, DeQuach JA, Seif-Naraghi SB, Littlefield RB, Schup-Magoffin PJ, Christman KL. Naturally derived myocardial matrix as an injectable scaffold for cardiac tissue engineering. Biomaterials 2009;30:5409-5416.